Guest Editor: Albert Viggiano

CHEMICAL AND MICROPHYSICAL CHARACTERIZATION OF AMBIENT AEROSOLS WITH THE AERODYNE AEROSOL MASS SPECTROMETER

M.R. Canagaratna,[1]* J.T. Jayne,[1] J.L. Jimenez,[2] J.D. Allan,[3] M.R. Alfarra,[4] Q. Zhang,[5] T.B. Onasch,[1] F. Drewnick,[6] H. Coe,[3] A. Middlebrook,[7] A. Delia,[8] L.R. Williams,[1] A.M. Trimborn,[1] M.J. Northway,[1] P.F. DeCarlo,[2] C.E. Kolb,[1] P. Davidovits,[9] and D.R. Worsnop[1]

[1]*Center for Aerosol and Cloud Chemistry, Aerodyne Research, Inc., 45 Manning Rd., Billerica, Massachusetts 01821*
[2]*Department of Chemistry and CIRES, University of Colorado-Boulder, Boulder, Colorado 80309*
[3]*School of Earth, Atmospheric and Environmental Sciences, University of Manchester, England*
[4]*Paul Scherrer Institut, Villigen, Switzerland*
[5]*Atmospheric Sciences Research Center, State University of New York, Department of Earth and Atmospheric Sciences, University at Albany, Albany, New York 12222*
[6]*Max Planck Institute for Chemistry, Particle Chemistry Department, 55128 Mainz, Germany*
[7]*NOAA Earth System Research Laboratory, Boulder, Colorado 80305*
[8]*Program in Atmospheric and Oceanic Science, University of Colorado, Boulder, Colorado 80309*
[9]*Chemistry Department, Boston College, Chestnut Hill, Massachusetts 02467*

Received 13 March 2006; received (revised) 17 May 2006; accepted 19 May 2006

Published online 17 January 2007 in Wiley InterScience (www.interscience.wiley.com) DOI 10.1002/mas.20115

The application of mass spectrometric techniques to the real-time measurement and characterization of aerosols represents a significant advance in the field of atmospheric science. This review focuses on the aerosol mass spectrometer (AMS), an instrument designed and developed at Aerodyne Research, Inc. (ARI) that is the most widely used thermal vaporization AMS. The AMS uses aerodynamic lens inlet technology together with thermal vaporization and electron-impact mass spectrometry to measure the real-time non-refractory (NR) chemical speciation and mass loading as a function of particle size of fine aerosol particles with aerodynamic diameters between ~50 and 1,000 nm. The original AMS utilizes a quadrupole mass spectrometer (Q) with electron impact (EI) ionization and produces ensemble average data of particle properties. Later versions employ time-of-flight (ToF) mass spectrometers and can produce full mass spectral data for single particles. This manuscript presents a detailed discussion of the strengths and limitations of the AMS measurement approach and reviews how the measurements are used to characterize particle properties. Results from selected laboratory experiments and field measurement campaigns are also presented to highlight the different applications of this instrument. Recent instrumental developments, such as the incorporation of softer ionization techniques (vacuum ultraviolet (VUV) photo-ionization, Li^+ ion, and electron attachment) and high-resolution ToF mass spectrometers, that yield more detailed information about the organic aerosol component are also described. © 2007 Wiley Periodicals, Inc., Mass Spec Rev 26:185–222, 2007

Keywords: *submicron particles; PM; atmospheric chemistry*

I. INTRODUCTION

A. Why Do We Care about Atmospheric Particles?

Taken individually, atmospheric aerosol particles are inconsequential things. The vast majority of airborne particles are tiny clumps of liquid and/or solid material with aerodynamic diameters between ~3 and ~1,000 nm. Some are emitted directly from combustion sources as soot or ash particles; others are produced from natural surfaces in the form of wind blown dust or sea salt particles produced by breaking waves. Many others are produced directly in the atmosphere by condensation of initially volatile chemicals that have been oxidized by

Contract grant sponsors: National Science Foundation (NSF); Department of Energy (DoE); Office of Naval Research (ONR); Environmental Protection Agency (EPA); Max Planck Institute for Chemistry, Mainz; Japanese Automobile Research Institute; National Aeronautics and Space (NASA); NOAA; Environment Canada; New York State Department of Environmental Conservation; Nordic Centre of Excellence BACCI (Biosphere-Aerosol-Cloud-Climate Interactions.
**Correspondence to:* M.R. Canagaratna, 45 Manning Road, Billerica, MA 01821. E-mail: mrcana@aerodyne.com

photochemical processes and/or condensation of semivolatile species that were thermally vaporized, and recondense when exposed to colder air. Condensing atmospheric vapors may nucleate to form new particles or deposit on existing particles, changing their size distribution and chemical content.

While the atmosphere can contain some particles with diameters as large as 5,000–20,000 nm (5–20 μm), in the absence of strong winds particles larger than a few μm are heavy enough that gravitational settling removes them quickly enough to prevent the build up of large number densities. On the other hand, particles smaller than a few microns can stay airborne for up to several weeks, long enough to be transported across continents and oceans. Continental atmospheres often contain between 1,000 and 100,000 particles/cm^3 with diameters between 10 and 1,000 nm and the mass loadings from a few up to ~100 μg/m^3.

The impacts of high airborne particle levels can be recognized on spatial scales ranging from local to hemispheric, and are the subject of a recently completed comprehensive assessment of the science of airborne particulate matter (PM) to inform policy makers dealing with PM health and haze effects (NARSTO, 2004). On local to metropolitan area scales, epidemiological studies have shown that persistent atmospheric particle mass loadings above ~10–20 μg/m^3 are strongly associated with adverse human health effects, including increased mortality from cardiopulmonary disease and lung cancer (Dockery et al., 1993; Pope et al., 2002; Dominici et al., 2006). High particle loadings also decrease visibility on local to regional scales, causing both transportation safety issues and aesthetic degradation (Watson, 2002).

Airborne PM can also have significant impacts at regional to hemispheric scales even though PM mass loadings are typically not as high away from urban and industrial areas unless smoke from biomass fires is present. Deposition of acidic particles, containing sulfate and nitrate, to sensitive, poorly buffered soils and lakes can contribute to significant ecosystem degradation (National Acid Precipitation Assessment Program, 1991). Nitrate deposition to better buffered lakes and estuaries can significantly contribute to their eutrophication, while its deposition to sensitive land ecosystems can also have significant impacts beyond contributing to acidification (Bytnerowicz & Fenn, 1996). Furthermore, heavy aerosol loadings from urban and industrial regions may reduce photosynthetic fluxes of solar radiation and ambient temperatures in downwind agricultural regions enough to significantly reduce their productivity (Chameides et al., 1999; Cohan et al., 2002).

Atmospheric PM is also now known to influence the climate on scales from regional to hemispheric through a variety of mechanisms. Submicron particles serve as cloud condensation nuclei (CCN) and the number density of effective CCN particles affects the ability of clouds to backscatter both sunlight and earthshine and to grow cloud droplets large enough to produce precipitation (McFiggans et al., 2005b). Aerosol particles may also cause significant direct perturbations to the transfer of infrared, visible, and ultraviolet light in the Earth's atmosphere through their ability to scatter and, in some cases, absorb radiation (NRC, 1996).

High levels of light absorbing atmospheric PM can also influence the thermal structure of the atmosphere and suppress cloud formation (Ramanathan et al., 2001). The degree to which airborne fine particulates perturb atmospheric radiation transport and therefore, impact climate on regional to semi-global scales is highly uncertain, but potentially very important (IPCC, 2001). In addition, atmospheric and ecological scientists are now able to define important couplings among the production of aerosol particles from biogenic emissions, the hydrological cycle, and the land ecosystems that produce most biogenic emissions (Barth et al., 2005).

B. The Scientific Challenge of Characterizing Atmospheric PM

The challenges of PM chemical characterization are daunting. First, as noted above, atmospheric PM comes in a wide range of sizes. The smallest nucleation mode consists of new particles formed in the atmosphere, and can span diameters ranging from 1–3 nm to ~50 nm. Atmospheric nucleation mode particles are believed to last only a few hours before agglomerating with larger particles. Particles with diameters between ~50 and 1,000 nm are termed accumulation mode particles, and have typical atmospheric lifetimes between a few days and a few weeks. The nucleation and accumulation mode particles are collectively called fine particles. Particles larger than a few μm are termed coarse mode particles and generally have relatively short atmospheric lifetimes before being removed by precipitation or gravity. It is possible to have atmospheric conditions where the nucleation mode particles dominate the PM number density, the accumulation mode particles define the PM surface area, and the coarse mode particles control the PM volume or mass loading. However, for many atmospheric conditions, especially when far from strong pollution emission sources, the accumulation mode often dominates many PM properties of interest.

The analytical problem posed by the wide range of atmospheric PM sizes is dynamic range; a 1 nm diameter particle will have a mass of ~10^{-21} g (zeptograms), whereas a 10 μm particle will have a mass of ~10^{-9} g (nanograms). Reliable sampling and accurate chemical composition determination of a single nanogram particle is a tough analytical challenge; for a zeptogram particle, it is nearly impossible. Traditional PM chemical composition measurement techniques rely on collecting many particles and measuring their average chemical composition. However, aerosol particle distributions can be externally mixed, that is, containing chemically differentiated particles emitted from different sources or products of different atmospheric chemical histories. The ideal atmospheric PM measurement would produce data on the chemical composition of individual particles as a function of particle diameter, for particle diameters ranging from a few nm to tens of μm.

In addition to PM size, composition, and mass loading, many other physical and chemical properties are of interest, and preferably measured simultaneously. For instance, climate scientists need to correlate size and chemical composition with a particle's ability to scatter and absorb radiation from the infrared to the near ultraviolet, and its ability to nucleate water droplets at low water supersaturation levels (IPCC, 2001). The former is influenced by a particle's shape and surface composition as well as its bulk composition. The latter depends

on a particle's surface structure and composition as well as on its size and bulk composition. Health scientists suspect that a particle's surface area and surface composition may be a key to understanding how it interacts with lung tissue to affect pulmonary functions and transfer chemicals into the blood stream (NARSTO, 2004), so measurements of particle morphology and surface adsorbed species are of growing interest. Finally, atmospheric chemists are interested in the physical phase (liquid or solid), surface area, and surface composition because these properties can strongly affect the interaction of atmospheric trace gases with airborne particles, impacting the chemical composition of both the gaseous and condensed phase components of the atmosphere.

C. Real-Time Atmospheric PM Instrumentation

The chemical complexity and labile nature of atmospheric PM strongly favors real-time instrumental analysis techniques that characterize pertinent physical and chemical properties without having to collect, store, and transport samples. Real-time instruments that measure physical properties such as particle number densities, mass loadings, and particle mobility or aerodynamic size distributions have been available for some time (McMurry, 2000; NARSTO, 2004). However, real-time instruments that characterize the chemical composition of atmospheric PM, ideally as a function of particle size, are a more recent development.

Some near real-time PM chemical composition instruments, operating with measurement cycles of 10–60 min, do a good job of characterizing the average PM content of one or more key PM constituents for an ensemble of particles in a size range defined by the sample collection system. Examples include the particle-into-liquid sampler (PILS) that utilizes automated ion chromatography to quantify average major anion or cation PM content (Weber et al., 2001) or an automated carbon analyzer to determine the water-soluble organic carbon (OC) (Sullivan et al., 2004), instruments based on particle collection followed by thermal decomposition and gas phase chemiluminescence or absorption spectroscopy allow for semi-continuous measurements of sulfate and nitrate (Stolzenburg & Hering, 2003). Other instruments analyze organic and total carbon content based on particle collection, thermal pyrolysis, and oxidation followed by carbon dioxide detection (Turpin, Cary, & Huntzicker, 1990; Bae et al., 2004). None of these methods produce significant information on the variation of PM chemical composition with particle size or a comprehensive picture of total PM composition.

The universal nature of mass spectrometric detection for atomic and molecular species recommends the technique as a comprehensive and sensitive technique to characterize the chemical content of atmospheric PM. Over the past decade, several research groups have made major strides in adapting mass spectrometric techniques to meet this challenge, and this work has been the subject of several review articles (Suess & Prather, 1999; Johnston, 2000; Noble & Prather, 2000; Sullivan & Prather, 2005; Coe & Allan, 2006). One major theme involves the use of lasers to both vaporize and ionize individual atmospheric particles sampled into a mass spectrometer's source region. This class of instruments focuses on single particle measurements and has been recently reviewed by Noble and Prather (2000) and Sullivan and Prather (2005). A review of design considerations for these instruments is presented by Murphy in this issue (Murphy, 2006).

A second class of aerosol mass instruments uses thermal vaporization of individual or collected particles followed by various ionization techniques (Allen & Gould, 1981; Sinha et al., 1982). Separation of the vaporization and ionization steps enables quantitative detection of PM chemical composition and mass loading. In addition, the simplicity of thermal vaporization allows the use of a variety of ionization techniques that will produce less sample fragmentation than traditional electron impact (EI) methods, such as chemical ionization techniques (Hoffmann et al., 1998; Voisin et al., 2003; Warscheid, Kuckelmann, & Hoffmann, 2003; Hearn & Smith, 2004), low energy photoelectron attachment (LaFranchi & Petrucci, 2004; Zahardis, LaFranchi, & Petrucci, 2005), and vacuum ultraviolet (VUV) single photon ionization (Woods et al., 2002; Öktem, Tolocka, & Johnston, 2004; Ferge, Muhlberger, & Zimmermann, 2005).

In this review, we will focus on the most widely used thermal vaporization aerosol mass spectrometer (AMS) which was designed and developed at Aerodyne Research, Inc. (ARI) and is currently used by approximately 40 laboratories worldwide. The initial version of the ARI AMS was designed to measure the real-time non-refractory (NR) chemical speciation and mass loading of fine aerosol particles with aerodynamic diameters between ~50 and 1,000 nm as a function of particle size (Jayne et al., 2000). The original ARI AMS utilizes a quadrupole mass spectrometer (Q) with EI ionization and produces ensemble average data of particle properties. Later versions, also described in this review, employ time-of-flight (ToF) mass spectrometers and can produce complete mass spectral data for single particles. The development of single photon and chemical soft ionization techniques for field deployment will also be presented. Results from selected laboratory experiments and field measurement campaigns will be discussed to demonstrate the instrument's strengths and weaknesses.

II. MEASUREMENT APPROACH USED IN THE AMS

A. Instrument Overview

A schematic representation of the Aerodyne AMS is shown in Figure 1. The instrument has three main sections: the aerosol inlet, the particle sizing chamber, and the particle composition detection section. The aerosol inlet samples sub-micron aerosol particles into the AMS through an aerodynamic lens, forming a narrow particle beam which is transmitted into the detection chamber where NR components are flash vaporized upon impact on a hot surface (~600°C) under high vacuum (~ 10^{-5} Pa) and chemically analyzed via EI ionization and mass spectrometry. The transmission of the beam to the particle detector can be modulated with a mechanical chopper that is operated at 100–150 Hz. The chopper is placed in one of the three positions: a "closed" position which blocks the beam completely, an "open" position which transmits the beam continuously, or a "chopped"

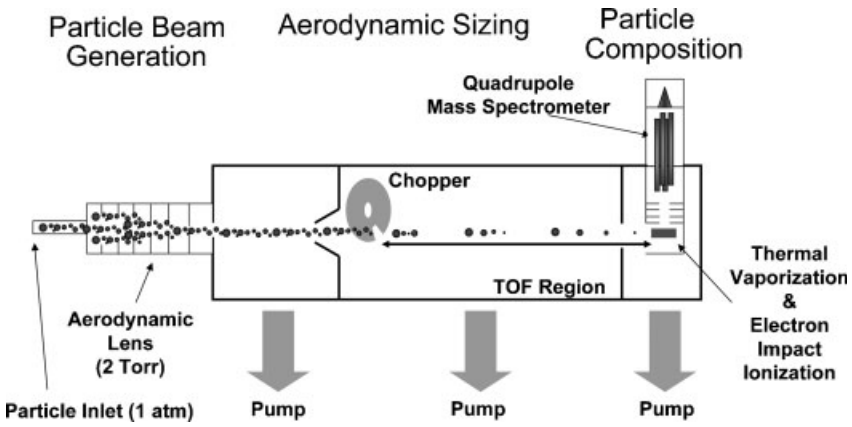

FIGURE 1. Schematic of an Aerodyne Aerosol Mass Spectrometer (AMS). Aerosols are sampled through the aerodynamic lens, focused into a narrow beam, and transmitted into a detection chamber where they are impacted on a heated surface. Vaporized aerosol species are ionized by electron impact and analyzed via mass spectrometry. Particle time-of-flight from a mechanical beam chopper to the vaporizer is measured to obtain chemically speciated size distributions. This figure shows the simplest version of the AMS. Other existing versions of the AMS which utilize several important instrumental modifications and developments that are not shown in this schematic are discussed in detail in the text of this manuscript.

position which modulates the beam transmission with a 1–4% duty cycle that is determined by the width of the chopper slit. The chopped mode is used to measure particle flight times from the chopper to the detector (Jayne et al., 2000).

Three versions of the AMS (Q-AMS, ToF-AMS, and HR-ToF-AMS) are currently in use. These versions that vary in the type of mass spectrometric detector, using a quadrupole mass spectrometer (Q), a ToF mass spectrometer, or a high resolution ToF mass spectrometer (HR-ToF). The three AMS versions are described in detail by Jayne et al. (2000), Drewnick et al. (2005) and DeCarlo et al. (2006), respectively. Despite the different mass spectrometers used, the basic measurement approach remains the same. Most of the results presented in this review are from Q-AMS instruments, and we will further describe the Q-AMS instrument in the following sections. A brief overview of the ToF-AMS and HR-ToF-AMS, which are newer versions of the AMS, will be provided in the last section of this review.

The AMS is typically alternated between two modes of operation: mass spectrum (MS) mode and particle ToF (PToF) mode (Jimenez et al., 2003b). In MS mode, the quadrupole is scanned (typically *m/z* 1–300) with the chopper in open position to obtain an ensemble averaged MS of the sampled aerosol. Signals from the ionization of background gases in the detection region are accounted for by subtracting the background MS obtained with the chopper in closed position. In the PToF mode, the quadrupole steps through 15–20 pre-selected ion fragment masses as the chopper modulates the particle beam. Most of the information provided by the Q-AMS in each of these modes is representative of the ensemble (averaged) aerosol. The Q-AMS provides some single particle information (Jimenez et al., 2003b), but limited to one *m/z* per particle because it cannot complete an entire mass spectral scan on the 100–200 μsec timescale of a particle vaporization event. The ToF-AMS, on the other hand, is not a scanning instrument and is capable of providing complete mass spectra for single particles (Drewnick et al., 2005).

By alternating between the PToF and MS modes, a broad chemical and microphysical picture of the ensemble aerosol can be obtained. The modes of operation are software controlled and automated so that focused studies can measure major components with fast time resolution (up to 10 Hz has been demonstrated) or can signal average over longer time scales for better sensitivity to minor chemical components or when sampling low concentrations. A third mode, known as the jump mass spec (JMS) mode has been implemented for applications where high time resolution and/or high sensitivity are critical. This mode is analogous to ''selected ion monitoring'' in commercial mass spectrometers: a small subset of *m/z*s (10–20) is selected and the quadrupole is tuned by jumping between them in order of increasing *m/z*, without scanning over the rest of the *m/z*s. The chopper is opened and closed every few seconds as in the MS mode. If 10 *m/z* are used, the duty cycle per *m/z* is increased by a factor of 30 with respect to the regular MS mode. This mode has been used during aircraft sampling (Crosier et al., 2006) and for performing chemically resolved eddy-covariance particle flux measurements.

B. Aerodynamic Lens and Focusing of Particle Beams

As described by Murphy (2006) in this issue, one of the advantages of aerodynamic lens inlets over capillaries and nozzle sampling inlets is that they provide efficient particle focusing over a wide size range. The aerosol inlet used by the AMS couples a critical orifice (which reduces the ambient pressure to ~267 Pa) with a series of apertures (Liu et al., 1995a,b; Zhang et al., 2002, 2004b) that focus particles into a narrow beam. The divergence of

gas phase molecules at the exit of the aerodynamic lens together with differential pumping in the vacuum chamber results in a particle flux to the detector region that is enriched by a factor of approximately 10^7 relative to the gases in the air sampled at the inlet. Computational fluid dynamics simulation of the AMS inlet system shows 100% transmission efficiency to the detector for particles in the aerodynamic diameter range 70–500 nm and substantial transmission for particles in the 30–70 nm and 500 nm–2.5 μm ranges for spherical particles (Jayne et al., 2000; Zhang et al., 2002, 2004b). This transmission curve has been verified experimentally for the 80 nm–1 μm range with NH_4NO_3 particles (Jayne et al., 2000; Liu et al., 2006). The computational tools described in Zhang et al. (2002, 2004b) can be used to design aerodynamic lens systems that move the lens transmission window to larger or smaller particle size ranges. Experiments are currently being conducted to confirm the computations. Based on the current transmission properties of the inlet, the AMS is referred to as a PM_1 instrument, reflecting its transmission efficiency of approximately 50% at a particle size of 1 micron. Thus, the current aerodynamic lens system is tailored to sample the bulk of ambient atmospheric accumulation mode particles.

The particle beam width at the exit plane of Liu type lenses is on the order of 100 microns (Heberlein et al., 2001), but the beam broadens as the particles travel through vacuum due to small radial velocity components from imperfect aerodynamic focusing, Brownian motion, and lift forces experienced by non-spherical particles (Liu, 1995c). The beam width at the point of detection depends on particle size, particle morphology, and distance of the detector from the lens exit. This can be a disadvantage if the particle beam solid angle becomes large enough such that significant portions of the beam miss the detector and are consequently not detected (Huffman et al., 2005). Recently, a novel beam width probe (BWP) has been used to measure, in real-time, the width of particle beams within the AMS (Jayne et al., 2000; Slowik et al., 2004; Huffman et al., 2005; Katrib et al., 2005a; Allan et al., 2006; Salcedo et al., 2006; Weimer et al., 2006). These measurements have been performed with the objectives of (a) quantifying the effect of particle beam divergence on AMS particle detection efficiency and (b) obtaining a real-time surrogate measurement of particle morphology versus particle size and composition. Results from these measurements are discussed below.

The BWP that is shown in Figure 2, consists of a small diameter wire (~400 μm) that is mounted at the end of the PToF chamber in front of the AMS vaporizer (Huffman et al., 2005). During measurements, the AMS signal is recorded as a function of BWP position as it is alternately positioned in either the non-blocking position, with the wire located outside the vaporizer

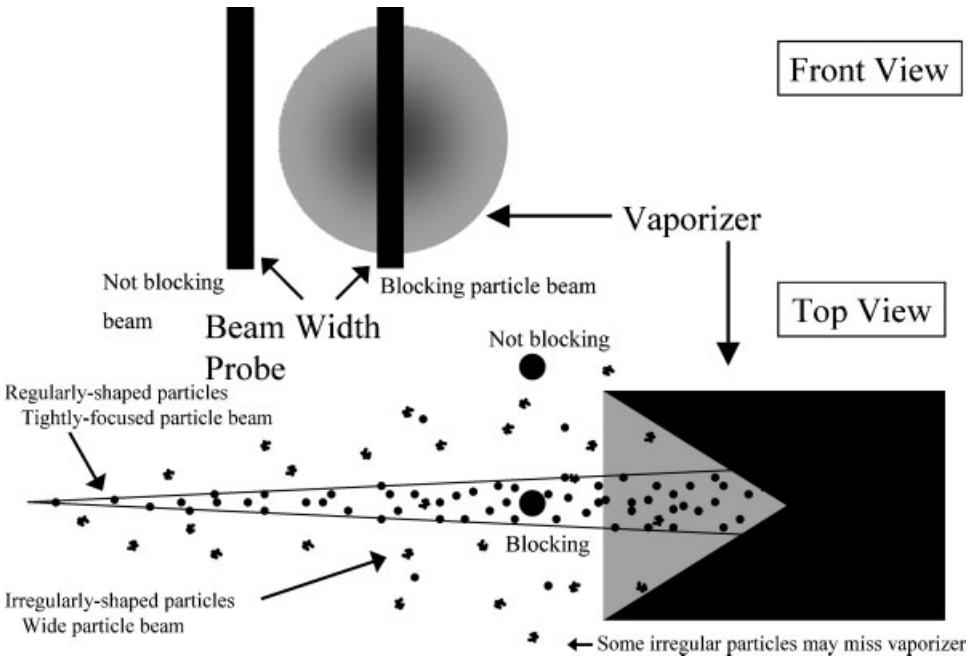

FIGURE 2. Two schematic views of the beam width probe (BWP) are shown. During BWP measurements, the probe is positioned in front of the vaporizer in either a non-blocking position or a blocking position. The non-blocking position provides the reference signal level for an unattenuated particle beam. The measured signal is attenuated in blocking positions because the BWP prevents a portion of the particle beam from impacting the vaporizer and being detected. A profile of the beam width is obtained by stepping the BWP through a series of blocking positions. The fraction of the particle beam blocked by the BWP at any given blocking position depends on the shape of the sampled particles. The top view of the BWP shows projections of particle trajectories for both regularly and irregularly shaped particles as they travel from the exit of the lens to the vaporizer. Regularly shaped particles are more tightly focused than irregularly shaped particles. (Aerosol Science & Technology: Huffman et al.: Design, modeling, optimization, and experimental tests of a particle beam width probe for the aerodyne aerosol mass spectrometer. (39):1143–1163. Copyright 2005. Mount Laurel, NJ, Reprinted with Permission.)

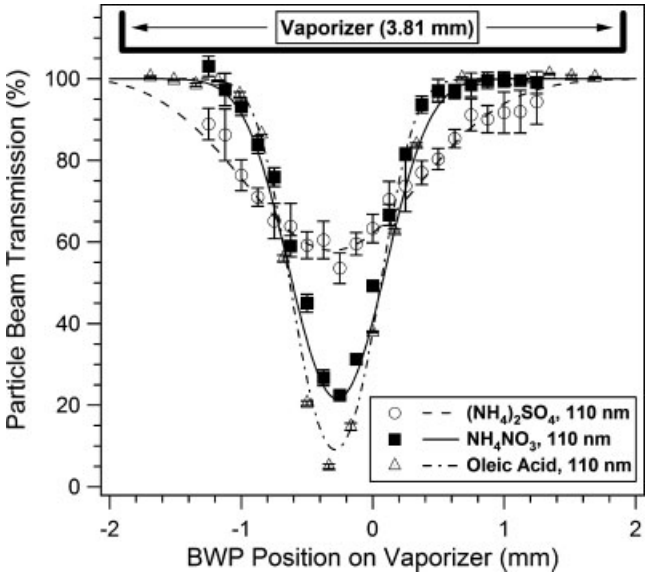

FIGURE 3. Beam width profiles reported by Huffman et al. (2005) for 110 nm pure component particles. The symbols denote experimental measurements of particle beam transmission and the error bars show the standard error of the measured mean. The dashed and solid lines show the predictions of the 2-D Gaussian distribution model. (Aerosol Science & Technology: Huffman:Design, modeling, optimization, and experimental tests of a particle beam width probe for the aerodyne aerosol mass spectrometer. (39):1143–1163. Copyright 2005. Mount Laurel, NJ, Reprinted with Permission.)

area, or one of a series of blocking positions. Figure 3 shows an example of data from an experiment in which the BWP was used to characterize the widths of pure component particle beams containing 110 nm particles of oleic acid (OA), NH_4NO_3, or $(NH_4)_2SO_4$ (Huffman et al., 2005). Each of the points in Figure 3 shows the particle transmission as the BWP wire was stepped across the different particle beams. The signal obtained in the unblocked BWP position is defined as 100% relative transmission. It is also clear from the figure that the well-focused, spherical OA particles and nearly spherical NH_4NO_3 particles have narrower beam width profiles than $(NH_4)_2SO_4$ particles. The beam widths from all of these particles are significantly smaller than the vaporizer diameter of 3.81 mm. The mild non-sphericity of $(NH_4)_2SO_4$ particles is consistent with the results of Zelenyuk, Yong, and Imre (2006b), who determined dynamic shape factors (χ_v) of 1.03–1.07 for submicron particles of this species.

Huffman et al. (2005) have recently developed a model which approximates the particle beam as a 2D circular Gaussian distribution and quantitatively relates measured BWP profiles to the width of the particle beam. The particle beam is defined in terms of a cone that is centered at the nozzle exit and has a solid angle that encompasses a certain fraction of the beam density. The standard deviation of the 2D Gaussian distribution, which encompasses ~48% of the probability density, is defined as the beam width (σ) by Huffman et al. (2005). Figure 4 shows a comparison of the particle beam widths determined for a range of published studies that have used Liu-type lenses (Huffman et al., 2005). The separation of the experimental data according to the sphericity of the measured particles highlights the observation that, in general, non-spherical particles are less well focused when compared to spherical particles (Liu et al., 1995a,b; Jayne et al., 2000; Tobias et al., 2000a). For a given chemical species, the beam widths also vary with the size of the sampled particles. The most focused beams are observed for particles with diameters around 300 nm for this type of lens. Smaller particles (<40 nm), which suffer from Brownian broadening (Liu, 1995; Liu et al., 1995b), and larger particles (>500 nm), which have greater inertia, are not focused as well by the aerodynamic lens (Zhang et al., 2004b).

The consistency between the results shown in Figure 4, which were obtained by different research groups with independently built aerodynamic lenses, indicates that the focusing behavior of a given aerodynamic inlet design is relatively constant. Huffman et al. have used the laboratory data shown in Figure 4 to estimate the relative detection bias between spherical particles and other particle types in the AMS. The calculations show that the detection bias for flame soot, which provides a reasonable limit for the non-sphericity of particles typically detected by the AMS under ambient conditions, is 1.05. (i.e., only approximately 5% of the particle signal is lost for flame soot due to excessive divergence of some particles). Lack of a significant sampling bias due to particle non-sphericity for ambient aerosols of varying composition has been confirmed by BWP measurements obtained in both urban areas (Salcedo et al., 2006; Weimer et al., 2006) and forests (Delia, 2004; Allan et al., 2006). The small detection biases in the AMS result from the large collection solid angle of the 3.81-mm diameter AMS vaporizer. Huffman et al. (2005) and Murphy (2006) estimate detection biases of at least a factor of 2 to 6 for the smaller collection angles used in laser vaporization MS instruments which rely on the overlap between the particle beam and a tightly focused laser spot.

C. Particle Sizing

The velocity acquired by particles when they exit an aerodynamic lens and expand into vacuum is directly related to their vacuum aerodynamic diameter. In the AMS, these particle velocities are determined by measuring particle flight times between a mechanical chopper that is used to modulate the particle beam and the vaporizer surface (Jayne et al., 2000).

Figure 5 shows an example of AMS PToF traces obtained while the quadrupole MS measured signal from two sulfate fragments (*m/z* 48, *m/z* 64) in ambient particles. The opening of the chopper slit, detected with an LED and photodiode, provides the start time for each PToF measurement cycle. The chopper operates at a frequency of approximately 100–150 Hz and has a 1–4% slit. Since the scan rate of the quadrupole (~300 msec per spectrum) is slow on the timescale of a PToF cycle (~10 msec), the quadrupole is operated at one *m/z* for approximately 40 PToF cycles, and then stepped to the next selected *m/z*, rather than scanned through the entire MS during these measurements. Particle arrival is indicated by the burst of ion signal at the selected *m/z* after a particle size-dependent delay from the opening of the chopper. The zero signal level for each PToF cycle is set by subtracting the observed signal, due to the background ion signal, within two user-definable DC regions

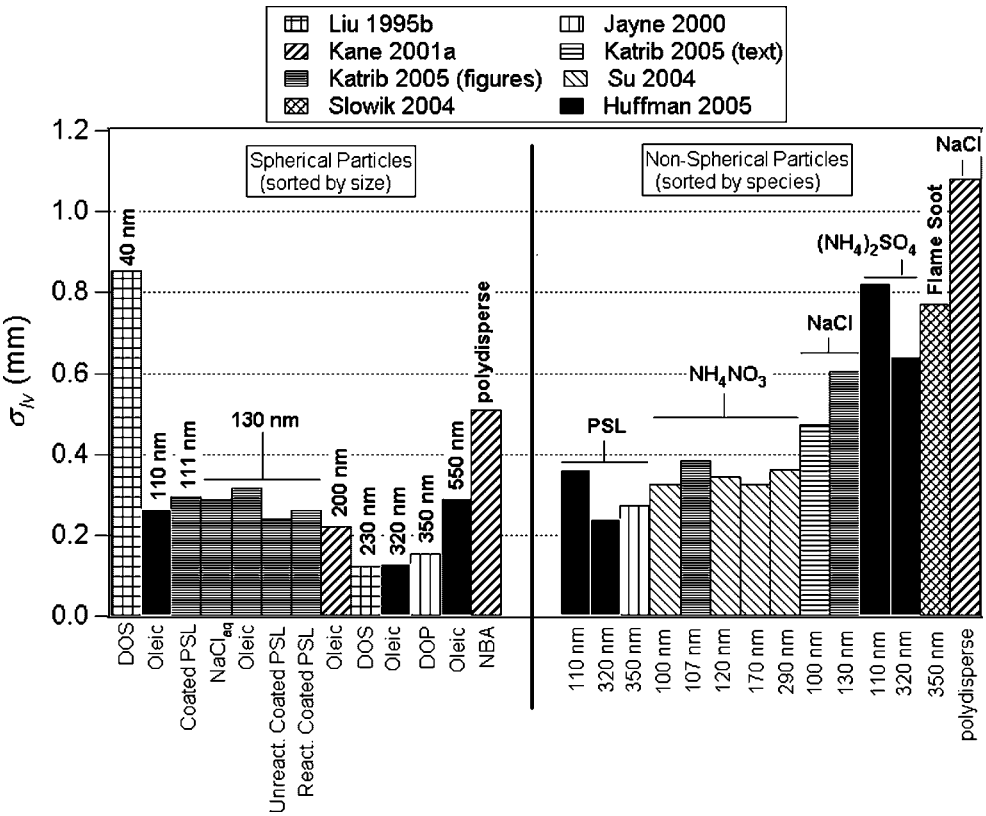

FIGURE 4. Particle beam widths estimated by Huffman et al. (2005) from published beam width studies of Liu-style lenses by various research groups. The particle beam widths (*lv*) are estimated for a flight distance of 450 mm, which correspond to the distance between the exit of the aerodynamic lens and the plane of the vaporizer surface in AMS instruments that have long chambers. The results have been sorted according to the sphericity or asphericity of the particles of interest. The spherical particle measurements are further sorted by size and the non-spherical particle measurements are sorted by species and then particle size.

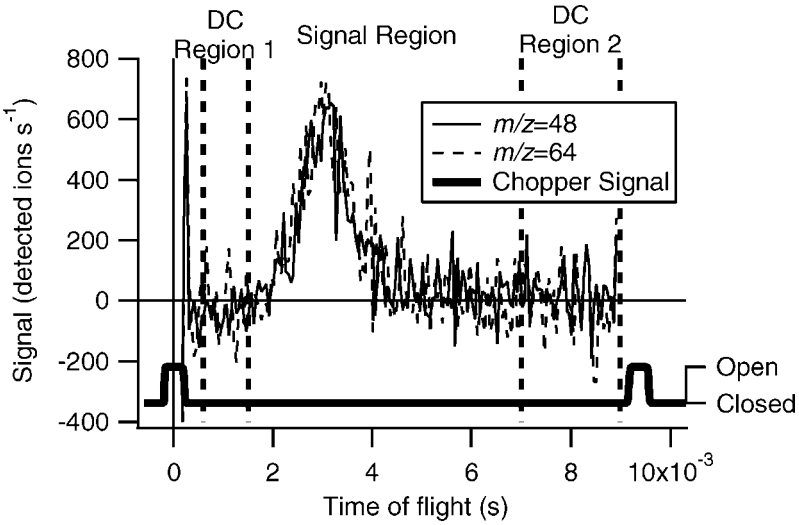

FIGURE 5. An example of data obtained in PToF mode for ambient particles. The figure shows quadrupole mass spectrometer signal measured at $m/z = 48$ and $m/z = 64$ as a function of particle time-of-flight. The chopper signal, which defines the beginning and end of each time-of-flight cycle, is also shown for reference. The DC regions of the PToF traces are used to obtain the baseline and noise levels for the measurements. (Reproduced/modified by permission of American Geophysical Union from Allan et al., 2003b. Copyright 2003 American Geophysical Union.)

(Allan et al., 2003b). The similar PToF traces obtained for *m/z* 48 and 64 in Figure 5 are due to both ions (SO^+ and SO_2^+) being produced in roughly equal amounts by sulfate-containing particles. The particle velocities determined in PToF measurements can be converted to particle vacuum aerodynamic diameters (d_{va}; DeCarlo et al., 2004) by using the relationships between velocity and size that are determined from calibrations performed with polystyrene latex size standards (Jayne et al., 2000). Since the AMS signal measured in PToF mode is proportional to particle mass, the resulting ensemble size distributions are mass-weighted.

Averaged mass-weighted size distributions for each fragment are obtained by averaging the signals from many PToF cycles. Signal bursts from larger (>100 nm if pure component) particles that reproducibly exceed the background signal at the scanned fragment, can be counted effectively to obtain number-weighted size distributions (Jayne et al., 2000; Jimenez et al., 2003b). Since this type of Q-AMS measurement is performed at only a few scanned *m/z*, the sensitivity and amount of single particle chemical information obtained in this manner is limited, and has been used more for laboratory than for field experiments. On the other hand, a ToF mass spectrometer provides a full spectrum for every ion extraction pulse, and detection of complete mass spectra of individual particles is possible as has been demonstrated with the ToF-AMS (Drewnick et al., 2005).

D. Detection Scheme

The AMS detection scheme was designed with the goal of developing a general method capable of providing quantitative measurements of aerosol mass for a wide range of aerosol compositions (Jayne et al., 2000). Key to accomplishing this goal is the ability to carry out ionization without plasma chemical charge transfer matrix effects which can create significant difficulty for quantitative analyses of combined laser vaporization/ionization mass spectral data (Reilly et al., 2000; Murphy, 2006). One proven method of accomplishing this goal is to separate the vaporization and ionization steps during the detection process (Allen & Gould, 1981; Morrical, Fergenson, & Prather, 1998; Lazar et al., 1999; Zelenyuk et al., 1999). Instruments that separate the vaporization and ionization steps generally vaporize particles with IR lasers (Morrical, Fergenson, & Prather, 1998; Zelenyuk et al., 1999) or heated surfaces (Allen & Gould, 1981; Sinha et al., 1982; Tobias et al., 2000b; Sykes et al., 2002; Voisin et al., 2003), and then ionize with lasers (Morrical, Fergenson, & Prather, 1998; Zelenyuk et al., 1999; Sykes et al., 2002), EI ionization (Allen & Gould, 1981; Tobias et al., 2000b), or chemical ionization techniques (Voisin et al., 2003).

In the AMS, particles are flash vaporized on a resistively heated porous tungsten surface and the vapor is ionized by EI. The vaporizer is coupled to an EI ionizer at the entrance of a mass spectrometer as shown in Figure 6. The vaporizer is simple to operate and has a large overlap with the particle beam, thus resulting in negligible detection bias (Huffman et al., 2005) (See section II.B for more details). EI is a linear and reproducible technique for ionizing molecules in the gas phase under vacuum conditions. Moreover, it is a universal ionization method that can be used for a wide range of molecules, both inorganic as well as organic (Crable & Coggeshall, 1958; Bartmess & Georgiadis, 1983; McLafferty & Turecek, 1993).

The effectiveness of the overall AMS detection approach in providing matrix-independent detection of aerosol species is illustrated in Figure 7. This figure shows linear quantitative detection of the nitrate and sulfate components as a function of varying $(NH_4)_2SO_4/NH_4NO_3$ ratio in the sampled aerosols (Hogrefe et al., 2003). The slope shown in the figure becomes the expected value of 1 once it has been corrected for fragments of both NO_3 and SO_4 that were not monitored during the experiment and for the relative ionization efficiencies of both species. Recent studies, discussed in a manuscript in preparation by Middlebrook

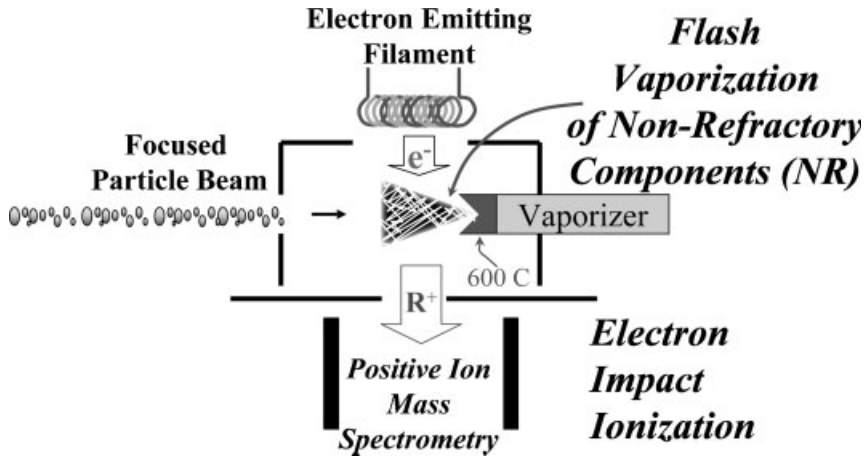

FIGURE 6. A schematic of the detection scheme used in the AMS. The particle beam first impacts on a vaporizer, and non-refractory aerosol components that vaporize are subsequently subjected to electron impact ionization. The unique feature of this detection scheme is the fact that a vaporizer is directly coupled into an electron impact ionizer to enable a two-step particle vaporization and ionization process. The separation of the vaporization and ionization processes allows for quantitative detection of aerosol mass with the AMS.

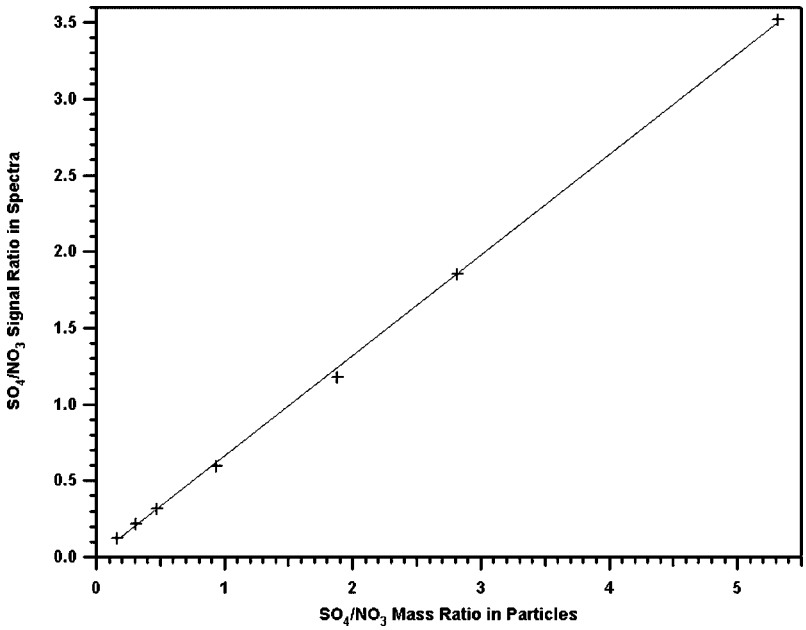

FIGURE 7. Sulfate to nitrate ratios measured with the AMS as a function of actual sulfate to nitrate content of sampled particles. As discussed in the text, the slope of the fitted line differs from 1 because AMS measurements only reflect the signal observed at the main fragments of sulfate and nitrate. (Aerosol Science & Technology: Hogrefe et al.: Development, operation and applications of an aerosol generation, calibration and research facility. (38):196–214. Copyright 2003. Mount Laurel, NJ, Reprinted with permission.)

et al., also show that the sensitivity of the AMS to nitrate and sulfate in NH_4NO_3 or $(NH_4)_2SO_4$ is independent of the water content of the sampled particles. These results indicate that the AMS can detect a wide range of chemical components including species like sulfate which laser-based detection schemes employing positive ion detection have difficulty ionizing and thus detecting (Murphy, 2006). Section III.B.2 of this review will assess the quantification capabilities of the AMS in the context of ambient measurements.

A limitation of using a thermal method for vaporizing the aerosol particles (compared to laser-based vaporization schemes) is that it can only detect NR materials, that is, species that evaporate sufficiently fast at the AMS vaporizer temperature and high vacuum conditions. Aerosol concentrations reported by the AMS, NR-PM_1, are usually qualified with the prefix NR to reflect this fact. During typical operation in the field, the vaporizer is held at approximately 600°C which is the optimum temperature for detecting NR organic aerosol components and major inorganic species like NH_4NO_3, $(NH_4)_2SO_4$, and NH_4Cl. Laboratory studies indicate that the NR material is efficiently vaporized and detected even if it is internally mixed in/on refractory particles (Katrib et al., 2004; Slowik et al., 2004). The main refractory materials that are not detected by the AMS are crustal materials (dust), soot, fly ash, metal oxides, and sea salt. These species, which are likely to be most significant close to the sources that emit them, can be better detected with laser vaporization instruments (Murphy, 2006). Other shortcomings of the thermal vaporization method include possible decomposition of labile species on flash heating and the need to account for non-unit collection efficiencies due to particle bounce effects (discussed in section III.B.2 below). The primary tradeoff with respect to EI ionization is that it introduces significant fragmentation which can make identification of the parent species difficult, especially when many species are present in the particles being analyzed. Recent advances in interpreting ambient organic mass (OM) spectra obtained with the AMS are discussed in section V; softer ionization methods to reduce ion fragmentation are discussed in section VI.

III. CHARACTERIZATION OF PARTICLE PROPERTIES WITH THE AMS

A. Determination of Aerosol Chemical Composition

Laboratory studies show that distinctive mass spectra are obtained when aerosol particles consisting of single chemical components are measured with the AMS (Jimenez et al., 2003b; Alfarra, 2004). Since the AMS uses standard 70 eV EI ionization, AMS spectra can be compared to, and are typically predicted by, mass spectra available in mass spectral databases such as that from the National Institute of Standards and Technology (NIST) (Linstrom & Mallard, 2001). Intercomparisons between AMS and NIST spectra for a range of chemical species have been performed (Alfarra, 2004). These studies indicate that most types of parent molecules that are resistant to thermal decomposition and fragmentation yield AMS mass spectra that are very similar to those in the NIST database (Dzepina et al., 2006). For certain classes of molecules, however, the vaporization step that precedes EI ionization in the AMS can introduce reproducible differences from NIST spectra. For example, AMS spectra of aliphatic (long-chain) organic molecules contain the same ion fragments as the NIST spectra but with ion intensities that are weighted

towards smaller ion fragments. This increased fragmentation likely reflects the additional thermal energy obtained during vaporization. Thermally induced decarboxylation and dehydration of di- and poly-carboxylic acids has also been observed. These molecules yield AMS spectra with significant signals at *m/z* 18 (H_2O^+), 28 (CO^+), and 44 (CO_2^+) which are not present with significant intensity in the corresponding spectra of the NIST database. As will be described below, these spectral differences do not affect the capability of the AMS to quantify the total mass of organic species because all fragments of a given chemical species are accounted for in the analysis.

Table 1 summarizes some of the main fragments observed by the AMS for the chemical species that are typically detected in ambient aerosol (Allan et al., 2004b). The use of these fragments for identification of chemical species in ambient particles is complicated by the fact that ambient particles may be composed of hundreds of individual chemical species, all of which are vaporized and ionized simultaneously in the AMS without any prior separation stage. The most common inorganic moieties like SO_4^{2-} and NO_3^- can usually be readily identified because of their simple fragmentation patterns and the fact that their main fragments typically do not experience significant interference from other chemical species in the aerosol, as they fall in the valleys between the main organic ion series (DeCarlo et al., 2006).

It is generally impossible for the AMS to identify individual organic compounds in ambient aerosols, except in a few special cases where species with a distinct fragmentation pattern like polycyclic aromatic hydrocarbons (Marr et al., 2005; Dzepina et al., 2006) are present in high concentration. The organic fragments listed in Table 1 can, however, be used to infer the presence of broad classes of organic molecules like oxidized organic species or hydrocarbon-like organic species (Alfarra et al., 2004; Zhang et al., 2005a). A more detailed discussion of analyzing ambient OM spectra is presented in section V.

AMS spectra obtained from ambient aerosols represent a linear superposition of the spectra of all individual species present, weighted by their relative concentrations and detection efficiencies. A generalized and flexible method of arithmetically deconvolving raw AMS spectra into partial mass spectra for distinct chemical species (or groups of species) has been developed by Allan et al. (2004b). In this method, the contribution of each chemical species at any given *m/z* is explicitly calculated based on a user-definable "fragmentation table" for each chemical species or a group of species. This fragmentation table is a series of non-circular linear dependencies between the contributions of various species to different *m/z*, constructed using laboratory-derived fragmentation ratios of all the pure species and knowledge of isotopic ratios of the various atoms (Hogrefe et al., 2003). The simplest example of this procedure is the determination of ammonium concentration from AMS spectra (Allan et al., 2004b). Laboratory calibrations show that this species produces fragments at *m/z* 15 (NH^+), 16 (NH_2^+), and 17 (NH_3^+). Significant interferences appear, however, at these *m/z* from CH_3^+ (*m/z* 15), O^+ (*m/z* 16) from O_2 and H_2O, and OH^+ (*m/z* 17) from H_2O. The fragmentation table in this case specifies several linear relationships, derived from empirical observations, that can be used to systematically correct for these interferences. For example, the signal from O^+ at *m/z* 16 arising from H_2O ionization and fragmentation can be estimated very reproducibly as a constant fraction (~4%, to be measured in each instrument) of the signal from H_2O^+ at *m/z* 18. After subtracting this and other small interferences, the signal due to NH_2^+ at *m/z* 16 can be obtained. Figure 8 shows the application of this technique to an

TABLE 1. Main ion fragments used to identify inorganic and organic aerosol species in AMS spectra. The fragments that are most useful in identifying these species are highlighted in bold text.

Group	Molecule/Species		Ion Fragments	Mass Fragments
Water	H_2O	$\xrightarrow{e^-}$	$\mathbf{H_2O^+}$, HO^+, O^+	**18**, 17, 16
Ammonium	NH_3	$\xrightarrow{e^-}$	NH_3^+, $\mathbf{NH_2^+}$, NH^+	17, **16**, 15
Nitrate	NO_3	$\xrightarrow{e^-}$	HNO_3^+, $\mathbf{NO_2^+}$, $\mathbf{NO^+}$	63, **46**, **30**
Sulfate	H_2SO_4	$\xrightarrow{e^-}$	$H_2SO_4^+$, HSO_3^+, SO_3^+ $\mathbf{SO_2^+}$, $\mathbf{SO^+}$	98, 81, 80 **64**, **48**
Organic *(Oxygenated)*	$C_nH_mO_y$	$\xrightarrow{e^-}$	H_2O^+, CO^+, $\mathbf{CO_2^+}$ $\mathbf{H_3C_2O^+}$, HCO_2^+, $C_nH_m^+$	18, 28, **44** **43**, 45, ...
Organic *(hydrocarbon)*	C_nH_m	$\xrightarrow{e^-}$	$C_nH_m^+$	27,29,**41**, **43,55,57**,69,71...

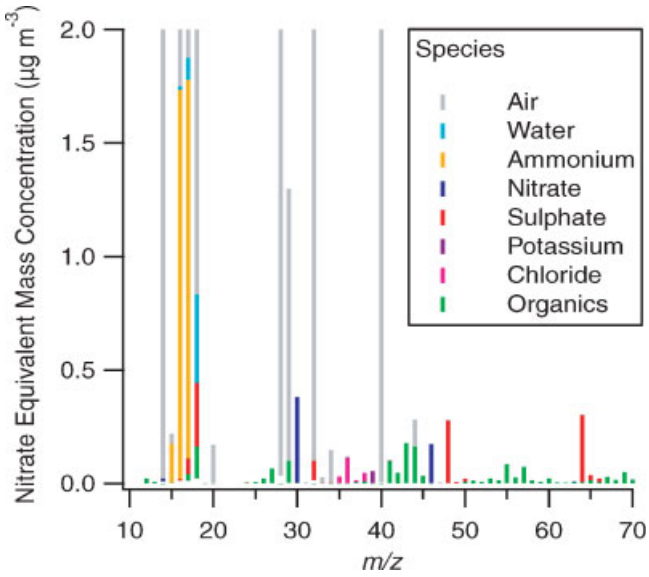

FIGURE 8. Application of the method developed by Allan et al. (2004b) to obtain aerosol chemical composition from ambient AMS mass spectra. The large air peaks have been allowed to go off scale in this figure to focus on the signal from aerosol components. The mass concentrations shown on the Y axis are calculated from the observed ion rate using Equation 4 (section III.B.1 of text) with all species dependent RIE_s set to 1. (Reproduced from Allan et al., 2004b, Copyright 2004, with permission from Elsevier.)

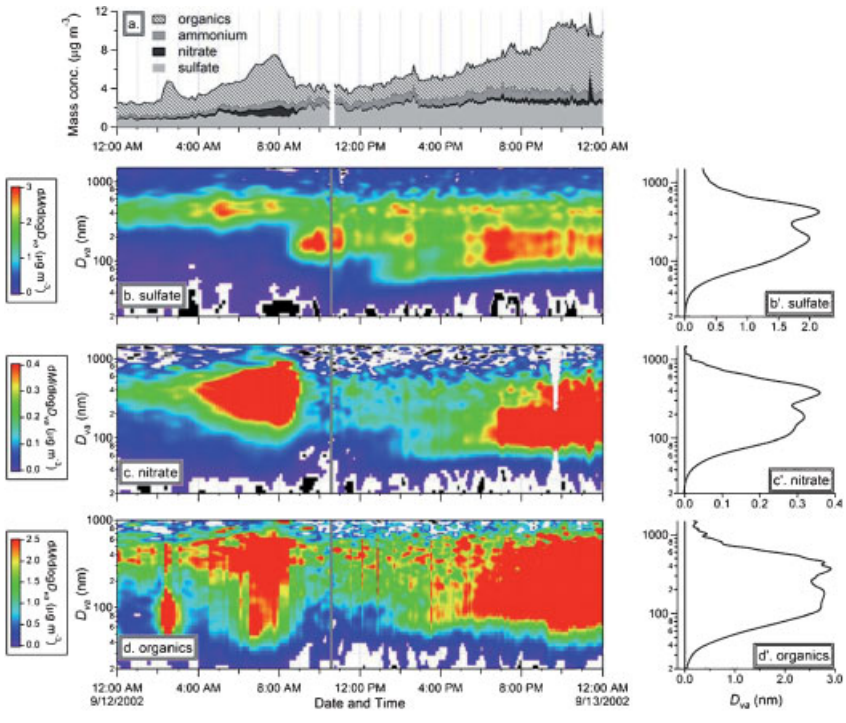

FIGURE 24. An example of the type of multi-dimensional information that can be obtained with the AMS. Panel a shows time trends in the mass concentrations of ambient aerosol species observed during the Pittsburgh Air Quality Study in 2002 (modified from Zhang et al., 2005b). Panels b–d show the corresponding time evolution of sulfate, nitrate, and organic mass-weighted size distributions. Measurements were averaged over 10-min timescales. Averages of the observed speciated size distributions over the entire time trend are shown in panels b′–d′.

ambient MS. The partial mass spectra calculated for the different species are shown in different colors. As described in the next section, the total mass of any species can be determined by summing up the measured signal at all *m/z*s in its partial MS.

In Figure 8, the air peaks, at *m/z* 18 (H_2O^+), 28 (N_2^+), 32 (O_2^+), 40 (Ar^+), and other ions, correspond to signal from gas phase species detected along with the particle signal. The fact that these signals are large even after the 10^7 reduction of gas-phase signal (relative to the particles) underscores the fact that the ambient concentrations of major air species are much larger than those of particles (e.g., $\approx$950 g m^{-3} of N_2 compared to total aerosol concentrations of 1–50 μg m^{-3}). It is important to note that although the air signals are offscale in Figure 8, the dynamic range in the AMS is large enough that these signals are quantified during routine measurements. In fact, as shown in the next section, the air signals provide a continuous internal standard that is used to gauge the general performance of the MS detector and to quantitatively correct the particle signals for changes in MS detection performance or sensitivity (Allan et al., 2003b).

B. Quantification of Chemically Speciated Aerosol Mass

The AMS uses a detection scheme that is capable of quantitative detection. In this section, we show how this capability extends to the measurement of ambient aerosol particles, which are a complex mixture of chemical species. The methodology used to convert observed mass spectra into mass concentrations of individual chemical species is described. Processes that need to be accounted for in the mass concentration calculations, such as ionization efficiency and particle collection efficiency (CE), are also discussed. Finally, the ability of the AMS to provide accurate speciated aerosol mass during ambient aerosol measurements is assessed by intercomparison with collocated quantitative aerosol instrumentation.

1. Ionization Efficiency

The basic theory for converting a detected ion rate (*I*, in counts per second or Hz) reported at a specific mass to charge ratio (*m/z*), to a mass concentration (*C*, in μg m^{-3}) was presented by Jimenez et al. (2003b) as follows:

$$C = \frac{10^{12}}{\mathrm{IE}} \frac{1}{Q} \frac{\mathrm{MW}}{N_A} \cdot I \tag{1}$$

where MW is the molecular weight of the species in question in g mol^{-1}, N_A is Avogadro's number, Q is the volumetric sample flow rate into the instrument in cm^3 s^{-1}, IE is the ionization efficiency, a dimensionless quantity equaling the number of ions detected per molecule of the parent species, and the 10^{12} factor is needed for unit conversion. The quantity IE is species specific and reflects not only the probability of a parent molecule becoming ionized, but also the possibly *m/z*-dependent transmission efficiency of the mass spectrometer and the detection efficiency of the electron multiplier. The *m/z* dependence of transmission efficiency is not significant for the components used by the Q-AMS.

Following from Equation 1, the total mass concentration of a particular species (s) that produces multiple ions at multiple *m/z* upon EI, can be expressed as:

$$C_s = \frac{10^{12}\mathrm{MW}_s}{\mathrm{IE}_s Q N_A} \sum_{\text{all } i} I_{s,i} \tag{2}$$

Here the summation is over all fragment ion rates in the partial MS of the species. The procedure for determining partial mass spectra of species has been outlined in the previous section.

In Equation 2, the species-dependent properties that are not always known when measuring complex aerosol particles are MW_s and IE_s. While explicit calibrations for IE_s can be performed for a small number of species, individual calibrations are not practical for the hundreds of known molecular organic species in ambient aerosol. Jimenez et al. (2003b) have suggested an empirical means of determining IE/MW that is based on the properties of EI ionization, as shown in Figure 9. The data in this figure indicate that the ionization cross section of a molecule, σ, is linearly related to the number of electrons, N_e, it contains. Moreover, since molecules with similar chemical structure and functionality have similar EI cross section-to-electron ratios, only three distinct proportionality constants, corresponding to inorganic, hydrocarbon, and oxygenated organic species, are needed to estimate these ratios for a range of molecules. To a first approximation, IE in the AMS is proportional to σ, and MW of a molecule is proportional to N_e, for molecules containing the small atoms typical of NR aerosol species (H, C, N, O, S). Thus, Jimenez et al. (2003b) proposed that a plot of IE versus MW for the AMS should contain simple linear relationships similar to those in Figure 9.

AMS studies of lab-generated particles do show a linear relationship between IE and MW. These studies show two distinct linear relationships for organic and inorganic species. These results suggest that the $\mathrm{IE}_s/\mathrm{MW}_s$ of any organic or inorganic molecule can be expressed as follows:

$$\frac{\mathrm{IE}_s}{\mathrm{MW}_s} = \mathrm{RIE}_s \frac{\mathrm{IE}_{\mathrm{NO_3}}}{\mathrm{MW}_{\mathrm{NO_3}}} \tag{3}$$

In Equation 3, the reference IE/MW is obtained from a well-characterized calibrant species like nitrate. RIE_s is defined as the relative ionization efficiency of species *s* relative to nitrate (Alfarra et al., 2004). Substitution of Equation 3 into Equation 2 results in

$$C_s = \frac{10^{12}\mathrm{MW}_{\mathrm{NO_3}}}{\mathrm{RIE}_s \mathrm{IE}_{\mathrm{NO_3}} Q N_A} \sum_{\text{all } i} I_{s,i} \tag{4}$$

The power of this method is that particle signals at any *m/z* can be directly interpreted as an equivalent aerosol mass concentration based on a single nitrate calibration. One only needs some chemical classification of the ion fragmentation pattern to choose the appropriate RIE_s. If the RIE_s factor is omitted from Equation 4, the result is referred to as the nitrate-equivalent concentration of the species (Jimenez et al., 2003b).

In practice, only *m/z* 30 and *m/z* 46 are used in the nitrate calibration (see below) and therefore, all RIE_s are stated relative to the sum of these ions rather than with respect to the total ion intensity from nitrate. The RIE values usually used in AMS

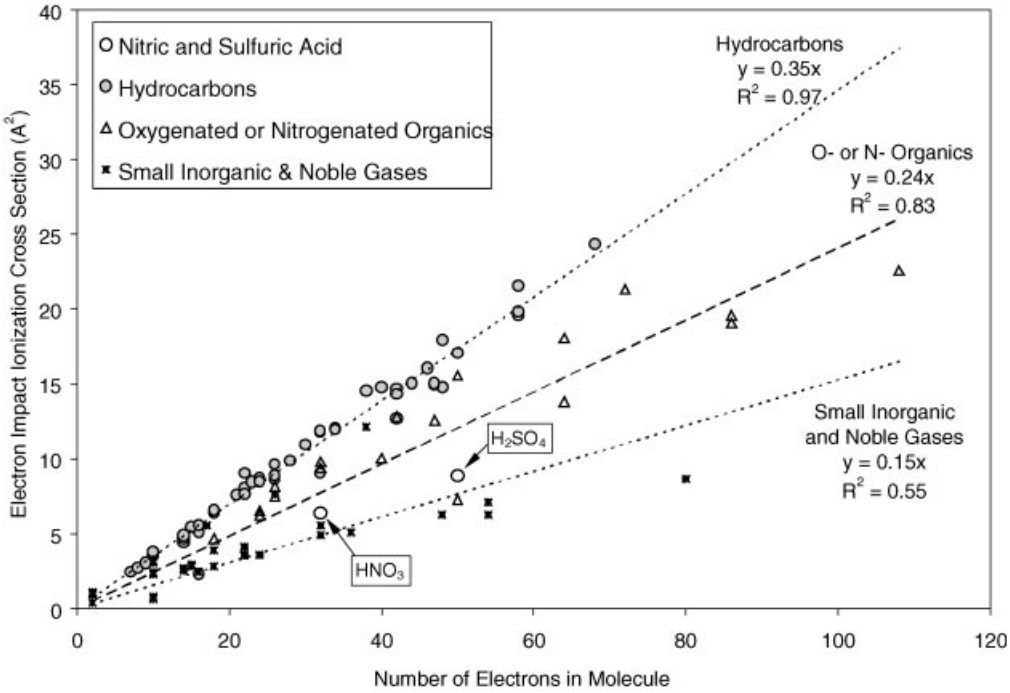

FIGURE 9. Electron impact ionization cross sections of small molecules as a function of the number of electrons they contain. (Reproduced/modified by permission of American Geophysical Union from Jimenez et al., 2003b. Copyright 2003 American Geophysical Union.)

ambient concentration calculations are 1.4 for organic molecules and 1.1, 1.15, and 3.5–6 for NO_3, SO_4, and NH_4 moieties, respectively. These values are based on many calibrations of laboratory-generated aerosols. The RIE_s for NO_3 is greater than 1 to account for the fact that although only *m/z* 30 and 46 are used to track NO_3 ion signal during calibrations, NO_3 signals at other ion fragments are included in the fragmentation table that is used for calculating NO_3 concentrations (Hogrefe et al., 2004; Allan et al., 2004b). The larger and more variable values for RIE_{NH4} are thought to be due to the increased response of the electron multiplier detector to ions of low *m/z*, and/or to more efficient extraction of these ions from the AMS ionizer, rather than to a truly more efficient ionization of this species by EI, which would not fit the framework of Figure 9.

Nitrate is chosen as the primary mass calibration species for the AMS because it is a common aerosol constituent that produces most of its signal at only two *m/z*s (30 and 46) and it is volatile enough that it evaporates with close to 100% efficiency in a few microseconds upon contact with the AMS vaporizer, leaving no significant residue in the mass spectrometer background. The experimental methodology for calibration of IE_{NO_3} has been provided in detail in other manuscripts (Jayne et al., 2000; Allan et al., 2003b; Zhang et al., 2005b). Briefly, ammonium nitrate (AN) particles are generated from an aqueous AN solution, dried size-selected with a differential mobility analyzer (DMA), and then introduced into the AMS. The number of nitrate ions measured at *m/z* 30 and *m/z* 46 per single particle vaporization event is measured in PToF mode. IE_{NO_3} is obtained by normalizing this value to the number of AN molecules estimated to exist in each size-selected AN particle. The latter estimation is based on the known size of the calibration particle, the bulk AN density, and the AN Jayne shape factor of 0.8 which is experimentally determined by comparing the mobility and vacuum aerodynamic diameters measured for the size-selected AN particles (Jayne et al., 2000) (see DeCarlo et al., 2004, for the interpretation of this shape factor).

It is important to note that evaporative losses of AN (Zelenyuk et al., 2006a) could cause significant uncertainties in the known size of the AN calibration particles. These losses could occur both as the size-selected particles travel from the DMA to the AMS and immediately after they are sampled into the AMS. Since the fractional loss of AN due to evaporation will not be constant across all calibration particle sizes, this problem can be diagnosed by the observation of size dependent trends in the calibrated IE_{NO_3} values and in the AN Jayne shape factor. No such trends have been observed within the experimental uncertainties of either of these measurements (Jayne et al., 2000). This suggests that AN evaporation is not significant under the conditions that are typically used for these IE_{NO_3} calibration measurements. The IE_{NO_3} values measured with the Q-AMS are usually on the order of 10^{-6}, in other words, approximately 1 out of every 1 million nitrate molecules is ionized and detected. Once IE_{NO_3} is known, IE_s/MW_s can be estimated for any species according to Equation 3.

The conversion of AMS mass spectral signal to ion rate (I_s, in ions s^{-1} or Hz) depends critically on an accurate knowledge of the electron multiplier gain (typically $\sim 2 \times 10^6$). Typically, multiplier gain calibrations are performed, with the help of the

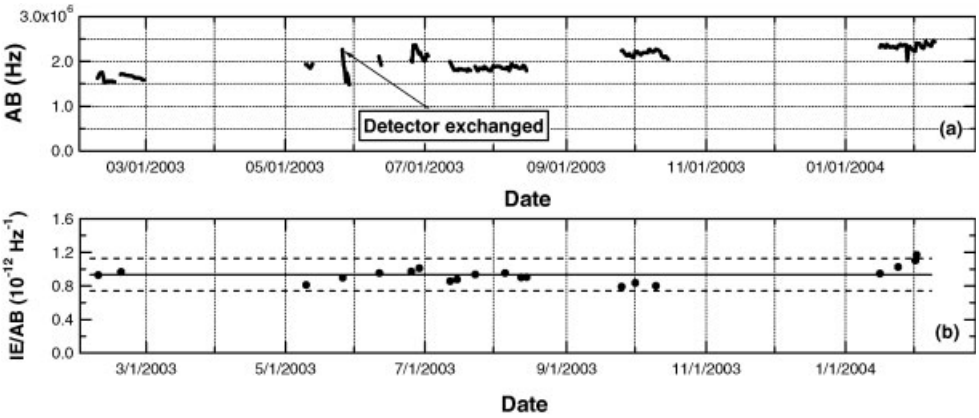

FIGURE 10. Long-term variability in observed (**a**) AB signal and (**b**) $IENO_3$/AB ratios during ambient AMS measurements in Tokyo, Japan. The average and 2σ variability in the observed $IENO_3$/AB are shown as solid and dashed lines, respectively. (Aerosol Science & Technology: Takegawa et al.: Characterization of an aerodyne aerosol mass spectrometer (AMS): Intercomparison with other aerosol Instruments. (39):760-770. Copyright 2005. Mount Laurel, NJ, Reprinted with Permission.)

AMS data acquisition software, every few days during a field campaign with continuous instrument operation, depending on the rate of multiplier degradation. The largest AMS signals are due to airbeam (AB) gas phase nitrogen and oxygen species at *m/z* 28 and 32. If the air flow into the instrument is constant, fluctuations in the AB signal intensities are due to changes in electron multiplier gain or ionization and transmission efficiencies. The changes in the AB signals provide a convenient way to obtain a continuous correction factor that is used to remove the influence of these instrumental drifts on the AMS ion signals (Allan et al., 2003b). Figure 10 shows an example of the stability of AB and IE_{NO_3} measurements over a period of almost 1 year during an ambient measurement campaign at a fixed site in Tokyo, Japan (Takegawa et al., 2005). The top panel shows the AB (from *m/z* 28) signal with some sensitivity and gain-related fluctuations as a function of time. In the bottom panel, the IE_{NO_3} calibrations measured during the campaign are normalized to the AB signals obtained at the time of calibration. Normalizing the various IE_{NO_3} measurements to simultaneously measured AB removes scatter in the results due to (a) variations of instrument sensitivity that should be captured equally by both figures of merit, and (b) experimental uncertainties in multiplier gain calibrations, since the multiplier gain is used in the calculation of both numbers and it cancels out in the ratio. The IE/AB measurements are within 25% of the average for the whole year, and within 10% for each of the weeks-long intensive measurement periods. This shows that the AMS instrument performance can be stable over long periods of time and that continuous

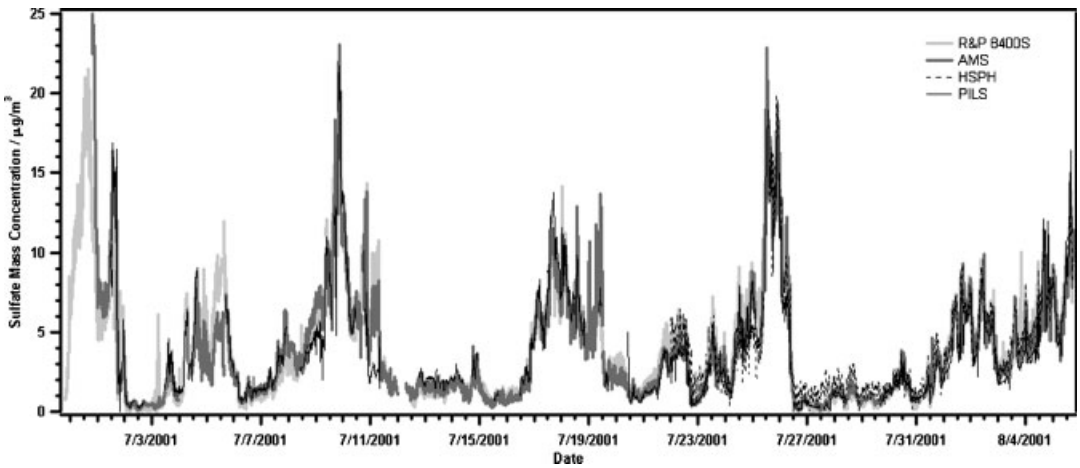

FIGURE 11. Aerosol sulfate mass concentrations measured with an AMS and three other semi-continuous sulfate measurements during the PMTACS-NY 2001 campaign. The AMS measurements have been scaled to the PILS data by multiplying with a single factor of 2.41. This factor is needed to account for apparent AMS collection efficiency losses. See the accompanying text of the manuscript for more details on AMS collection efficiency. Information about the PILS, R&P 8400S, and HSPH measurements can be found in Drewnick et al. (2003) and references therein. (Reprinted from Drewnick et al. (2003). Copyright 2003, with permission from Elsevier.)

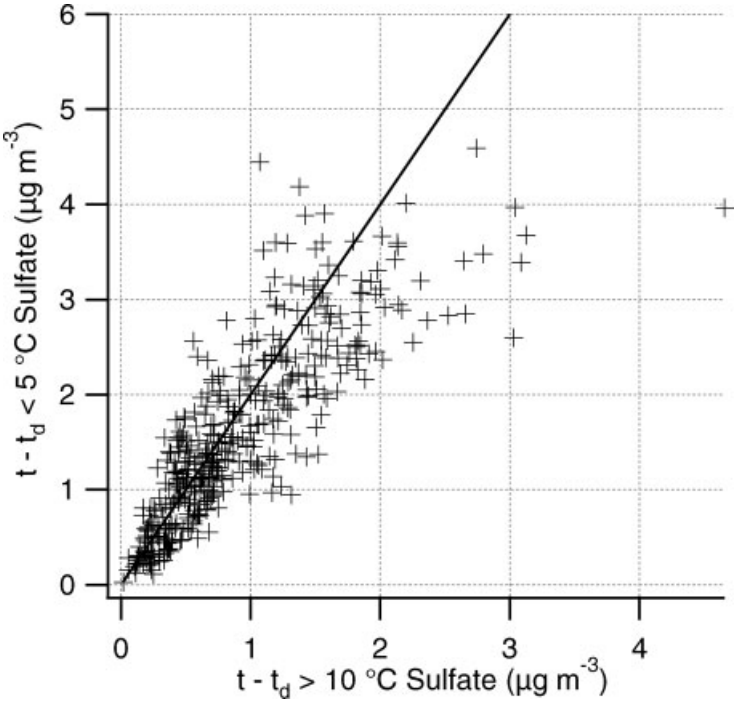

FIGURE 12. Illustration of the dependence of measured aerosol sulfate mass on AMS inlet temperature. The symbols t and t_d in the figure refer to the AMS inlet temperature and the ambient dewpoint, respectively. The data is binned according to points that correspond to $t - t_d < 5^\circ$C and $t - t_d > 10^\circ$C. The scatter plot of the data obtained in these two categories shows enhanced measurement of sulfate mass when the AMS inlet temperature is close to the dewpoint. (Reproduced/modified by permission of American Geophysical Union from Allan et al., 2004a. Copyright [2004] American Geophysical Union.)

sampling of polluted air does not degrade the performance of the instrument significantly.

2. *Collection Efficiency*

Figure 11 shows a comparison of sulfate mass concentrations measured with an AMS and with three other semi-continuous instruments during a field campaign in New York City (Drewnick et al., 2003). This figure shows that the AMS mass concentrations tracked the other measurements very well over an order of magnitude in concentration. The agreement in absolute mass loading was obtained after multiplying by a single factor of 2.41 to uniformly scale the AMS sulfate measurements to the PILS-IC (Particle-into-liquid sampler with ion chromatography, Weber et al., 2001) measurements. These observations indicate that while the response of the AMS to ambient sulfate aerosol mass was linear, the apparent CE of ambient sulfate particles was less than 100%.

The need to apply a constant CE factor to match AMS sulfate measurements with other sulfate measurements has been observed in many other field campaigns (Alfarra, 2004; Drewnick et al., 2004a; Hogrefe et al., 2004; Takegawa et al., 2005; Zhang et al., 2005b). In most cases, the CE factors that are used are ~ 0.5 with variation that likely arises from dependence on location, season, and type of ambient aerosol being sampled. In all of these situations, once the CE factor was applied, the quantitative agreement between the compared instruments was on the order of 25% or better, except in cases where the size distribution continued past the transmission limit of the AMS (see below). Thus, the equation for calculating mass loadings for various species is modified from Equation 4 to include CE as follows (Alfarra et al., 2004):

$$C_s = \frac{10^{12}}{\mathrm{CE}_s} \frac{\mathrm{MW}_{\mathrm{NO_3}}}{\mathrm{RIE}_s \mathrm{IE}_{\mathrm{NO_3}} Q N_A} \sum_{\mathrm{all}i} I_{s,i} \qquad (5)$$

In situations where CE_s factors cannot be explicitly determined by scaling with respect to collocated measurements like the PILS-IC, a default CE factor of 0.5 is used for sulfate. Chemically speciated size distributions obtained during most field campaigns suggest that sulfate is generally internally mixed with other inorganic species and oxidized organic species. Thus, the same CE is used for sulfate, nitrate, and organic species since they will all experience the same collection efficiency losses (Alfarra et al., 2004). In cases where externally mixed aerosols are observed, however, the use of size and composition-dependent CE values needs to be investigated (Weimer et al., 2006).

Allan et al. (2004a) used a temperature controlled sampling inlet to investigate the effect of relative humidity on CE. In this experiment, the inlet temperature (T) was ramped up and down on a 40-min cycle with the minimum temperature corresponding to the ambient dew point (T_d) and the maximum temperature being approximately 20°C greater than T_d. Since drastic changes in

ambient ammonium sulfate concentrations were not expected on the time scale of individual temperature cycles, any large changes in measured concentrations could be linked to changes in CE due to particle deliquescence or drying.

Figure 12 shows a plot of the data from this experiment after it has been sorted into two groups according to whether $T - T_d$ is less than 5°C or greater than 10°C. When $T - T_d < 5$°C, it is expected that the particles would deliquesce and become more spherical due to water uptake, whereas when $T - T_d > 10$°C, the ammonium sulfate is likely solid with a slightly non-spherical shape. From the figure, it is clear that the sulfate concentration detected by the AMS approximately doubled when the inlet temperature approached the dewpoint temperature. Interestingly, the ratio of dry-to-wet sulfate concentrations is very close to the CE factors used in field campaigns. There is significant scatter in Figure 12, part of which will be due to real variations in the particle concentration. The results shown in Figure 12 are consistent with recent laboratory studies by Matthew et al. (manuscript in preparation) which show that the CE of sulfate from $(NH_4)_2SO_4$ is dependent on the phase of the sampled particles.

Possible explanations for the observations of Allan et al. (2004a) are (a) shape-related collection losses (E_s) at the vaporizer from inefficient focusing of the non-spherical solid sulfate particles and (b) collection losses at the vaporizer due to bouncing (E_b) of less ''sticky'' solid sulfate particles before they are completely vaporized (Huffman et al., 2005). Here, E_s and E_b account for detection efficiency losses in particle mass *after* particles are transmitted into the AMS by the aerodynamic lens. Huffman et al. (2005) have also introduced another loss factor, E_L, that takes into account particle losses in the aerodynamic inlet as a function of particle diameter. This factor is particularly important in cases where the PM_1 AMS mass is compared with mass measured by an instrument that has a different inlet transmission. For example, undetected mass between PM_1 and $PM_{2.5}$ could introduce significant uncertainty in the CE derived from an intercomparison between the AMS and a $PM_{2.5}$ instrument (Drewnick et al., 2003, 2004a; Zhang et al., 2005b).

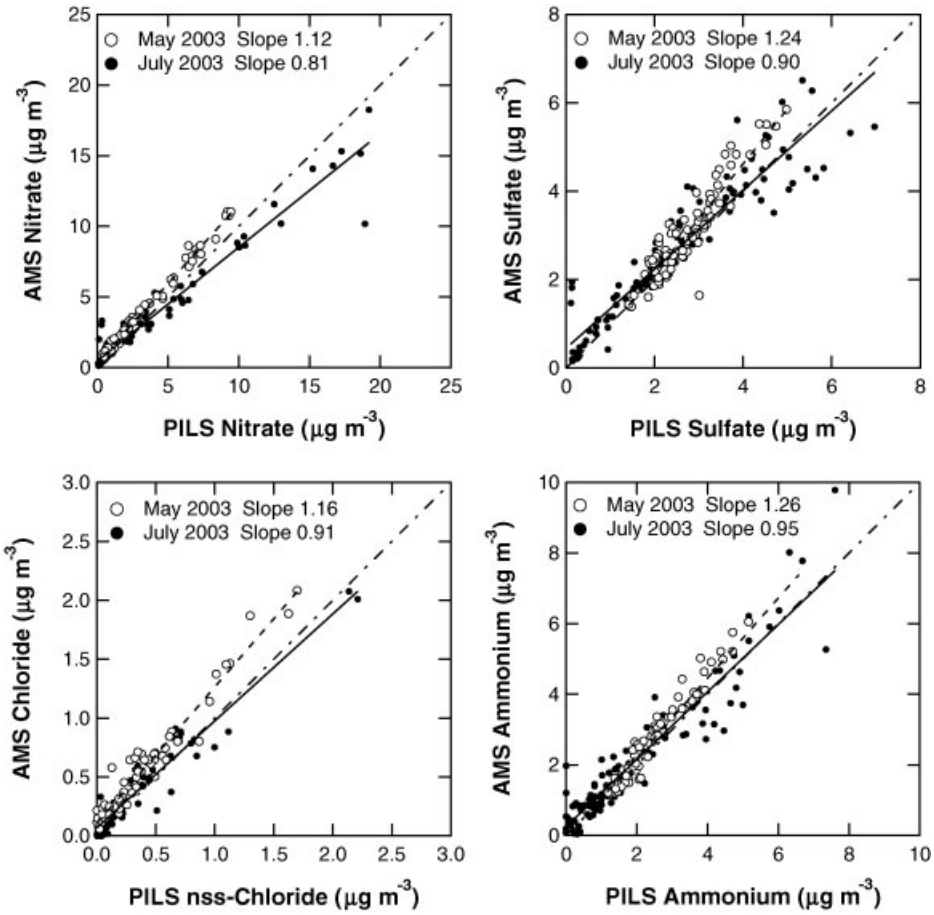

FIGURE 13. Scatter plots of the aerosol nitrate, sulfate, chloride, and ammonium mass concentrations measured with both an AMS and a co-located PILS instrument during ambient measurements in Tokyo, Japan. (Aerosol Science & Technology: Takegawa et al.: Characterization of an aerodyne aerosol mass spectrometer (AMS): Intercomparison with other aerosol instruments. (39):760–770. Copyright 2005. Mount Laurel, NJ, Reprinted with Permission.) The AMS measurements have been scaled to the PILS data by multiplying with a single factor of 2. This factor is needed to account for the apparent AMS collection efficiency losses. See the accompanying text of the manuscript for more details on AMS collection efficiency.

When all the individual detection losses are taken together, the collection efficiency of the AMS can be expressed as $CE = E_L * E_s * E_b$. As discussed above, lab and field-based BWP measurements indicate that the imperfect focusing of ambient non-spherical particles does not play a significant role in the AMS (Huffman et al., 2005). In fact, the current state of understanding, based on a manuscript in preparation by Onasch et al., is that detection losses in the AMS are primarily due to particle bounce off the vaporizer. The effect of vaporizer geometry on the occurrence of particle bounce has been reported previously in the literature (Sinha et al., 1982).

3. *Instrument Intercomparisons*

Figure 11 presented one of the first successful intercomparisons of the AMS with collocated sulfate instruments (Drewnick et al., 2003). Figure 13 summarizes the results of another intercomparison, this time of AMS sulfate, nitrate, ammonium, and non-seasalt (NSS) chloride measurements, with PILS-IC measurements of the same species during two ambient measurement campaigns in Tokyo, Japan (Takegawa et al., 2005). In this case, the default CE values of 0.5 were used. The scatter plots indicate a high degree of correlation between the AMS and PILS-IC measurements. The data shown were obtained during two separate sampling periods in May and July of 2003, and much of the scatter in the overall plot is due to systematic differences between the two sampling periods, whose causes have not been identified. Even with this scatter, these AMS and PILS measurements agree with each other to within 26% for nitrate, sulfate, NSS chloride, and ammonium. Note that NSS chloride is likely in the form of NH_4Cl, which is NR and is detected with the AMS, while sea salt-chloride is not detected at typical AMS vaporizer temperatures.

The performance of the AMS in measuring oranic mass (OM) is not as straightforward to assess as in the case of inorganic species because most other organic semi-continuous and filter measurements use detection schemes that measure the mass of organic carbon (OC) instead of OM. OC measures only the mass due to C contained in organic material, whereas OM includes mass contributions from not only C, but also other abundant organic constituents such as H, O, N, and S. Thus, a range of OM/OC ratios is possible depending on the exact chemical composition of the organic aerosol. Figure 14 shows a comparison between the organic aerosol mass detected by the AMS and the mass of OC detected by a semi-continuous thermal-optical EC/OC instrument (Sunset Labs) during the same ambient measurement campaign in Tokyo (Takegawa et al., 2005). The data is divided into two sampling time periods (July and October) and the AMS OM is calculated with a CE of 0.5 for both. Both plots show good correlation between the instruments, and they indicate OM/OC ratios of 1.79 and 1.61 for July and September data, respectively. Turpin and Lim estimate that the OM/OC ratio for urban aerosols is 1.6 ± 0.2, whereas the ratio for aged organic aerosol is 2.1 ± 0.2 (Turpin & Lim, 2001). The OM/OC ratios observed in Japan are consistent with these ratios. Similar OM/OC ratios have been observed in other field measurement campaigns indicating that AMS OM loadings are consistent with other measures of organic aerosol mass (Topping et al., 2004; Zhang et al., 2005b). The OM/OC ratio can also be estimated directly from the AMS spectra of organic chemical classes (Zhang et al., 2005c), as described below.

These intercomparison results, when taken together with those obtained in other campaigns (Drewnick et al., 2003, 2004a; Hogrefe et al., 2004; Zhang et al., 2005b), indicate that despite the uncertainties associated with RIE and CE factors for different species, in practice the AMS PM_1 mass concentrations for inorganic and organic ambient aerosol species are reproducibly

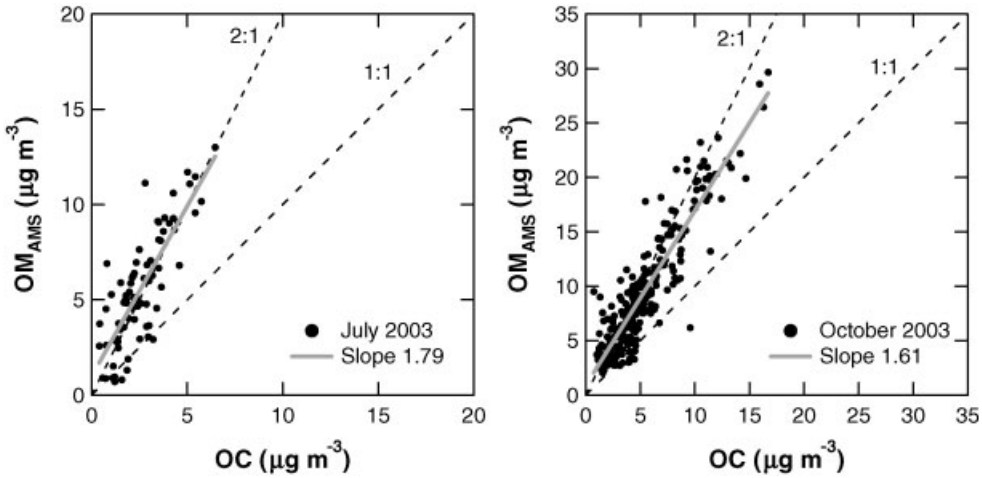

FIGURE 14. Scatter plots of organic mass (OM) measured by the AMS and organic carbon (OC) measured by a collocated semi-continuous thermal-optical EC/OC instrument during ambient measurements in Tokyo, Japan. (Aerosol Science & Technology: Takegawa et al.: Characterization of an aerodyne aerosol mass spectrometer (AMS): Intercomparison with other aerosol Instruments. (39):760–770. Copyright 2005. Mount Laurel, NJ, Reprinted with Permission.) The AMS measurements have been scaled by multiplying with a single factor of 2 which is needed to account for the apparent losses in AMS collection efficiency. See the accompanying text of the manuscript for more details on AMS collection efficiency.

accurate to approximately ±25%. The reported detection limits (3σ in 10 min) for various species reported during three different Q-AMS field campaigns, estimated while sampling particle-free ambient air after a HEPA filter, are in the ranges 0.01–0.05 μg m^{-3} for nitrate, 0.02–0.09 for sulfate, 0.11–0.49 for ammonium, 0.04–0.05 for chloride, and 0.15–0.73 for organics (Takegawa et al., 2005; Zhang et al., 2005b; Salcedo et al., 2006).

C. Aerosol Size Distributions

The particle velocities determined in PToF measurements can be converted to particle vacuum aerodynamic diameters (d_{va}, see below) using the relationships between velocity and size that are determined from calibrations performed with polystyrene latex sphere sizing standards (Jayne et al., 2000). Note that since the AMS signal is proportional to particle mass, the resulting ensemble size distributions are mass-weighted ($dM/d\log d_{va}$).

Particle size distributions are obtained at individual pre-selected ion fragments and therefore, provide chemically speciated size information (Jayne et al., 2000; Allan et al., 2003b; Jimenez et al., 2003b). Figure 15 shows the size distributions (averaged over the particle ensemble and over the entire sampling time period) for ambient aerosol in Pittsburgh (Zhang et al., 2005b) containing sulfate (*m/z* 48, 64), nitrate (*m/z* 30), oxygenated organics (*m/z* 44), and hydrocarbon-like organics (*m/z* 57). The area under the curve for each fragment corresponds to the absolute contribution it makes towards the total mass of its parent species. A comparison of the size distributions obtained for the different species provides insight into the possible mixing state of the particles. For example, the similar distributions of nitrate, sulfate, and oxygenated species suggest that these species are internally mixed in the same particles. The distinctly different bimodal size distribution of the hydrocarbon-like organic species, on the other hand, suggests that some of the smaller particles that contain hydrocarbon-like organic species do not contain significant SO_4, NO_3, or oxygenated organic species.

The aerodynamic diameter is classically defined as the diameter of a sphere of standard density (1 g cm^{-3}) that settles with the same terminal velocity as the particle of interest (Hinds, 1982). It can also be defined as the diameter of a sphere of standard density that would experience the same change in velocity following a given perturbation to the carrier gas velocity as the particle of interest. The aerodynamic diameter measured for a given particle depends on the flow regime under which the measurement is performed. Size-dependent particle velocities are created at the exit of the aerodynamic lens at a pressure of ~100 Pa which corresponds to free molecular regime flow conditions for particles in the submicron size range. For this reason, the aerodynamic diameter measured by the AMS (and other instruments that use Liu-type aerodynamic lenses) is referred to as a vacuum aerodynamic diameter (d_{va}) (Jimenez et al., 2003a; DeCarlo et al., 2004). This is in contrast to the classical aerodynamic diameter (d_{ca}) measured by instruments that operate in the continuum flow regime, such as the aerodynamic particle sizer (APS) (Jimenez et al., 2003a; DeCarlo et al., 2004). DeCarlo et al. (2004) present a detailed review of the physical basis of the dependence of d_{va} on particle properties, and of its relationship to other diameter measurements. Briefly, for a sphere, d_{va} is equal to its physical diameter (d_p) multiplied by its density. For a non-spherical particle, d_{va} is defined in terms of the volume equivalent diameter, d_{ve}, as shown below:

$$d_{va} = \frac{\rho_p}{\rho_0}\frac{d_{ve}}{\chi_v} \tag{6}$$

where d_{ve} is the d_p of the spherical particle that would result if the non-spherical particle of interest were melted into a sphere, while preserving any internal void spaces (see DeCarlo et al. for a treatment of particles with internal void spaces). Particle density and standard density (1 g cm^{-3}) are denoted as ρ_p and ρ_0, respectively. The dynamic shape factor of the particle in the free molecular regime, χ_v, is the ratio of the drag experienced by the real non-spherical particle relative to the drag experienced by a spherical particle with identical d_{ve}. For a sphere, χ_v is equal to one and for non-spherical particles, $\chi_v > 1$. Equation 6 means that the measured d_{va} for a particle of given d_{ve} depends not only on physical size, but also on the density and shape of the particle as well.

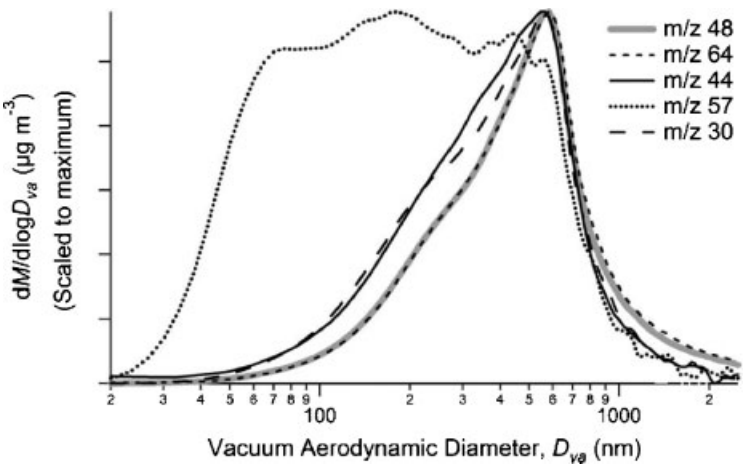

FIGURE 15. An example of mass weighted chemically speciated size distributions obtained with the AMS during ambient measurements by Zhang et al. (2005b), modified.

D. Aerosol Morphology and Density

Particle morphology and density can be characterized by combining d_{va} measurements with other measures of particle size that have different dependences on the fundamental particle properties, such as the mobility diameter (d_m) (Jimenez et al., 2003a; DeCarlo et al., 2004). The mobility diameter, which is usually measured with a DMA, is the diameter of a sphere possessing a single unit of charge that has the same migration velocity in a constant electric field as the particle of interest when it is singly charged with the same electrical polarity. It can be shown (DeCarlo et al., 2004) that d_m and d_{ve} are related as follows:

$$\frac{d_m}{C_c(d_m)} = \frac{d_{ve}\chi_t}{C_c(d_{ve})} \quad (7)$$

where $C_c(d)$ is the Cunningham slip correction factor that is needed to account for changes in drag experienced by the particle outside of the continuum flow regime. χ_t is the dynamic shape factor under the transition regime flow conditions of the DMA.

Figure 16 illustrates the different effects of shape on measurements of d_{va} and d_m. The top panel shows the trajectories of two spherical and one non-spherical particle as they travel through the DMA (DeCarlo et al., 2004). The non-spherical particle has the same d_{ve} as the small sphere. However, the greater drag it experiences due to its non-sphericity results in a trajectory through the DMA that is the same as that of the larger sphere. Thus, non-spherical particles generally have an apparent measured d_m that is greater than their d_{ve}. Zelenyuk et al. 2006b) have shown that particle alignment effects in the DMA can also influence the determination of d_m. The second panel of

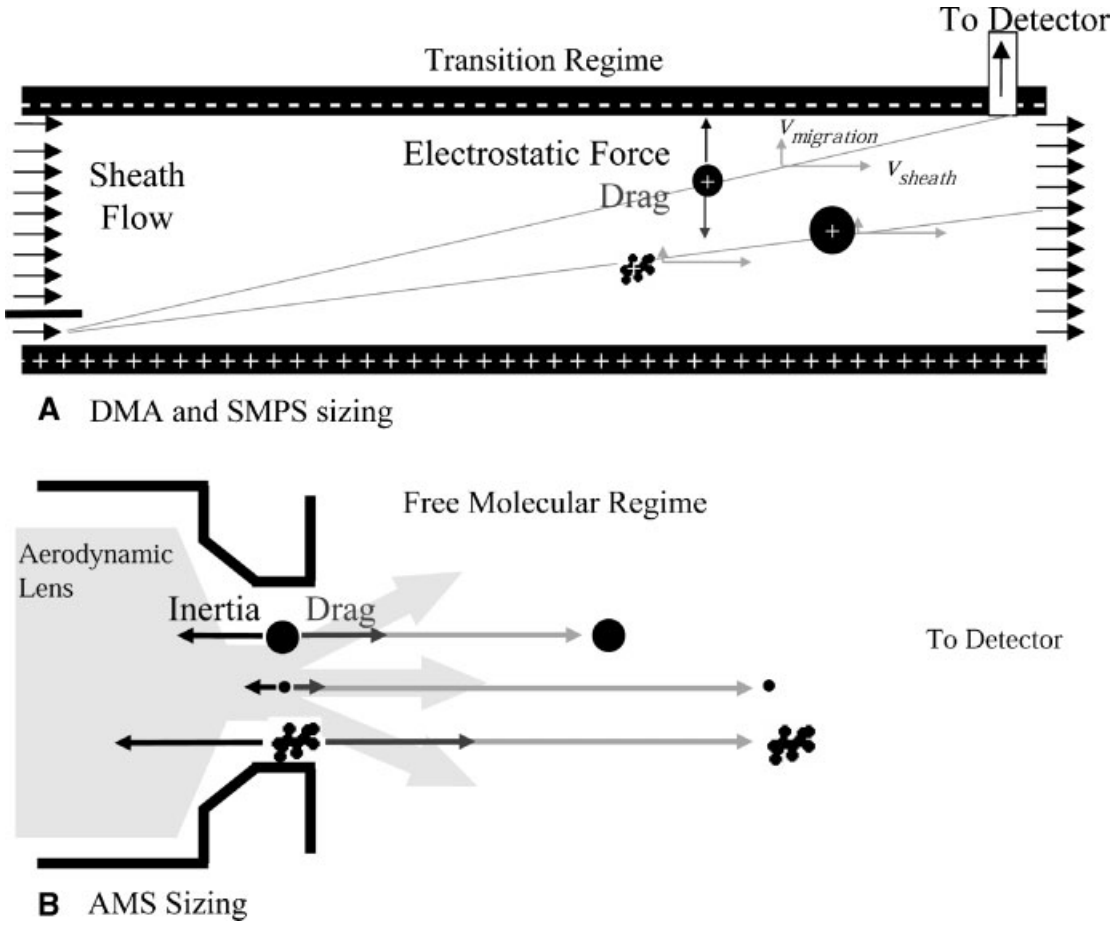

FIGURE 16. Schematic of the effect of particle shape on the particle size measured by different sizing techniques. Panel A shows particle trajectories in DMA (Differential Mobility Analyzer) and SMPS (Scanning Mobility Particle Sizer) instruments and Panel B shows particle velocities measured by the AMS. In each panel, three particles (two spherical and one irregularly shaped) of standard density are shown. The irregular particle in Panel A has the same mass as the small sphere, but it has the same trajectory and electrical mobility in a DMA as the larger spherical particle. On the other hand, in Panel B, the irregular particle has the same mass as the larger sphere but it acquires the same velocity as the smaller sphere. (Aerosol Science & Technology: DeCarlo et al.: Particle morphology and density characterization by combined mobility and aerodynamic diameter measurements. Part 1: Theory. (38): 1185–1205. Copyright 2004. Mount Laurel, NJ, reprinted with permission.)

Figure 16 shows three particles of identical material density as they travel through the AMS. In this case, the non-spherical particle has the same d_{ve} as the larger sphere; however, in the gas expansion at the exit of the lens, greater drag results in more force in the forward direction and a faster particle velocity. Thus, the AMS measures a d_{va} that is smaller than its d_{ve}.

AMS and DMA sizing measurements of the same particles can be combined together to obtain particle ''effective'' densities which are a function of both the true density and the shape of the particle (Jimenez et al., 2003a; DeCarlo et al., 2004).

$$\rho_{\text{eff}} = \frac{d_{\text{va}}}{d_{\text{m}}}\rho_0 \tag{8}$$

For a spherical particle, ρ_{eff} is the particle density, while for a non-spherical particle, $\rho_{\text{eff}} < \rho_p$. For a more detailed discussion of ρ_{eff} and a comparison to other effective density definitions in the literature, see DeCarlo et al. (2004).

An estimate of particle mass can be derived solely from the d_{va} and d_m measurements. This provides a method of determining particle mass from AMS measurements even when part of the particle is composed of refractory materials such as soot. This is important because the direct measurement of soot particle mass can currently only be performed with aerosol particle mass analyzers (APM) (Ehara & Shin, 1998; McMurry et al., 2002) which have only very recently been commercialized and whose use is not as widespread as that of AMS–DMA combinations. The particle mass estimate can be calculated as:

$$m_{\text{p}} \cong \frac{\pi}{6}\rho_{\text{eff}}d_{\text{m}}^3 = \frac{\pi}{6}\rho_0 d_{\text{va}}d_{\text{m}}^2 \tag{9}$$

where m_p is the particle mass. The error in this approximate formula can be evaluated for any particle if the assumption is made that the dynamic shape factor is the same in the free molecular and transition regimes ($\chi_v = \chi_t$). DeCarlo et al. (2004) and Zelenyuk et al. (2006b) show that this is a reasonable approximation for mildly non-spherical particles. This mass estimate can be shown to be within a factor of 2 for submicron particles, with smaller errors for small particles and for mildly non-spherical particles. Slowik et al. (2004) show that if the density of the particle can be estimated from its composition (measured with the AMS), the error in this estimate is further reduced.

Particle mass estimates can also be used to estimate the fractal dimension of a particle using the mass–mobility relationship (Park et al., 2003):

$$m_{\text{p}} = Cd_{\text{m}}^{D_{\text{f}}} \tag{10}$$

where C is a proportionality constant and the fractal dimension, D_f, varies from a minimum value of 1 for a very long linear chain of spheres to a maximum value of 3 for a sphere.

E. Light Scattering

The intensity of light scattered by a particle provides a measure of its optical size. Murphy et al. (2004) have used simultaneous measurements of optical and aerodynamic diameters to obtain information about single particle densities and refractive indices. The AMS has recently been equipped with a light scattering module to allow for similar estimations of particle density in real-time, and to allow the sizing of refractory particles that would otherwise escape chemical detection (Cross et al., 2006). This module monitors scattering of a beam of 405 nm (green) laser light by individual particles in the focused particle beam while the AMS is operated in PToF mode. The light scattering signal is monitored as a function of PToF, allowing calculation of the d_{va} and the optical size of the particle. Moreover, the single particle light scattering signal can be directly correlated with the mass spectral signal to obtain chemical information about the scattering particle.

A unique feature of the laser beam in this scattering probe is that it is relatively broad and unfocussed compared to the tightly focused beams usually used by other optical sizing instruments (Murphy et al., 2004). The broader beam allows for greater overlap with the width of the particle beam. This means that the light scattering probe detects nearly all scattering particles (refractory and non-refractory) before they impact the vaporizer. Thus, this probe provides a method of determining the fraction of particles that are not vaporized in the detector due to either particle bounce effects or the need for higher vaporization temperatures. Moreover, in the ToF-AMS, where true single particle detection is possible, the light scattering signal can be used as a trigger for the saving of raw single particle data.

IV. EXAMPLE APPLICATIONS OF THE AMS

A. Lab Studies

The highly time-resolved measurements possible with the AMS make it an attractive choice for kinetic studies and for detailed characterization of aerosol properties under controlled laboratory conditions. The AMS has been utilized in flow tube and smog chamber studies designed to investigate several broad topics including:

(a) Transformation of aerosol chemical properties as a function of heterogeneous oxidation (Morris et al., 2002; Katrib et al., 2004; Katrib, 2005a) and reactive uptake (Kroll et al., 2005b; Liggio, Li, & McLaren, 2005a,b; Garland et al., 2006)
(b) Kinetics and products of secondary aerosol formation in urban and biogenically influenced terrestrial (Bahreini et al., 2005; Kroll et al., 2005a; Alfarra et al., 2006), biogenically influenced marine (O'Dowd et al., 2002; Jimenez et al., 2003a; McFiggans et al., 2004), and extra-terrestrial environments (Trainer et al., 2004a,b).
(c) The effect of chemical composition on aerosol density (Bahreini et al., 2005; Katrib et al., 2005b) and water uptake (Garland et al., 2005). A few of these studies are highlighted in this section.

A commonly used model for understanding heterogeneous oxidation processes has been the reaction of oleic acid, $C_{18}H_{34}O_2$ (OA), with ozone. The first AMS experiments on this system by Morris et al. (2002) provided information about the size dependent chemistry and kinetics, the reaction stoichiometry, and qualitative information about the volatility of the reaction products. In subsequent AMS studies, some specific oxidized organic products of this reaction (Katrib et al., 2004) and the

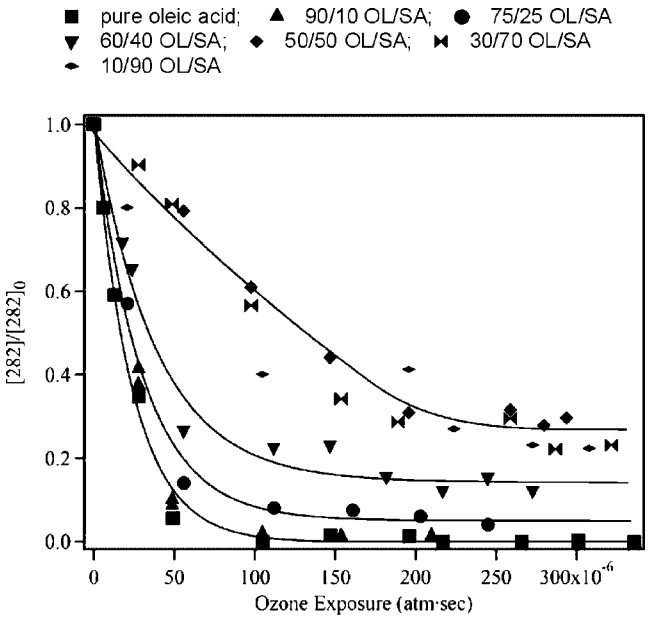

FIGURE 17. Kinetics of the reaction of ozone with oleic acid (OA) in mixed OA/SA (stearic acid) particles of varying compositions. The decrease in oleic acid concentration as the reaction proceeds is monitored at *m/z* 282. (Reprinted with permission from Katrib et al. (2005a). Copyright 2005 American Chemical Society.)

changes in aerosol density (Katrib et al., 2005b) resulting from the oxidation process were measured. The effect of particle phase and composition on the observed OA/O_3 reaction was also investigated by Katrib et al. (2005a). Figure 17 shows the reaction kinetics of OA (measured at its molecular ion at *m/z* 282) when it is mixed with various mass fractions of stearic acid (SA). The rate of initial decay of OA decreases linearly with increasing SA content of particles with a particularly sharp decrease observed for particle compositions with >50% SA. In addition, large residual OA concentrations at high O_3 concentrations are observed for particles with SA >50%. Simultaneous measurements of particle beam width with a BWP indicate that the results shown in Figure 17 can be correlated with the phase of the mixed OA/SA before and during reaction. For example, the decrease in initial decay rates correlates with solidification of supersaturated liquid mixed particles (with SA fractions between 25 and 40%) upon reaction. Katrib et al. (2005a) postulate that this solidification is accompanied by the formation of a semi-permeable gel that reduces the molecular diffusivity and thus the observed OA decay rate. The high residual fraction of OA for particles with SA >50% correlates with the fact that these particles are solid even before reaction. In this case, it is postulated that the residual fraction corresponds to significant amounts of OA that is locked inside pockets of the solid SA matrix.

The kinetics of secondary aerosol formation and the characteristics of the resulting products have been explored by Bahreini et al. (2005) in a series of smog chamber studies. These studies focused on aerosol formation from the oxidation of a variety of model compounds representative of biogenic and anthropogenic secondary organic aerosol precursors. The effective densities and the effects of acidic and non-acidic inorganic seeds on the resulting secondary organic aerosol (SOA) were examined. The mass spectra from these experiments were analyzed in terms of standard CH_2 ion series (i.e., mass peaks separated by 14 amu) observed in the spectra. Accordingly, each *m/z* in the spectrum was assigned a Δ value where $\Delta = m/z - 14n + 1$ (where n is the "nominal" number of CH_2 groups in the fragment). The value of Δ is indicative of the likely functional groups present in the ion fragment that appears at that *m/z*. On this Δ scale, $\Delta = 2$ corresponds to linear saturated hydrocarbons, $\Delta > 2$ correspond to organics with heteroatoms like oxygen, and a $\Delta < 2$ corresponds to unsaturated and branched hydrocarbons (McLafferty & Turecek, 1993). Figure 18 shows mass spectra from the oxidation reactions of various anthropogenic and biogenic precursors classified according to their average delta values in the *m/z* ranges corresponding to $n = 1–4$, $n = 5–6$, and $n = 7–15$. These experiments indicate that SOA from similar precursors yield similar AMS mass spectra and that different ion series patterns in AMS spectra may be useful to distinguish between biogenic and anthropogenic sources of SOA.

As shown in Figure 19, smog chamber experiments (Baltensperger et al., 2005; Alfarra et al., 2006) have also focused on the mass spectral signatures observed from the photooxidation of 1,3,5-trimethylbenzene (TMB, an anthropogenic SOA precursor) and α-pinene (a biogenic SOA precursor) in the presence of nitrogen oxides. While the mass spectra observed from both types of precursors are similar in many ways, they also have significant differences in less intense mass spectral peaks that can be used to distinguish between them. Comparisons of the smog chamber SOA spectra with ambient measurements show that ambient organic aerosol measured in urban, rural, remote, and forested environments are more similar to spectra of α-pinene SOA than 1,3,5-TMB SOA. Although the relative importance of *m/z* 44 in the photooxidation products of both precursors increased with irradiation time, it was typically lower than that observed in rural and remote ambient spectra indicating that the latter are more oxygenated and/or photochemically aged than the SOA produced in the smog chamber experiment after 8 hr of irradiation.

The overall fragmentation patterns observed in both types of SOA mass spectra did not change significantly with irradiation time in the smog chamber experiments. This could be consistent with work by Kalberer et al. (2004) that indicates that up to 50% of the mass of SOA produced from the 1,3,5-TMB photooxidation could be due to oligomers. Increased polymerization as a function of irradiation may not give rise to changes in AMS spectra because the polymers likely undergo thermally induced fragmentation into their monomer units upon vaporization in the AMS. The use of lower thermal vaporization temperatures and especially softer ionization methods (See Section VI) may provide a means of increasing the sensitivity of the AMS to larger oligomeric units.

B. Source Characterization

Direct sampling of aerosols from specific sources can be used to obtain specific profiles or signatures useful for estimating the relative contributions of different types of sources to ambient aerosols. The AMS has been utilized to characterize a wide variety of specific sources such as diesel vehicles operating on-

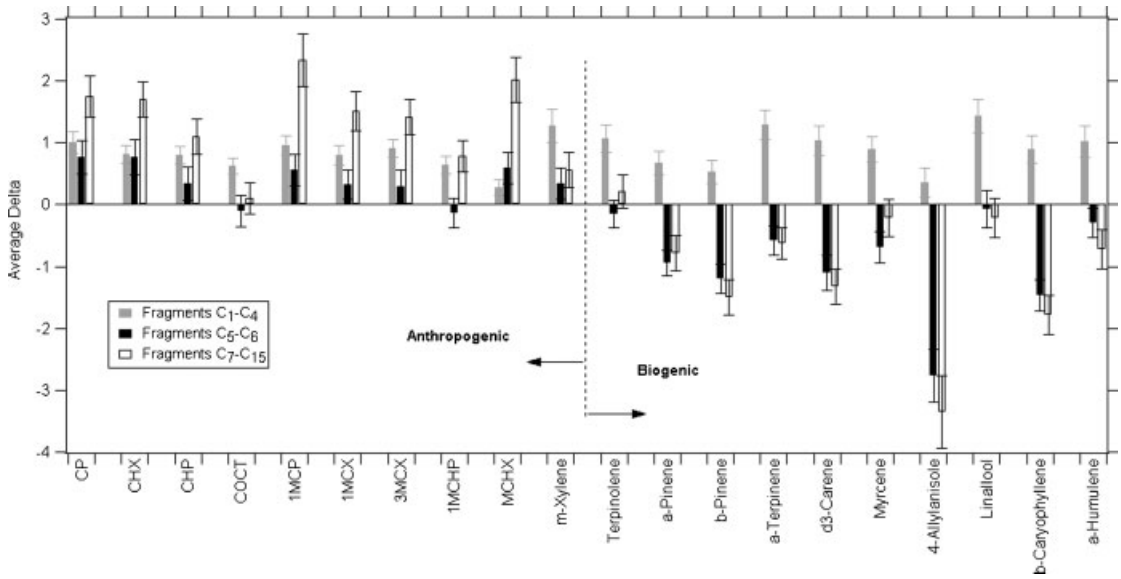

FIGURE 18. Average delta values determined from AMS mass spectra of secondary organic aerosol (SOA). The SOA were produced by photo-oxidation of a variety of gas phase precursors in a smog chamber. The results are categorized and sorted according to the anthropogenic or biogenic nature of the SOA precursors. Detailed information about the chemical structure and formulas of each of the precursors can be found in the manuscript by Bahreini et al. (2005). (Reproduced with permission from Bahreini et al., 2005. Copyright 2005 American Chemical Society.)

road or on a chassis dynamometer (Canagaratna et al., 2004; Scheer et al., 2005; Schneider et al., 2005b), aircraft exhaust aerosol (Anderson et al., 2005; Schneider et al., 2005a; Akiyama, 2005), biomass burning (Weimer, 2003; Schneider et al., 2006), propane flame soot (Slowik et al., 2004), and firework aerosols (Allan et al., 2003a; Williams et al., 2005; Drewnick et al., 2006). This section will highlight AMS measurements on two related sources: vehicle emissions and propane flame soot emissions.

The AMS has been deployed on a mobile laboratory (Kolb et al., 2004) which was used to measure emissions from individual in-use diesel vehicles in real time (Canagaratna et al., 2004). Figure 20 shows an AMS time trend of total NR-PM_1 (obtained with 2-sec time resolution) as well as analogous trends in the 1-sec measurements of CO_2 mixing ratio measured during a single vehicle chase event. The simultaneous peaks in the particle and CO_2 signals, which usually last for approximately 10–20 sec, represent separate instances during the chase when the sampling inlet of the mobile lab captured the target vehicle's exhaust plume. The baseline signal levels in the gas and particle time trends represent ambient background concentrations of the various species during the chase event. The linear proportionality constant between the NR-PM_1 and CO_2 species during these exhaust plume measurements was used to obtain a fuel-consumption based aerosol mass emission index for each sampled vehicle. An average spectrum MS obtained from many diesel chase event plume captures is shown in Figure 21. Also shown in the figure for comparison are mass spectra for lubricating oil and diesel fuel which are known to be the major components of diesel PM. An analysis of the three mass spectra suggests that while they all contain the same CH_2 ion series, the relative intensities of the series in the diesel exhaust spectrum more closely matches that seen for lubricating oil. This is consistent with measurements by Tobias et al. (2001) who also concluded that the hydrocarbon content of diesel exhaust particles was dominated by lubricating oil. On average, the mass-weighted size distributions of the particles in fresh diesel exhaust plumes were measured to peak at vacuum aerodynamic diameters around 90 nm with a typical full-width at half maximum of 60 nm.

Schneider et al. (2005b) have measured vehicle exhaust from diesel-fueled vehicles under various conditions including on chassis dynamometers, on the side of a busy highway, and by chasing individual vehicles. These studies show that nucleation particles (d_{va} ~55 nm) in diesel exhaust consist of organic species and sulfur, and their formation is strongly dependent on conditions such as exhaust dilution, sulfate content of the fuel, and the operating engine load. Evidence indicates that the nucleating agents for this mode are sulfuric acid and water which are present in the exhaust when high sulfur fuels are used. As shown in Figure 22, a larger exhaust aerosol mode (d_{va} ~100 nm), was also observed with remarkable similarity with the highway and dynamometer AMS measurements. Thermodenuder studies indicate that this mode contains a non-volatile core of soot and variable amounts of condensed sulfate and semivolatile organic species depending on the engine load and the sulfur level in the fuel.

The technique for particle shape characterization with DMA-AMS measurements described in section III.D has been used by Slowik et al. (2004) to characterize the morphology of flame soot generated in laboratory experiments. Nascent soot particles were produced from flames with different fuel/oxygen ratios (ϕ). At each ϕ, a DMA was used to size-select particles at

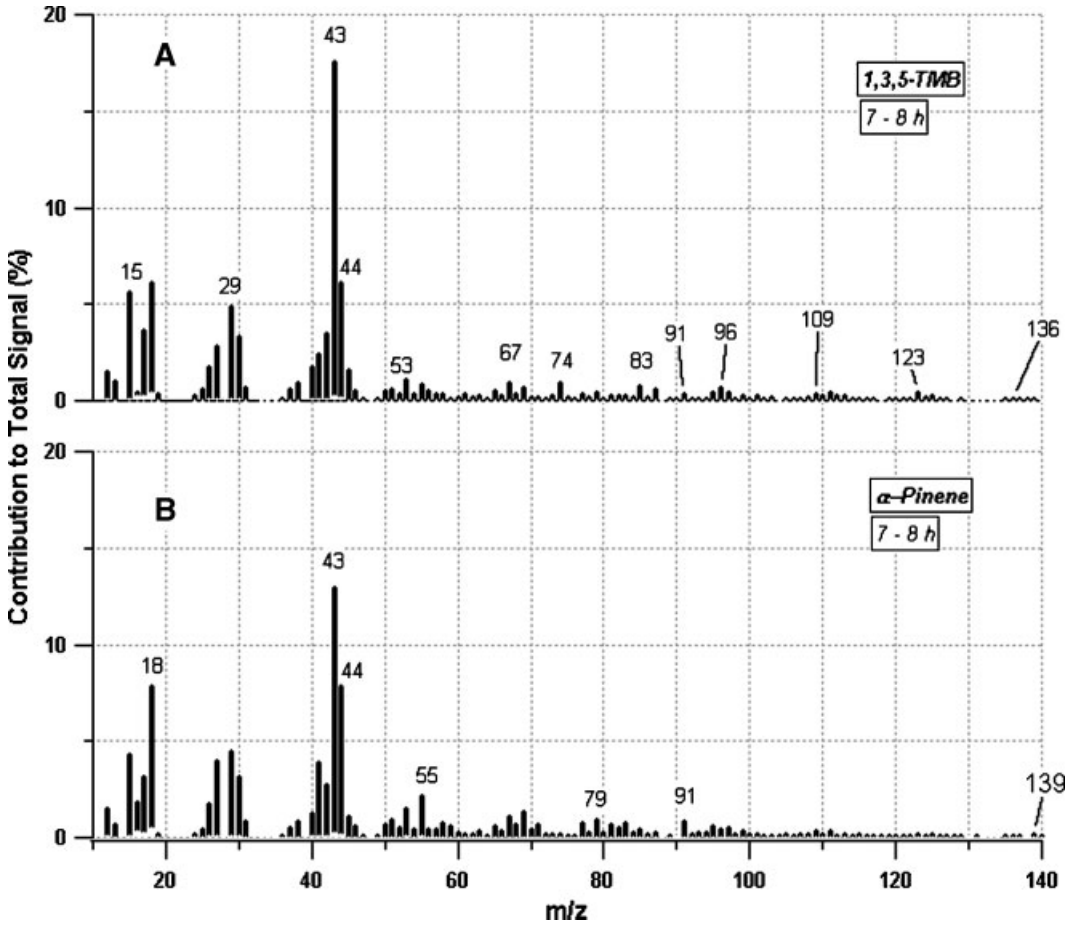

FIGURE 19. AMS mass spectra of the organic aerosol species produced during the photo-oxidation of 1,3,5-TMB and α-Pinene in a smog chamber. These mass spectra were averaged for irradiation times between 7 and 8 hr.

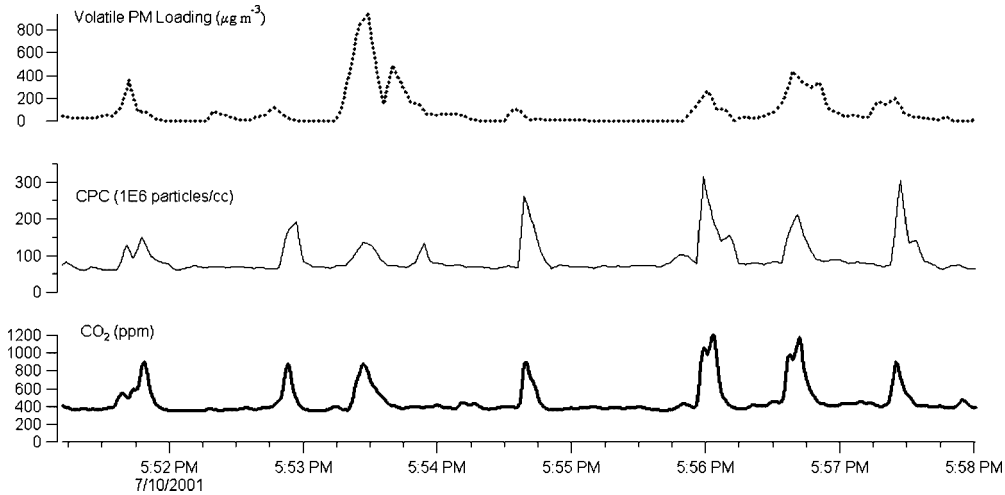

FIGURE 20. Example of vehicle chase data obtained while following an individual vehicle with the mobile laboratory. The NR-PM_1 loadings are obtained with the AMS. Each peak in the CO_2 signal signifies a "capture" of the target vehicle's exhaust plume. The valleys between plume captures reflect ambient gas and PM loadings. Peaks in the AMS aerosol signal which correlate with peaks in the CO_2 time trace, are indicative of direct measurements of vehicle exhaust aerosol. Particle number concentrations measured with a Condensation Particle Counter (CPC) correlate well with the AMS measurements.

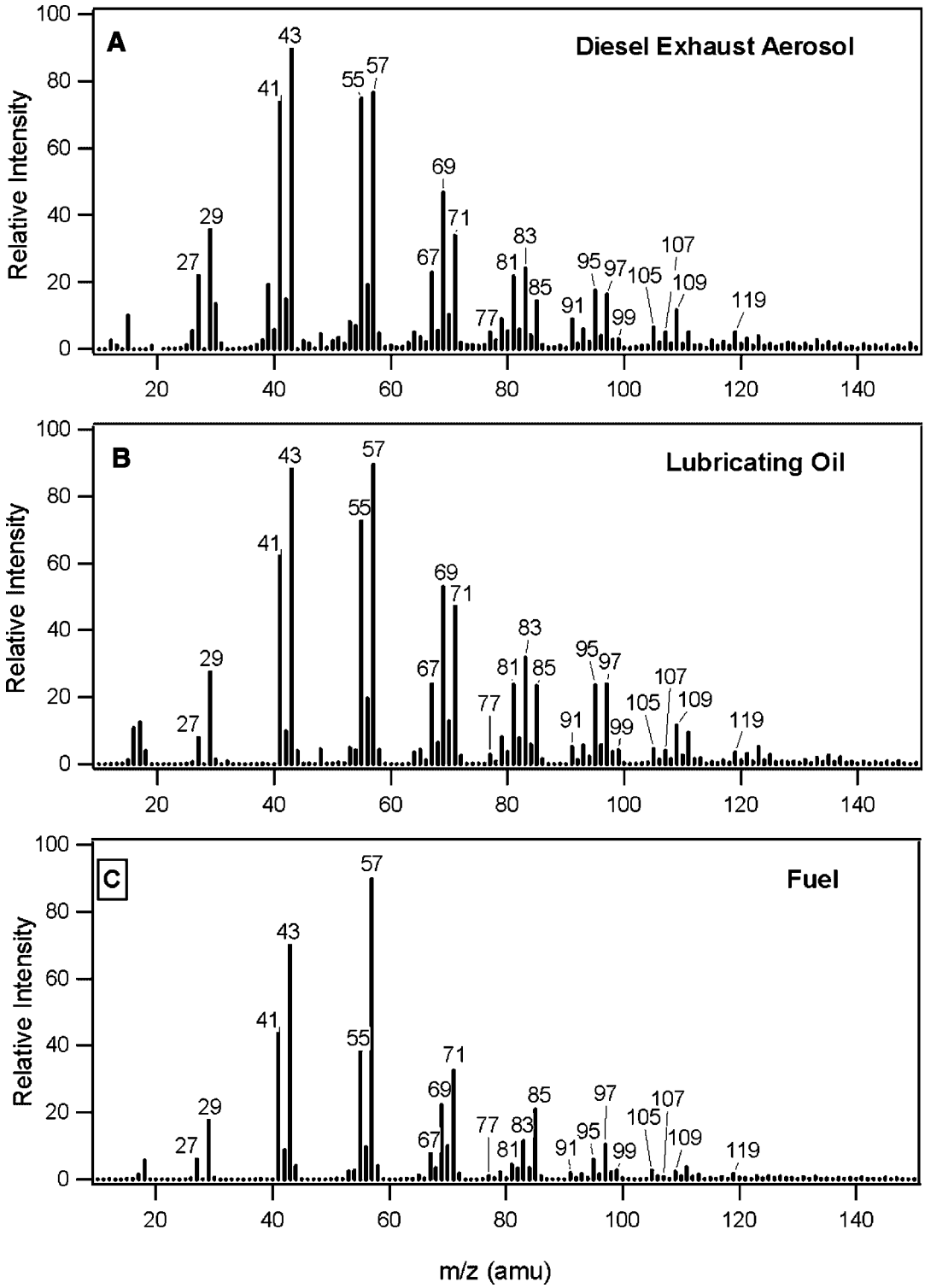

FIGURE 21. AMS mass spectra obtained from diesel bus exhaust (**A**), pure lubricant oil (**B**), and pure diesel fuel (**C**) aerosols. The lubricant oil and diesel fuel spectra were obtained from lab aerosols and the diesel bus exhaust spectrum is an average of PM exhaust mass spectra obtained during all the diesel vehicle chases performed with the mobile laboratory during the New York City measurement campaign. (Aerosol Science & Technology: Canagaratna et al.: Chase studies of particulate emissions from in-use New York City vehicles. (38) 555–573. Copyright 2004. Mount Laurel, NY, Reprinted with permission.)

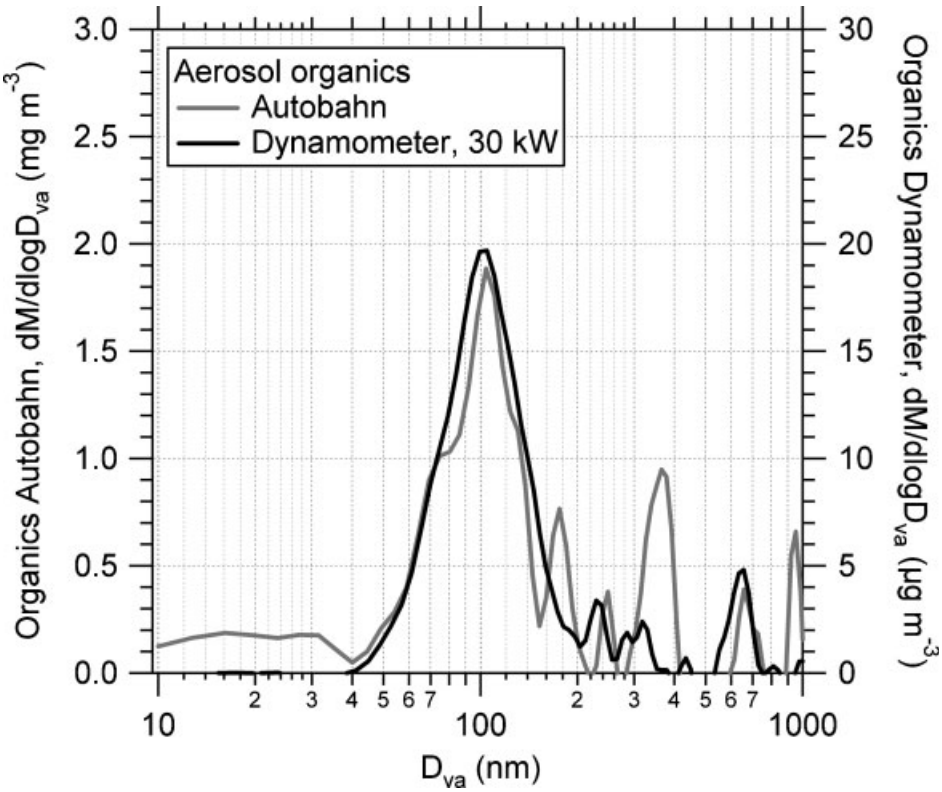

FIGURE 22. A comparison of organic aerosol size distributions measured with the AMS during highway and dynamometer studies. (Reproduced with permission from Schneider et al., 2005b. Copyright 2005 American Chemical Society.)

mobility diameters between 100 and 460 nm. The chemical composition, size distributions, and morphologies of the size-selected particles were determined with an AMS. Two distinct types of flame soot were observed depending on the value of ϕ. Flames with $\phi < 4$ were found to produce fractal soot particles with a constant d_{va} centered at 100 nm regardless of selected d_m. The observed values of χ for these particles ranged from 1.3 ($\phi = 2.8$, $d_m = 100$ nm) to 3.6 ($\phi = 2.3$, $d_m = 460$ nm). The fractal dimension for these particles was 1.7 ± 0.1 and they were composed mostly of black carbon. For flames with $\phi \geq 4$, a near-step change was observed with the soot particles becoming near spherical as indicated by fractal dimensions of 2.95. Shape factors of these particles were found to be 1.2 for all d_m, and they appeared to consist of approximately equal amounts of black carbon and NR organics. Similar results for soot particles from various sources (diesel, kerosene, biomass) were found by Weimer (2003) and Schneider et al. (2006).

Figure 23 shows the observed relationship between dynamic shape factor and mobility diameter for flame soot. The two types of soot are represented by the solid symbols. The open symbols are diesel engine exhaust measurements made by Park et al. (2003). The remarkable degree of agreement between the diesel exhaust observations and those for fractal propane flame soot suggests that the Type 1 fractal laboratory soot particles may be a good model system for fractal sooty particles in vehicle exhaust. This observation is further underscored by the fact that the constant d_{va} of 100 nm measured for fractal laboratory soot is also very similar to the small exhaust mode shown in Figure 22 that is observed in chase, highway, and dynamometer studies of diesel vehicle exhaust (Canagaratna et al., 2004; Schneider et al., 2005b).

C. Field Studies

The AMS has been fielded in urban (Allan et al., 2003a; Alfarra et al., 2004; Drewnick et al., 2004a,b; Broekhuizen et al., 2005; Takegawa et al., 2005; Zhang et al., 2005b; Salcedo et al., 2006; Volkamer et al., 2006), remote (Allan et al., 2004a; Schneider et al., 2004; Topping et al., 2004; Takami et al., 2005), rural (Alfarra et al., 2004; Boudries et al., 2004; Hogrefe et al., 2004; Rupakheti et al., 2005), marine (Bates et al., 2005; Dall'Osto et al., 2005; Coe et al., 2005), and forested environments (Delia, 2004; Allan et al., 2006) around the world. The AMS has also been deployed on mobile platforms such as ships (Bates et al., 2005), mobile laboratories (Canagaratna et al., 2004), and aircraft (Bahreini et al., 2003; Conant et al., 2004; Schneider et al., 2005a; Crosier et al., 2006). Figure 24 (on page with Figure 8) shows an example of the type of information that is usually obtained from the AMS during ambient measurement campaigns. Plot (a) in Figure 24 on page with Figure 8 shows the time-resolved mass concentrations of sulfate, nitrate, and organic aerosol species. Plots b–d show time trends of speciated mass-weighted size distributions; the right hand side of these plots

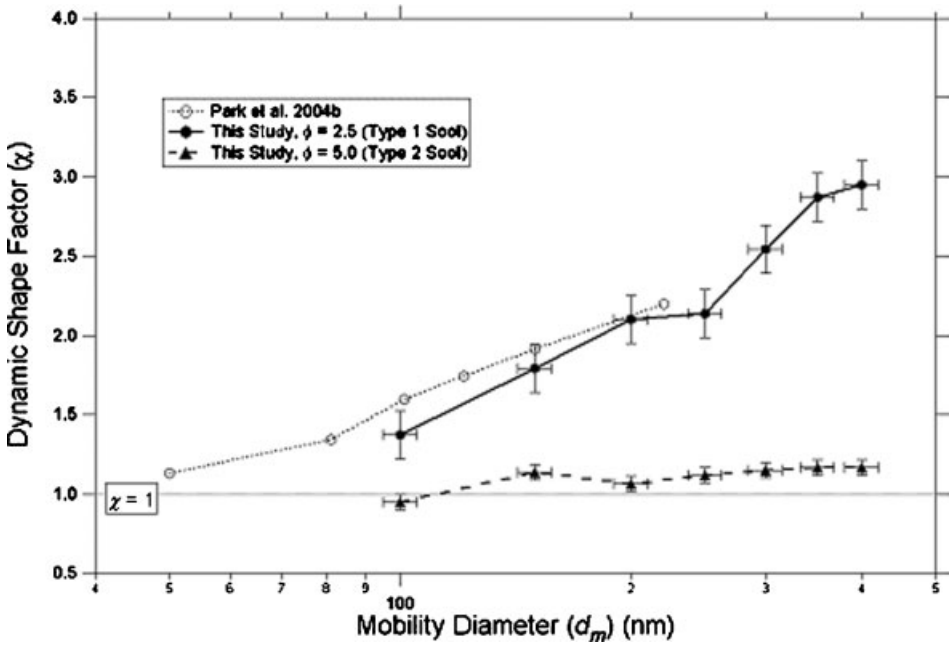

FIGURE 23. Dynamic Shape Factors measured as a function of Mobility Diameter for the Type 1 and Type 2 soot generated in the laboratory with a propane flame. Diesel engine exhaust measurements by Park et al. are included for comparison with the propane soot. (Aerosol Science & Technology: Slowik et al.: Particle morphology and density characterization by combined mobility and aerodynamic diameter measurements. Part 2: Application to combustion generated soot particles as a function of fuel equivalence ratio. (38): 1206–1222. Copyright 2004. Mount Laurel NJ, Reprinted with permission.)

shows the size distributions for each species averaged over the entire time period. Real-time measurements of speciated aerosol mass, size, and composition provide a rich picture of the dynamic evolution of aerosol that would not be captured in time-averaged measurements of the same properties. Indeed, as will be illustrated below, a great deal of information about aerosol sources, properties, and processes can be obtained with a systematic detailed analysis of this type of multidimensional dataset.

AMS measurements show that in most environments, a large fraction of the ambient NR-PM_1 can be accounted for by the inorganic species $(NH_4)_2SO_4$, NH_4HSO_4, and NH_4NO_3, with NH_4Cl typically playing a smaller role in some environments (Takegawa et al., 2005; Salcedo et al., 2006). Total organic species typically have concentrations of the same order of the total inorganic species. Distinct diurnal trends in organic aerosol size and composition have been observed in different environments (Alfarra et al., 2004; Drewnick et al., 2004a,b; Takegawa et al., 2005). Figure 25 shows an intercomparison between organic aerosols measured in rural and urban sites (Alfarra, 2004; Boudries et al., 2004). While this figure contains data measured in rural and urban sites in Canada, the results are representative examples of similar observations seen in multiple deployments of the AMS throughout the world (Allan et al., 2003a, 2004a; Drewnick et al., 2004a,b; Schneider et al., 2004; Topping et al., 2004; Cubison et al., 2005; Takami et al., 2005; Takegawa et al., 2005; Zhang et al., 2005b; Salcedo et al., 2006).

As shown in Figure 25, organic aerosol species in rural and urban sites are typically found in accumulation mode particles in the 200–500 nm range. The lower panel of this figure shows that the mass spectra of the accumulation mode particles are characteristic of oxidized organic molecules (Alfarra, 2004; Schneider et al., 2004; Topping et al., 2004; Allan et al., 2004a; Drewnick et al., 2004a; Cubison et al., 2005; Zhang et al., 2005b). Analysis of speciated size distribution time trends further indicate that the oxidized organic species in the accumulation mode are typically internally mixed with inorganic species such as $(NH_4)_2SO_4$, and that photochemical processing of the accumulation mode particles largely occurs on a regional rather than a local scale (Alfarra et al., 2004; Boudries et al., 2004; Topping et al., 2004; Cubison et al., 2005; Zhang et al., 2005b). In polluted environments, afternoon peaks in the diurnal concentrations of accumulation mode organic and inorganic species that correlate with gas phase photochemical markers (Zhang et al., 2005b,c; Salcedo et al., 2006) reflect local photochemical production and subsequent condensation of secondary aerosol. Allan et al. (2003a) have also observed an increase in the size of the accumulation mode that correlates with the apparent increase in the mass of photochemically formed material that is available to condense on the accumulation mode particles in the summer relative to the winter. Under clean and clear (sunny) conditions, when background accumulation aerosol concentrations are low, locally formed sulfate and oxidized organic species are also observed to condense onto nucleated ultrafine particles (40–80 nm diameter) (Zhang et al., 2004a).

Figure 25 shows that in urban areas (Allan et al., 2003a; Drewnick et al., 2004b; Zhang et al., 2005b) or during aerosol events influenced by urban pollution (Allan et al., 2004a; Boudries et al., 2004), a distinct organic mode at ''smaller'' sizes (~100 nm) is observed in addition to the accumulation mode. These particles are almost completely made up of organic

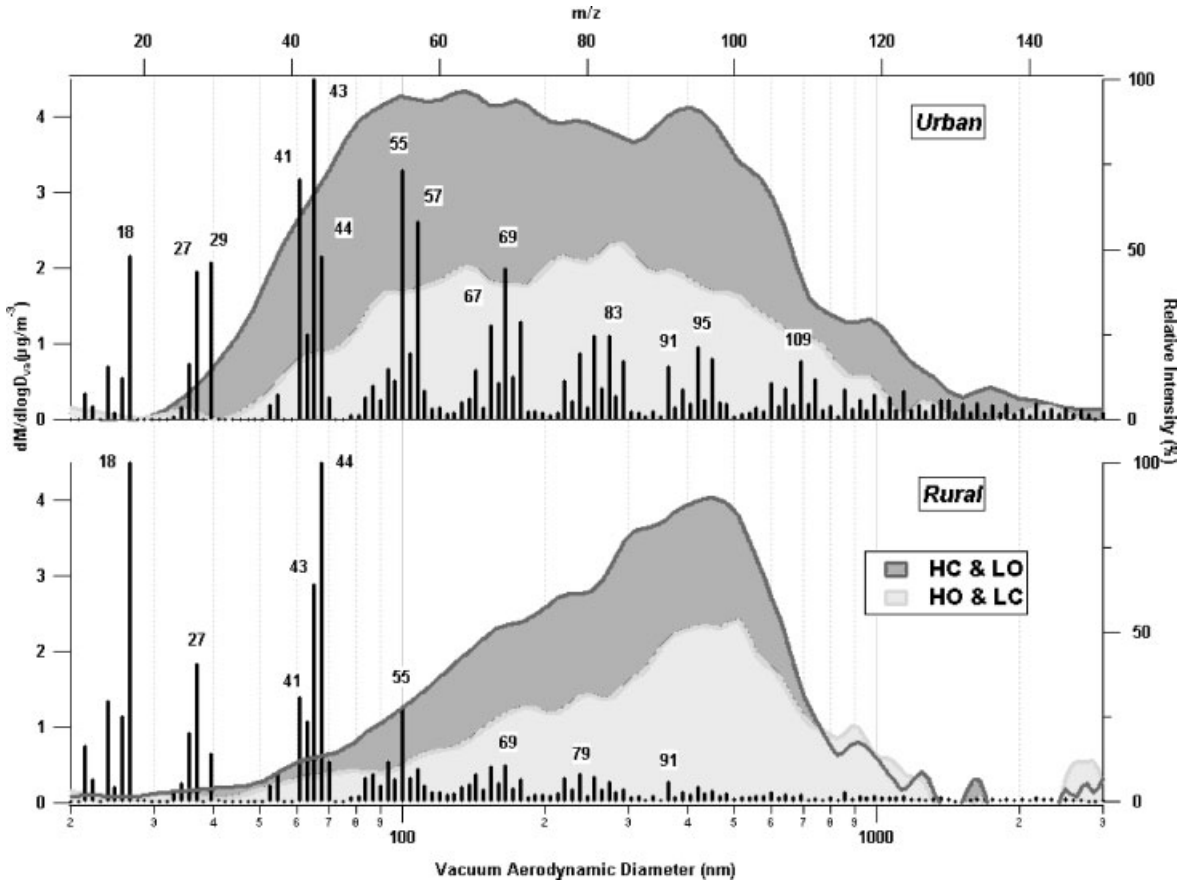

FIGURE 25. Organic aerosol size distributions and mass spectra measured with the AMS in an urban site and a rural site during the PACIFIC 2001 field campaign (Alfarra et al., 2004). At each site, the size distributions have been conditionally averaged according to the observed gas phase concentrations of carbon monoxide (CO) and ozone (O_3). Time periods that are likely influenced by motor vehicle emissions are identified by high CO and low O_3 concentrations (HC & LO). Time periods during which photochemical activity is likely enhanced are identified by high O_3 and low CO concentrations (HO & LC). The average urban mass spectrum was averaged over HC & LO conditions while the rural mass spectrum was averaged over HO & LO conditions.

species that contain a strong *m/z* 57 peak and the prominent CH_2 ion series characteristic of hydrocarbon species. Concentrations of the ''small'' mode hydrocarbon species typically peak in the early morning and have a positive correlation with gas phase tracers of traffic exhaust like CO (Allan et al., 2003a) and various volatile organic compounds (Allan et al., 2004a). Moreover, the size distributions and mass spectra of these particles are remarkably similar to particles directly sampled behind in-use vehicles (Canagaratna et al., 2004; Schneider et al., 2005b). AMS measurements of these ''small'' hydrocarbon-like organic particles are useful for probing the relative importance of fresh vehicle emissions to ambient aerosol budgets (Alfarra, 2004; Drewnick et al., 2004b; Zhang et al., 2005b,c) and in understanding the aging process of these freshly emitted particles (Cubison et al., 2005; Zhang et al., 2005c).

The AMS has the fortuitous capability of distinguishing between ''smaller'' fractal soot emissions and more spherical ambient accumulation mode particles because d_{va} decreases with increasing asphericity (See Eq. 6). This is in contrast to mobility diameter measurements where the apparent sizes of soot emission particles become closer to that of ambient accumulation mode particles with increasing asphericity. Thus, as shown by Zhang et al. (2005b), it is important to take particle shape effects into account when comparing ambient size distributions measured by the AMS with those obtained by other instruments.

Aircraft deployments of the AMS have provided a picture of how aerosol concentrations vary with altitude (Bahreini et al., 2003; Conant et al., 2004; Schneider et al., 2005a; Crosier et al., 2006). Figure 26 shows an example of altitude profiles obtained with an AMS that was deployed aboard the DOE G-1 aircraft during the New England Air Quality Study—2002 campaign off the New England Coast. The distinct sulfate aerosol layers observed during this measurement were found to correlate with differing altitude-dependent pollution histories of the air masses. Similar layers of accumulation mode particles containing sulfate and oxidized organic species were also observed during aircraft measurements sampling the outflow of eastern Asia (Bahreini et al., 2003) and the Po Valley in Italy (Crosier et al., 2006).

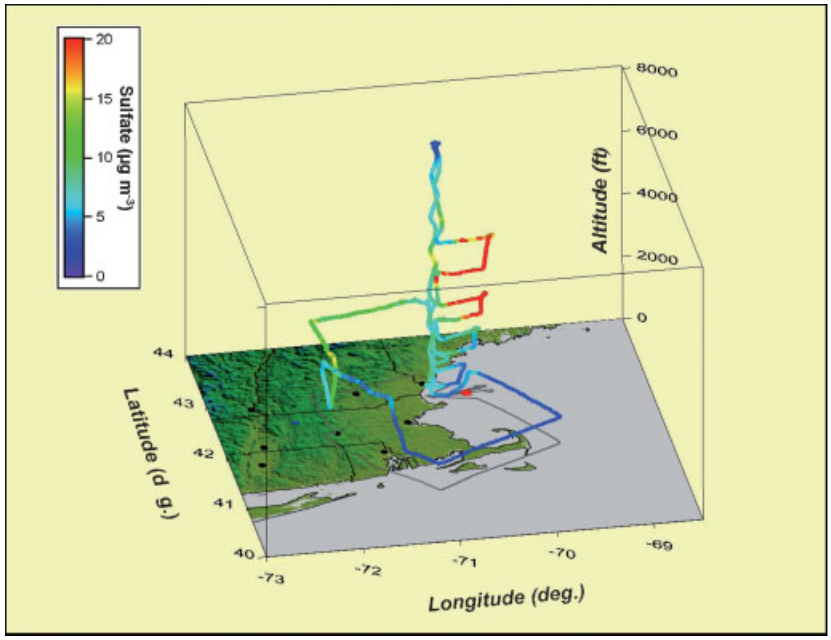

FIGURE 26. Vertical profiles of sulfate aerosol concentrations measured with an AMS that was deployed aboard the DOE G-1 aircraft during the New England Air Quality Study in 2002.

V. ANALYSIS OF ORGANIC SPECTRA

The total mass concentration of organic aerosol components, which is determined from the AMS spectrum after removing signals of inorganic and gas phase species, shows good correlation with the carbon concentration measured by thermal-optical carbon analyzers (Bates et al., 2005; de Gouw et al., 2005; Takegawa et al., 2005; Zhang et al., 2005b; Weimer et al., 2006). Since the total organic concentration is calculated as the sum of the intensity of all *m/z*s in the AMS organic spectrum, this supports the concept that each ensemble organic spectrum is quantitative and thus, can be decomposed into a linear combination of the spectra of individual organic species and/or classes. These inherently linear spectra, together with the high time resolution of the measurements, enable statistical multivariate analysis to unravel the main types of organic species contributing to the AMS mass spectra.

A deconvolution technique has recently been developed and applied successfully to an urban AMS dataset acquired in Pittsburgh, US to yield information on the concentrations, mass spectra, and size distributions of hydrocarbon-like and oxygenated organic aerosols (HOA and OOA, respectively) (Zhang et al., 2005a,c). This technique involves a series of multivariate linear regressions, conceptually similar to the alternating regressions method (Paatero & Tapper, 1994), that

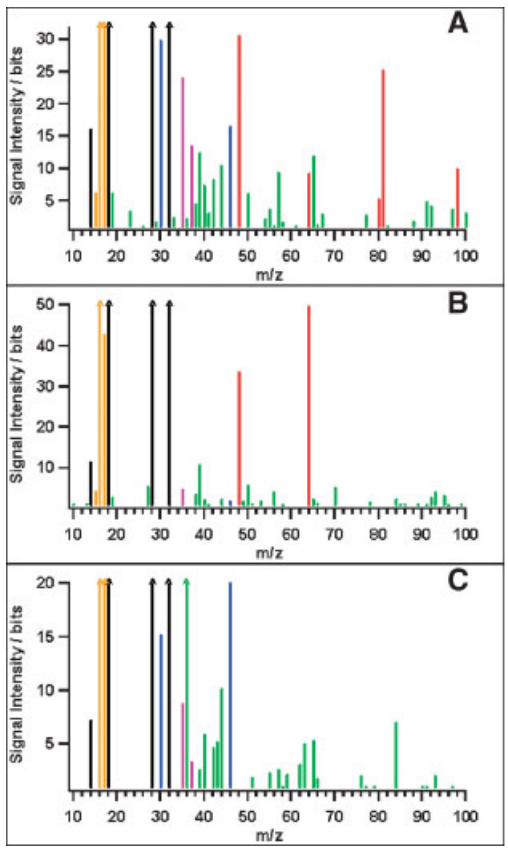

FIGURE 29. Mass spectra of three different types of single particles observed by Drewnick et al. during the first deployment of the ToF-AMS. (Aerosol Science & Technology: Drewnik et al.: A new time-of-flight aerosol mass spectrometer (ToF-AMS)—Instrument description and first field deployment. (39): 637–658. Copyright 2005. Mount Laurel, NJ, Reproduced with permission.)

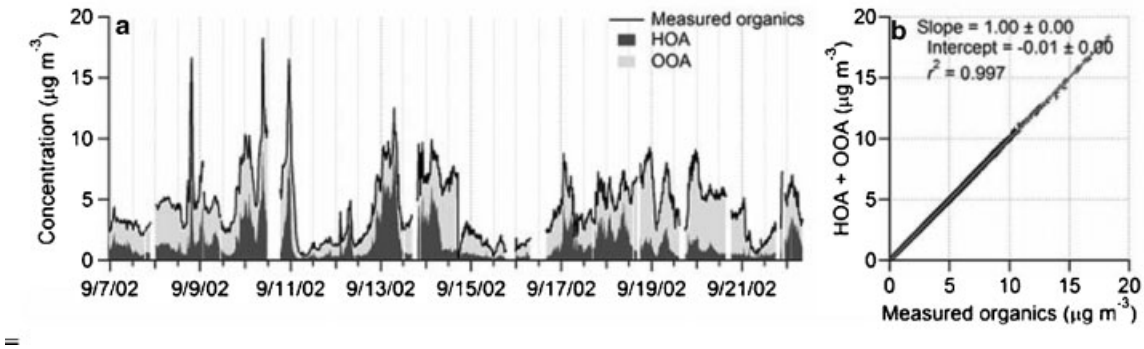

FIGURE 27. Panel a shows time trends of organic aerosol mass concentration and deconvolved HOA and OOA components during the Pittsburgh Air Quality Study. OOA is stacked on top of HOA. Panel b shows a scatter plot between the reconstructed two-component organic mass concentration (HOA + OOA) and the actual organic mass concentration measured with the AMS. Results of a linear fit between the reconstructed and measured organic concentrations are also shown (Zhang et al., 2005a), modified.

use the time series of AMS spectral tracers *m/z* 57 (mostly $C_4H_9^+$) and 44 (mostly CO_2^+) as the seed principal components, and an iterative algorithm to optimize the deconvolution. In the analysis of a 16-day field dataset from Pittsburgh in September 2002, the reconstructed organic concentrations (=HOA + OOA) agree well with the measured values of total OM ($r^2 = 0.997$, slope ≈ 1, Fig. 27) and the reconstructed organic data matrix (size = 3,199 time steps × 300 *m/z*s) explains ~99% of the variance in the measured matrix (Zhang et al., 2005a). In addition, as shown in Figure 28, the extracted mass spectra of HOA and OOA are very different and can be interpreted chemically. The HOA spectrum reveals ion series characteristic of long chain hydrocarbons and is similar to the spectrum of fresh vehicle exhaust aerosol (Fig. 21). The OOA spectrum peaks at *m/z* 28 and 44, and closely resembles that of highly processed organic aerosols sampled from rural and remote locations (Fig. 25).

A multicomponent version of this technique is being applied to more than 30 AMS datasets acquired from multiple urban and rural/remote locations around the world (Zhang et al., in preparation). A major utility of this technique is that it greatly simplifies the complex AMS OM spectral data into a physically meaningful and much smaller set of results. Note that the success of using only two components (i.e., HOA and OOA) to explain most of the variance in measured organic aerosol concentration in urban atmospheres indicates that these two types of aerosols account for the large majority of the mass in some urban areas, are very different chemically from each other, and have different temporal emission, production, and transport patterns that are exploited by the principal component analysis technique.

Analysis of datasets from rural and remote locations suggests the presence of significant amounts of components other than HOA and OOA. For instance, a less oxidized component that appears to be associated with biogenic sources has been identified in several sites that are strongly influenced by biogenic emissions (Zhang et al., in preparation). New techniques are currently under development to resolve more organic aerosol components using the AMS data. Preliminary results from a modified version of the spectral deconvolution method described above show some promise of resolving three or even four physically meaningful components. Alternatively, Marcolli et al. (2006) shows that a hierarchical clustering

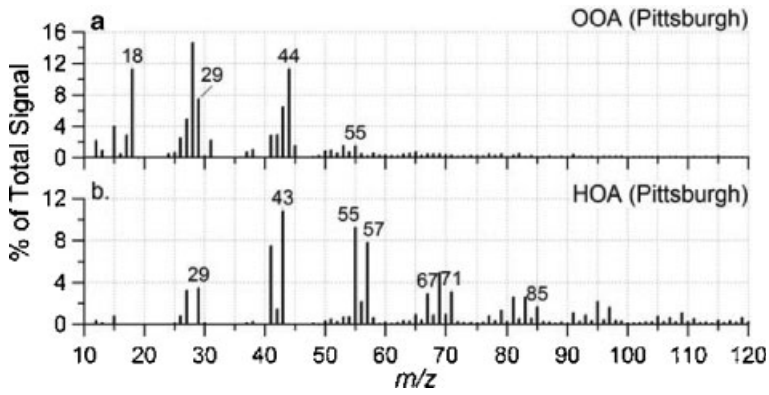

FIGURE 28. Deconvolved mass spectra of the OOA and HOA components observed during the Pittsburgh Air Quality Study. The y-axis of the spectra is scaled to reflect the contribution of each fragment to the total signal intensity (Zhang et al., 2005a), modified.

algorithm, which has been used in the past to analyze single particle spectra obtained from laser-based instruments (Murphy, Middlebrook, & Warshawsky, 2003), can be successfully applied to Q-AMS spectra to obtain several mass spectral clusters.

Detailed organic analysis is difficult to achieve with the unit mass resolution EI Q-AMS data because extensive fragmentation reduces the differences in mass spectra between species. However, it is expected that recent developments in AMS technology, such as softer ionization techniques (VUV, Li^+ ion, and electron attachment) and the high-resolution ToF-AMS (see section VI) will produce more detailed spectra, from which additional information about the organic aerosol components may be extracted.

VI. ENHANCEMENTS AND FUTURE DIRECTIONS

A. ToF-AMS

In the ToF-AMS, the vaporization and ionization system shown in Figure 6 is directly coupled to a compact ToFMS that has been developed by Tofwerk AG (Thun, Switzerland). This approach takes advantage of the quantitative vaporization/ionization system while adding the high ion throughput of a ToF mass spectrometer (Drewnick et al., 2005). Since the ToFMS technique is inherently pulsed, it is most efficiently used in combination with pulsed ionization techniques like laser ionization instead of continuous ionization sources like EI. In the ToF-AMS, however, the continuous stream of ions generated in the AMS EI ionizer is imaged and extracted into a well-collimated (~1 mm) beam which is then transferred to an orthogonal extraction chamber (Chen et al., 1998; Guilhaus, Selby, & Mlynski, 2000). The ion beam enters the extractor region of the Tofwerk ToF mass spectrometer from the ionizer side and is extracted with a pulsed electric field. This results in a fraction of the continuous ion beam being sampled in discrete sections. This way, the ion beam is monitored section by section, providing fast, quasi-continuous sampling that is appropriate for analysis of vaporized particle bursts. For the ToF-AMS, the extraction efficiency has a significant but predictable dependence on *m/z*, a correction for which is routinely applied during data analysis (Drewnick et al., 2005). The resolving power of a ToF mass spectrometer is limited by the recorded ions' distribution of kinetic energies. In the ToF-AMS this is minimized by optimizing the transfer optics between the ion source and the ToFMS (DeCarlo et al., 2006). A second limit on resolution is separation of adjacent *m/z* values in time-of-flight space. The reflectron configuration increases flight path and leads to larger temporal separation, while maintaining a field-portable footprint.

Typically, the extractor is pulsed at a rate of 66.7 kHz (15 μsec). Each extraction yields a complete MS that is processed by a data acquisition board and computer at a rate of 1 GHz. During a single particle vaporization event, which can range from 30 to 120 μsec depending on particle size, the extractor is pulsed several times. Thus, unlike the quadrupole, this mass spectrometer has the capability to provide size distributions for all *m/z* (or alternatively complete size-resolved mass spectra), and also to provide complete mass spectra as a function of particle size for individual particles. Moreover, since this mass spectrometer will analyze the extracted ions at all *m/z*, the ToF-AMS has an increased sensitivity by a factor of ~30 (depending on the species) over the Q-AMS due to its much higher duty cycle (DeCarlo et al., 2006). Figure 29 demonstrates single particle mass spectra observed during the first field deployment of the ToF-AMS. Panel A shows an accumulation mode single particle with $d_{va} = 405$ nm that is composed of mixed AN/ammonium sulfate particles and also contains some organics and chloride. Panel B shows a single particle with $d_{va} = 315$ nm which is dominated by ammonium sulfate. Finally, panel C shows a particle with $d_{va} = 190$ nm that is made up of AN internally mixed with organic species. The most common particle type observed during this campaign was type A.

B. HR-ToF-AMS

The resolution of the standard ToF-AMS instrument is ~1,000. The standard ToFMS spectrometer is referred to as the C-ToF due to the shape of the ion path in the instrument resembling a "C." Recently, a HR-ToF-AMS capable of resolution ranging from 2,500 (in V-mode) or 4,500 to 5,000 (in W mode) has been developed, where the V and W represent the path of the ions in the flight chamber (DeCarlo et al., 2006). In V-mode, ions follow a traditional reflectron path, whereas in W-mode, the ions are reflected three times, thereby increasing the effective drift length. The high mass resolution allows the separation of each unit mass peak into separate contributions for specific elemental compositions based on small differences in mass defect. Figure 30 compares the mass spectral signal observed at a common organic fragment (*m/z* 43) with a standard C-ToF and a HR-ToF-AMS operating in the V and W modes. The high resolution of the HR-ToF-AMS has already been demonstrated in the field (DeCarlo et al., 2006) and will provide valuable insight into the elemental composition of organic-containing PM.

C. Soft Ionization

While EI ionization has many advantages, such as universal detection of all vaporized molecules with similar sensitivity, it can cause extensive fragmentation and result in complex mass spectra which do not permit unambiguous molecular detection and identification of specific organic compounds. Accurate classification (and sometimes identification) of organic aerosol species can be greatly improved by reducing the fragmentation of organic molecules when ionized. One means of achieving this goal is the use of ionization methods that are softer (deposit less energy in the ions) than 70 eV EI ionization. Soft ionization methods would also enhance the specificity of the AMS technique to target specific groups of species that are preferentially ionized by a given technique. For example, dissociative electron attachment is very sensitive to oxygenated organic molecules while blind to other types of organic molecules (Zahardis, LaFranchi, & Petrucci, 2005).

Chemical ionization techniques for mass spectrometric PM analyses have been recently investigated (Hoffmann et al., 1998; Voisin et al., 2003; Warscheid, Kuckelmann, & Hoffmann, 2003; Hearn & Smith, 2004), as has the use of low energy photoelectron attachment (LaFranchi & Petrucci, 2004; Zahardis, LaFranchi, &

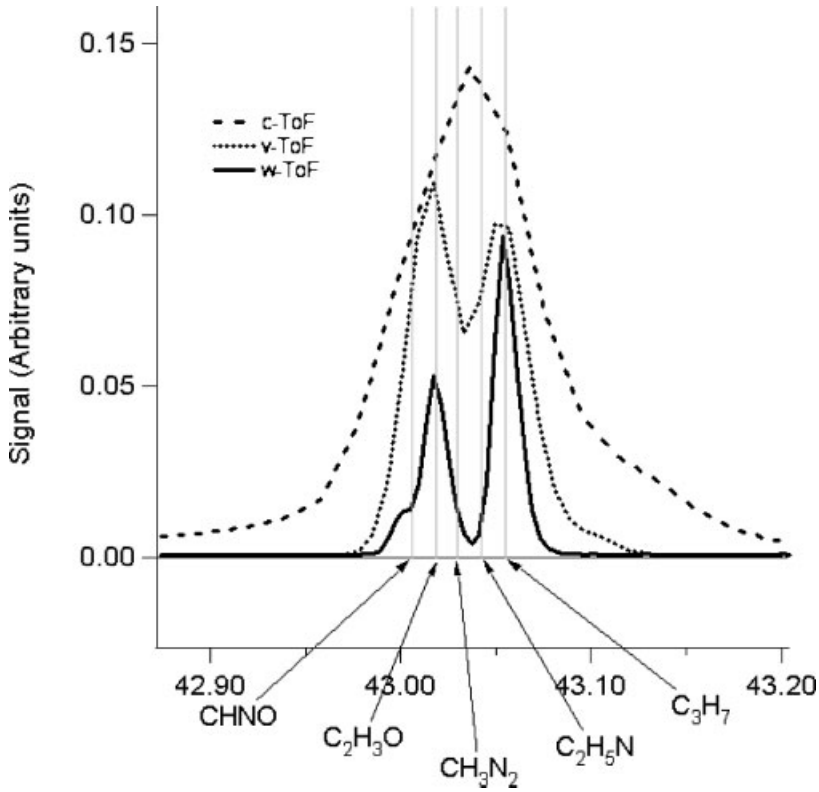

FIGURE 30. An illustration of the detailed chemical information that can be obtained with high resolution ToF spectrometers. The spectral resolution c-ToF, v-ToF, and w-ToF are approximately 1,000; 2,500; and 4,500–5,000, respectively. (DeCarlo, 2006, modified.)

Petrucci, 2005). Svane, Hagstrom, and Pettersson (2004) and Svane et al. (2005) have also developed a specialized Aerosol MS instrument that exploits the ability of hot surfaces to thermally vaporize and ionize species with very low ionization potentials and have used it to measure the alkali metal content of ambient PM.

Several groups have used VUV single photon ionization to reduce sample fragmentation after vaporizing single particle or collected PM thermally or by infrared laser heating. Baer and co-workers, Johnston and co-workers, and Zimmermann and co-workers have all used 118 nm radiation from a Xe cell or third harmonic generation of a tripled Nd:YAG laser pump source to demonstrate single UV photoionization of organic PM constituents (Woods et al., 2002; Öktem, Tolocka, & Johnston, 2004; Ferge, Muhlberger, & Zimmermann, 2005). Recently, Baer and co-workers showed that thermal vaporization produced fewer vibrationally excited organic molecules than CO_2 infrared laser vaporization, and less fragmentation during VUV ionization (Nash et al., 2005). They also showed that using 142 nm (8.75 eV) VUV produced less fragmentation than 118 nm (10.48 eV) radiation for vaporized OA, since it better matched the 8.6 eV ionization potential of that species. Baer and co-workers (Mysak et al., 2005) have also demonstrated the use of tunable UV radiation from a synchrotron coupled to a thermal particle desorption vaporization source. While coherent laser pumped and synchrotron VUV ionization sources are terrific for laboratory studies of organic PM, they are unlikely to be useful for field instruments designed for ambient atmospheric studies in the near future.

Recently, the use of single-photon ionization using VUV light from a krypton discharge lamp that emits radiation at 10 and 10.6 eV has been demonstrated at ARI and deployed in field measurements at University of California–Riverside and in chamber studies at the Paul Scherrer Institute in Switzerland (Northway et al., 2006). In this technique, a VUV resonance lamp is integrated into the AMS vaporization/ionization region and used in alternation with the standard EI ion source to optimize quantitative information. VUV photons have only slightly more energy than the ionization potential of most organic species, which limits the amount of excess internal energy deposited in the molecular ion after ionization. Since this excess energy can result in bond cleavage, the lower internal energy of the molecular ions achieved with VUV ionization results in reduced fragmentation. The top two panels of Figure 31 show the MS of OA resulting from EI and VUV photoionization with the krypton discharge lamp. VUV ionization reduces fragmentation enough that the parent molecular ion at *m/z* 282 is observed.

A second soft ionization technique under development for AMS deployment is Li^+ ion attachment (LIAMS) (Hodges & Beauchamp, 1976; Fujii, Ogura, & Jimba, 1989). LIAMS has the advantage that it generally occurs without fragmentation or the occurrence of side reactions and therefore, almost solely results

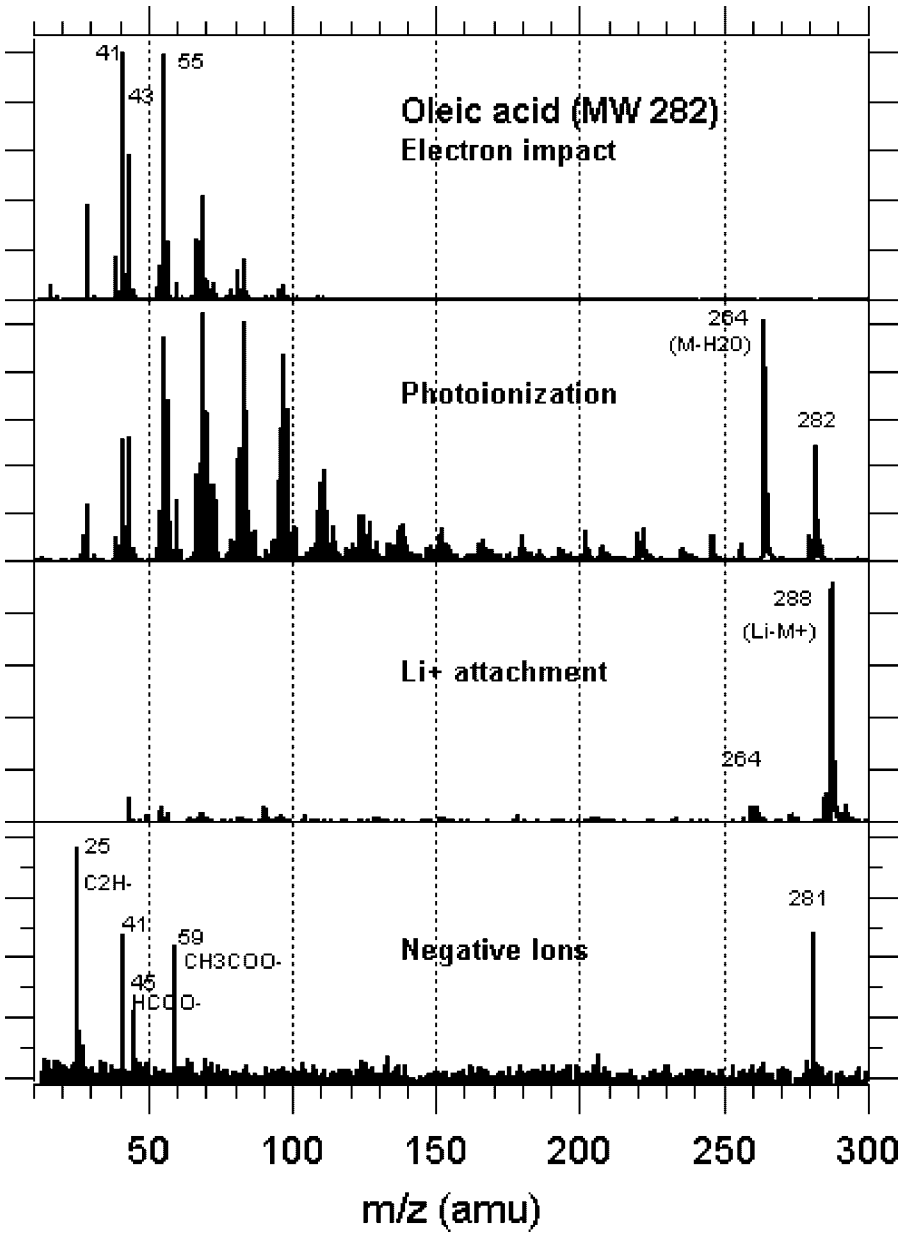

FIGURE 31. A comparison between AMS mass spectra obtained with electron impact and various soft-ionization methods. The molecular weight of oleic acid is 282 g/mol. All mass spectra in the figure have linear y-axes with arbitrary units.

in the formation of quasi-molecular $Li(M)_x^+$ adduct ions. The resulting mass spectra are relatively simple and easy to interpret. An Li^+ ion source has been integrated into the ionizer/vaporizer of the AMS. The third panel in Figure 31 shows the lithium ion attachment spectrum for OA. The dominant peak is due to $[M–Li]^+$ at $m/z = 288$ and the MS shows almost no fragmentation of the parent molecule.

A third soft ionization technique, dissociative electron attachment, takes advantage of low energy electrons that are present during the EI process. These electrons attach to other molecules resulting in negatively charged species in a manner similar to the low energy photoelectron capture detector developed by Pertrucci and co-workers (LaFranchi & Petrucci, 2004; Zahardis, LaFranchi, & Petrucci, 2005). The ToFMS can be tuned to detect negative ions and the resulting MS is shown in the bottom panel of Figure 31. The parent molecular peak appears at m/z 281 due to loss of an H. Some fragmentation is observed, but not nearly as much as in the positive ion EI spectrum in the top panel.

As indicated in Figure 31, the reduced fragmentation in the soft-ionization mass spectra results in clear parent ion signals in the mass spectra that are not observed in the EI mass spectra.

Thus, organic molecules could be more readily identified with the soft-ionization spectra than the EI spectrum. Compared to EI, however, the soft ionization techniques have lower inherent ionization cross sections, are less universal, and are not as capable of providing quantitative total organic aerosol mass concentrations. Thus, the ideal operating mode for the AMS will likely involve continuous switching (e.g. every 5 min) between EI and soft-ionization detection schemes to enable near-simultaneous measurement of both types of complementary information.

VII. SUMMARY AND OUTLOOK

The AMS discussed in this review represents one of the widely used instrumental approaches to addressing the challenging problem of real-time characterization of atmospheric PM. This instrument combines aerodynamic lens inlet technology with thermal vaporization and electron-impact mass spectrometry to provide measurements of speciated PM mass concentrations and size distributions. The unique feature of this instrument, compared to laser vaporization aerosol mass spectrometric techniques reviewed by Murphy in this issue, is its use of a detection technique which does not rely on high powered lasers. This allows a robust and relatively compact design that can be deployed for field measurements at fixed sites as well as on small aircraft, in mobile laboratories, and aboard research vessels.

The most commonly used versions of the AMS use a resistively heated metal surface to vaporize the sampled aerosol particles and EI mass spectrometry (Q or ToF) to detect the vaporized aerosol species. This detection scheme is general for a wide range of aerosol compositions. It is inherently linear, and since the vaporization and ionization steps are decoupled, it does not suffer from the plasma chemical charge transfer matrix effects that affect combined laser vaporization/ionization methods. It is, thus, capable of providing quantitative measurements of the mass concentration of aerosol constituents.

The quantitative and multidimensional data produced by the AMS have many atmospheric science applications. Measurements taken in close proximity to sources of particles can be used to derive emission profiles (Allan et al., 2003a; Canagaratna et al., 2004; Schneider et al., 2005b), identify local sources (Li et al., 2004), or quantify particle chemical fluxes. These can be used to improve emissions inventories, which are in turn used in regional and global atmospheric composition models.

AMS composition data is also being used more directly in regional chemistry models to either provide realistic initialization and boundary conditions or validate the products (Tang et al., 2004; Johnson et al., 2005). Parameterized forms of AMS data can contribute to models in other ways. For example, Quinn and Bates (2005) used an extensive comparison of *in situ* measurements to produce empirical predictions of the humidity-dependent optical properties of aerosols based on their compositions. These quantities are important when modeling the aerosol direct radiative forcing effect on climate or when developing retrieval techniques for data produced by satellites or other remote sensing methods.

The composition-dependent hygroscopicity of aerosol particles is another key process for which AMS field data is being used to validate models through closure studies (Conant et al., 2004; McFiggans et al., 2005a). These models, when fully developed, can be used to predict the optical and cloud-forming properties of aerosols much more explicitly, which can again be used (in a parameterized form) to improve predictions of climate, atmospheric composition, and meteorology.

AMS data is also being used in the more fundamental aspects of atmospheric science. For instance, it is useful in studying complex processes such as the reactive uptake of chemical species (Kroll et al., 2005b; Liggio, Li, & McLaren, 2005a,b; Garland et al., 2006) and the formation of secondary organic aerosol (e.g., Kroll et al., 2005a) in detail in the laboratory. Accurate kinetic data obtained can then be employed in larger chemical process models.

While the atmospheric applications of the AMS have been stressed in this review, the potential of diagnosing disease from the analysis of aerosols in exhaled breath, the growing need for the real-time characterization of the size and chemical composition of aerosolized pharmaceutical drugs during their production phase and their delivery by inhalers, and the need to detect potentially deadly bioagents are all areas that are gaining increasing attention and that could benefit from the detailed real-time aerosol characterization that is possible with the AMS.

Remaining development challenges for the AMS include improving its quantification capability, interpreting the mass spectral complexity, particularly for organic species, and extending its capability to detect refractory species. The flexibility of the AMS detection approach allows for progress in these directions through the development of aerodynamic inlets that have higher transmission efficiencies for supermicron and small particles, new vaporizer designs that could reduce bounce-related collection efficiency losses, soft ionization schemes that could simplify mass spectral fragmentation patterns, and the incorporation of other techniques such as light scattering that can be used to detect NR species.

Experimental possibilities will also open up as nanoscience evolves, and new methods of characterizing nanoparticles are developed and deployed within the AMS framework. While the capabilities of the AMS will continue to evolve, it is unlikely, given the dynamic range in atmospheric aerosol properties, that any one instrument can provide all the information needed to completely characterize the atmospheric aerosol properties of interest. Thus, simultaneous aerosol measurements with the AMS and other aerosol instrumentation such as DMAs or laser vaporization AMSs will be necessary to obtain a comprehensive understanding of atmospheric PM.

ACKNOWLEDGMENTS

Many fruitful discussions with the broader AMS user community are gratefully acknowledged.

REFERENCES

Alfarra MR. 2004. Insights into atmospheric organic aerosols using an aerosol mass spectrometer. PhD Thesis. University of Manchester.

Alfarra MR, Coe H, Allan JD, Bower KN, Boudries H, Canagaratna MR, Jimenez JL, Jayne JT, Garforth A, Li S-M, Worsnop DR. 2004.

Characterization of urban and regional organic aerosols in the lower Fraser Valley using two Aerodyne Aerosol Mass Spectrometers. Atmos Environ 38:5745–5758.

Alfarra MR, Paulsen D, Gysel M, Garforth AA, Dommen J, Prevot ASH, Worsnop DR, Baltensperger U, Coe H. 2006. A mass spectrometric study of secondary organic aerosols formed from the photooxidation of anthropogenic and biogenic precursors in a reaction chamber. Atmos Chem Phys 6:5279–5293.

Allan JD, Alfarra MR, Bower KN, Williams PI, Gallagher MW, Jimenez JL, McDonald AG, Nemitz E, Canagaratna MR, Jayne JT, Coe H, Worsnop DR. 2003a. Quantitative sampling using an Aerodyne Aerosol Mass Spectrometer. Part 2: Measurements of fine particulate chemical composition in two UK Cities. J Geophys Res Atmos 108:4091, doi:4010.1029/2002JD002359.

Allan JD, Jimenez JL, Williams PI, Alfarra MR, Bower KN, Jayne JT, Coe H, Worsnop DR. 2003b. Quantitative sampling using an Aerodyne Aerosol Mass Spectrometer. Part 1: Techniques of data interpretation and error analysis. J Geophys Res Atmos 108:4090, doi:4010.1029/2002JD002358.

Allan JD, Bower KN, Coe H, Boudries H, Jayne JT, Canagaratna MR, Millet DB, Goldstein AH, Quinn PK, Weber RJ, Worsnop DR. 2004a. Submicron aerosol composition at Trinidad Head, California, during ITCT 2K2: Its relationship with gas phase volatile organic carbon and assessment of instrument performance. J Geophys Res Atmos 109:D23S24, doi:10.1029/2003JD004208.

Allan JD, Delia AE, Coe H, Bower KN, Alfarra MR, Jimenez JL, Middlebrook AM, Drewnick F, Onasch TB, Canagaratna MR, Jayne JT, Worsnop DR. 2004b. A generalised method for the extraction of chemically resolved mass spectra from Aerodyne aerosol mass spectrometer data. J Aerosol Sci 35:909–922, doi:910.1016/j.jaerosci.2004.1002.1007.

Allan JD, Alfarra MR, Bower KN, Coe H, Jayne JT, Worsnop DR, Aalto PP, Kulmala M, Hyötyläinen T, Cavalli F, Laaksonen A. 2006. Size and composition measurements of background aerosol and new particle growth in a Finnish forest during QUEST 2 using an Aerodyne Aerosol Mass Spectrometer. Atmos Chem Phys 6:315–327.

Allen J, Gould RK. 1981. Mass spectrometric analyzer for individual aerosol particles. Rev Sci Instrum 52:804–809.

Anderson BE, Branham H-S, Hudgins CH, Plant JV, Ballenthin JO, Miller TM, Viggiano AA, Blake DR, Boudries H, Canagaratna M, Maike-Lye RC, Onasch T, Wormhoudt J, Worsnop D, Brunke KE, Culler S, Penko P, Sanders T, Han H-S, Lee P, Pui DYH, Thornhill KL, Winstead EL. 2005. Experiment to Characterize Aircraft Volatile Aerosol and Trace-Species Emissions (EXCAVATE). National Aeronautics and Space Administration. Report (NASA/TM-2005-213783).

Bae MS, Schauer JJ, DeMinter JT, Turner JR. 2004. Hourly and daily patterns of particle-phase organic and elemental carbon concentrations in the urban atmosphere. J Air Waste Manage Assoc 54:823–833.

Bahreini R, Jimenez JL, Wang J, Flagan RC, Seinfeld JH, Jayne JT, Worsnop DR. 2003. Aircraft-based aerosol size and composition measurements during ACE-Asia using an Aerodyne aerosol mass spectrometer. J Geophys Res-Atmos 108:8645, doi:8610.1029/2002JD003226.

Bahreini R, Keywood M, Ng NL, Varutbangkul V, Gao S, Flagan RC, Seinfeld JH, Worsnop DR, Jimenez JL. 2005. Measurements of secondary organic aerosol from oxidation of cycloalkanes, terpenes, and m-xylene using the Aerodyne Aerosol Mass Spectrometer. Environ Sci Technol:10.1021/es048061a.

Baltensperger U, Kalberer M, Dommen J, Paulsen D, Alfarra MR, Coe H, Fisseha R, Gascho A, Gysel M, Nyeki S, Sax M, Steinbacher M, Prevot ASH, Sjögren S, Weingartner E, Zenobi R. 2005. Secondary organic aerosols from anthropogenic and biogenic precursors. Faraday Discussions 130:265–278, DOI: 210.1039/b417367h.

Barth M, McFadden JP, Sun J, Wiedinmyer C, Chuang P, Collins D, Hannigan M, Karl T, Kim S-W, Lasher-Trapp S, Levis S, Litvak M, Mahowald N, Moore K, Nandi S, Nemitz E, Nenes A, Potosnak M, Raymond TM, Smith J, Still C, Stroud C. 2005. Coupling between land ecosystems and the atmospheric hydrologic cycle through biogenic aerosol pathways. Am Meteorol Soc 86:1738–1742.

Bartmess JE, Georgiadis RM. 1983. Empirical methods for determination of ionization gauge relative sensitivities for different gases. Vacuum 33:149–153.

Bates TS, Quinn PK, Coffman DJ, Johnson JE, Middlebrook AM. 2005. Dominance of organic aerosols in the marine boundary layer over the Gulf of Maine during NEAQS 2002 and their role in aerosol light scattering. J Geophys Res 110:D18202, doi:10.1029/2005JD005797.

Boudries H, Canagaratna MR, Jayne JT, Alfarra R, Allan J, Coe H, Pryor SC, Jimenez JL, Brook JR, Li S, Worsnop DR. 2004. Chemical and physical processes controlling the distribution of aerosols in the Lower Fraser Valley, Canada, during the PACIFIC 2001 field campaign. Atmos Environ 38:5759–5774.

Broekhuizen K, Chang RY-W, Leaitch WR, Li S-M, Abbatt JPD. 2005. Closure between measured and modeled cloud condensation nuclei (CCN) using size-resolved aerosol compositions in downtown Toronto. Atmos Chem Phys Discuss 5:6263–6293.

Bytnerowicz A, Fenn ME. 1996. Nitrogen deposition in California forests—A review. Environ Pollut 92:127–146.

Canagaratna MR, Jayne JT, Ghertner DA, Herndon S, Shi Q, Jimenez JL, Silva PJ, Williams P, Lanni T, Drewnick F, Demerjian KL, Kolb CE, Worsnop DR. 2004. Chase studies of particulate emissions from in-use New York city vehicles. Aerosol Sci Technol 38:555–573, 510.1080/02786820490465504.

Chameides WL, Hu H, Liu SC, Bergin M, Zhou X, Mearns L, Wang G, Kiang CS, Saylor RD, Luo C, Huang Y, Steiner A, Giorgi F. 1999. Case study of the effects of atmospheric aerosols and regional haze on agriculture: An opportunity to enhance crop yields in China through emission controls? Proc Nat Acad Sci 26:3626–13633.

Chen YH, Gonin M, Fuhrer K, Dodonov A, Su CS, Wollnik H. 1998. Orthogonal electron impact source for a time-of-flight mass spectrometer with high mass resolving power. Int J Mass Spectrom 185–187:221–226.

Coe H, Allan JD, Alfarra MR, Bower KN, Flynn MJ, McFiggans GB, Topping DO, Williams PI, O'Dowd CD, Dall'Osto M, Beddows DCS, Harrison RM. 2005. Chemical and physical characteristics of aerosol particles at a remote coastal location, Mace Head, Ireland, during NAMBLEX. Atmos Chem Phys Discuss 5:11643–11678.

Coe H, Allan JD. 2006. Mass spectrometric methods for aerosol composition measurements. In: Analytical techniques for atmospheric measurement. Oxford: Blackwell Publishing. p 265–310.

Cohan D, Xu J, Bergin MH, Chameides WL. 2002. The impact of aerosol light attenuation on C-uptake by green plants. Global Biogeochem Cycle 16:1090.

Conant WC, VanReken TM, Rissman TA, Varutbangkul V, Jonsson HH, Nenes A, Jimenez JL, Delia AE, Bahreini R, Roberts GC, Flagan RC, Seinfeld JH. 2004. Aerosol-cloud drop concentration closure in warm cumulus. J Geophys Res Atmos 109:D13204.

Crable GF, Coggeshall ND. 1958. Application of total ionization principles to Mass Spectrometric Analysis. Anal Chem 30:310–313.

Crosier J, Allan J, Bower K, Coe H, Alfarra MR, Jimenez J, Canagaratna M, Jayne J, Worsnop D. 2006. Description and use of the new Jump Mass Spectrum mode of operation for the Aerodyne Quadrupole Aerosol Mass Spectrometer. Aerosol Sci Technol (Submitted).

Cross ES, Slowik JG, Davidovits P, Allan JD, Worsnop DR, Jayne JT, Lewis DK, Canagaratna MR, Onasch TB. 2006. Laboratory and ambient particle density determinations using light scattering in conjunction with aerosol mass spectrometry. Aerosol Sci Technol (submitted).

Cubison M, Alfarra M, Allan J, Bower K, Coe H, McFiggans G, Whitehead J, Williams P, Zhang Q, Jimenez JL, Hopkins J, Lee J. 2005. The characterisation of pollution aerosol in a changing photochemical environment. Atmos Chem Phys Discuss 5:10055–10096.

Dall'Osto M, Harrison RM, Furutani H, Prather KA, Coe H, Allan JD. 2005. Studies of aerosol at a coastal site using two aerosol mass spectrometry instruments and identification of biogenic particle types. Atmos Chem Phys Discuss 5:10799–10838.

de Gouw JA, Middlebrook AM, Warneke C, Goldan PD, Kuster WC, Roberts JM, Fehsenfeld FC, Worsnop DR, Canagaratna MR, Pszenny AAP, Keene WC, Marchewka M, Bertman SB, Bates TS. 2005. Budget of organic carbon in a polluted atmosphere: Results from the New England Air Quality Study in 2002. J Geophys Res Atmos 110: doi:10.1029/2004JD005623.

DeCarlo P, Slowik JG, Worsnop DR, Davidovits P, Jimenez JL. 2004. Particle morphology and density characterization by combined mobility and aerodynamic diameter measurements. Part 1: Theory. Aerosol Sci Technol 38:1185–1205.

DeCarlo PF, Kimmel JR, Trimborn A, Northway MJ, Jayne JT, Aiken AC, Gonin M, Fuhrer K, Horvath T, Docherty KS, Worsnop DR, Jimenez JL. 2006. Field-deployable, high-resolution, time-of-flight aerosol mass spectrometer. Anal Chem ASAP Article; DOI: 10.1021/ac061249n.

Delia AE. 2004. Real-time measurement of non-refractory particle composition and interactions at forested sites. Thesis. Boulder: University of Colorado.

Dockery DW, Pope CA, Xu XP, Spengler JD, Ware JH, Fay ME, Ferris BG, Speizer FE. 1993. An Association between Air-Pollution and Mortality in 6 United-States Cities. New Eng J Med 329:1753–1759.

Dominici F, Peng DK, Bell ML, Pham L, McDermott A, Zeger SL, Samet JM. 2006. Fine particulate air pollution and hospital admission for cardiovascular and respiratory diseases. JAMA 295:1127–1134.

Drewnick F, Schwab JJ, Hogrefe O, Peters S, Husain L, Diamond D, Weber R, Demerjian KL. 2003. Intercomparison and evaluation of four semi-continuous $PM_{2.5}$ sulfate instruments. Atmos Environ 37:3335–3350.

Drewnick F, Schwab JJ, Jayne JT, Canagaratna M, Worsnop DR, Demerjian KL. 2004a. Measurement of ambient aerosol composition during the PMTACS-NY 2001 using an Aerosol Mass Spectrometer. Part I: Mass concentrations. Aerosol Sci Technol 38:92–103.

Drewnick F, Schwab JJ, Jayne JT, Canagaratna M, Worsnop DR, Demerjian KL. 2004b. Measurement of ambient aerosol composition during the PMTACS-NY 2001 using an Aerosol Mass Spectrometer. Part II: Chemically speciated mass distributions. Aerosol Sci Technol 38:104–117.

Drewnick F, Hings SS, DeCarlo PF, Jayne JT, Gonin M, Fuhrer K, Weimer S, Jimenez JL, Demerjian KL, Borrmann S, Worsnop DR. 2005. A new Time-of-Flight Aerosol Mass Spectrometer (ToF-AMS)—Instrument description and first field deployment. Aerosol Sci Technol 39:637–658.

Drewnick F, Hings SS, Curtius J, Eerdekens G, Williams J. 2006. Measurement of fine particulate and gas-phase species during the New Year's Fireworks 2005 in Mainz, Germany. Atmos Environ 40:788–795.

Dzepina K, Arey J, Marr LC, Worsnop DR, Salcedo D, Zhang Q, Molina LT, Molina MJJ. 2006. Detection of particle-phase polycyclic aromatic hydrocarbons in Mexico City using an aerosol mass spectrometer. Int J Mass Spec (submitted).

Ehara K, Shin S. 1998. Measurement of density distribution of aerosol particles by successive classification of particles according to their mass and diameter. J Aerosol Sci 29(Suppl. 1):19–20.

Ferge T, Muhlberger F, Zimmermann R. 2005. Application of infrared laser desorption vacuum-UV single-photon ionization mass spectrometry for analysis of organic compounds from particulate matter filter samples. Anal Chem 77:4528–4538.

Fujii T, Ogura M, Jimba H. 1989. Chemical ionization Mass Spectrometry with lithium ion attachment to the molecule. Anal Chem 61:1026–1029.

Garland RM, Wise ME, Beaver MR, DeWitt HL, Aiken AC, Jimenez JL, Tolbert MA. 2005. Impact of palmitic acid coating on the water uptake and loss of ammonium sulfate particles. Atmos Chem Phys 5:1951–1961.

Garland RM, Elrod MJ, Kincaid K, Beaver MR, Jimenez JL, Tolbert MA. 2006. Acid-catalyzed reactions of hexanal on sulfuric acid particles: Identification of reaction products. Atmos Environ 40:6863–6878.

Guilhaus M, Selby D, Mlynski V. 2000. Orthogonal acceleration time-of-flight mass spectrometry. Mass Spectrom Rev 19:65–107.

Hearn JD, Smith GD. 2004. A chemical ionization mass spectrometry method for the online analysis of organic aerosols. Anal Chem 76:2820–2826.

Heberlein J, Postel O, Girshick S, McMurry P, Gerberich W, Iordanoglou D, Di Fonzo F, Neumann D, Gidwani A, Fan M, Tymiak N. 2001. Thermal plasma deposition of nanophase hard coatings. Surf Coat Technol 142:265–271.

Hinds WC. 1982. Aerosol technology: Properties, behavior, and measurement of airborne particles. New York: Wiley-Interscience.

Hodges RV, Beauchamp JL. 1976. Application of alkali ions in chemical ionization Mass Spectrometry. Anal Chem 48:825–829.

Hoffmann T, Bandur R, Marggraf U, Linscheid M. 1998. Molecular composition of organic aerosols formed in the alpha-pinene/O_3 reaction: Implications for new particle formation processes. J Geophys Res 103:25569–25578.

Hogrefe O, Drewnick F, Lala GG, Schwab JJ, Demerjian KL. 2003. Development, operation and applications of an aerosol generation, calibration and research facility. Aerosol Sci Technol 38(S1):196–214.

Hogrefe O, Schwab JJ, Drewnick F, Lala GG, Peters S, Demerjian KL, Rhoads K, Felton HD, Rattigan OV, Husain L, Dutkiewicz VA. 2004. Semicontinuous PM2.5 sulfate and nitrate measurements at an urban and a rural location in New York: PMTACS-NY summer 2001 and 2002 campaigns. J Air Waste Manage Assoc 54:1040–1060.

Huffman JA, Jayne JT, Drewnick F, Aiken AC, Onasch T, Worsnop DR, Jimenez JL. 2005. Design, modeling, optimization, and experimental tests of a particle beam width probe for the Aerodyne Aerosol Mass Spectrometer. Aerosol Sci Technol 39:1143–1163, doi:1110.1080/02786820500423782.

IPCC. 2001. Climate change 2001. In: Houghton JT, Ding Y, Griggs DJ, Noguer M, van der Linden PJ, Dai X, Maskell K, Johnson CA, editors. The scientific basis, contribution of working group I to the Third Assessment Report of the Intergovernmental Panel on climate change. New York: Cambridge University Press.

Jayne JT, Leard DC, Zhang X, Davidovits P, Smith KA, Kolb CE, Worsnop DR. 2000. Development of an aerosol mass spectrometer for size and composition analysis of submicron particles. Aerosol Sci Technol 33:49–70.

Jimenez JL, Bahreini R, Cocker DR, Zhuang H, Varutbangkul V, Flagan RC, Seinfeld JH, O'Dowd C, Hoffmann T. 2003a. New particle formation from photooxidation of diiodomethane (CH_2I_2). J Geophys Res Atmos 108:4318, doi:4310.1029/2002JD002452.

Jimenez JL, Jayne JT, Shi Q, Kolb CE, Worsnop DR, Yourshaw I, Seinfeld JH, Flagan RC, Zhang X, Smith KA, Morris JW, Davidovits P. 2003b. Ambient aerosol sampling with an Aerosol Mass Spectrometer. J Geophys Res 108:8425, doi:8410:1029/2001JD001213.

Johnson D, Utembe SR, Jenkin ME, Derwent RG, Hayman GD, Alfarra MR, Coe H, McFiggans G. 2005. Simulating regional scale secondary organic aerosol formation during the TORCH 2003 campaign in the southern UK. Atmos Chem Phys Discuss 5:7829–7874.

Johnston MV. 2000. Sampling and analysis of individual particles by aerosol mass spectrometry. J Mass Spectrom 35:585–595.

Kalberer M, Paulsen D, Sax M, Steinbacher M, Dommen J, Prevot ASH, Fisseha R, Weingartner E, Frankevich V, Zenobi R, Baltensperger U. 2004. Identification of polymers as major components of atmospheric organic aerosols. Science 303:1659–1662.

Katrib Y, Martin ST, Hung HM, Rudich Y, Zhang H, Slowik J, Davidovits P, Jayne JT, Worsnop DR. 2004. Products and mechanisms of ozone

reactions with oleic acid for aerosol particles having core-shell morphologies. J Phys Chem A 108:6686–6695.

Katrib Y, Biskos G, Buseck PR, Davidovits P, Jayne JT, Mochida M, Wise ME, Worsnop DR, Martin ST. 2005a. Ozonolysis of mixed oleic-acid/stearic-acid particles: Reaction kinetics and chemical morphology. J Phys Chem A 109:10910–10919.

Katrib Y, Martin ST, Rudich Y, Davidovits P, Jayne JT, Worsnop DR. 2005b. Density changes of aerosol particles as a result of chemical reaction. Atmos Chem Phys 5:275–291.

Kolb CE, Herndon SC, McManus JB, Shorter JH, Zahniser MS, Nelson DD, Jayne JT, Canagaratna MR, Worsnop DR. 2004. Mobile laboratory with rapid response instruments for real-time measurements of urban and regional trace gas and particulate distributions and emission source characteristics. Environ Sci Technol 38:5694–5703.

Kroll JH, Ng NL, Murphy SM, Flagan RC, Seinfeld JH. 2005a. Secondary organic aerosol formation from isoprene photooxidation under high-NOx conditions. Geophys Res Lett 32:L18808.

Kroll JH, Ng NL, Murphy SM, Varutbangkul V, Flagan RC, Seinfeld JH. 2005b. Chamber studies of secondary organic aerosol growth by reactive uptake of simple carbonyl compounds. J Geophys Res Atmos 110: D23207, doi: 10.1029/2005JD006004.

LaFranchi BW, Petrucci GA. 2004. Photoelectron resonance capture ionization (PERCI): A novel technique for the soft-ionization of organic compounds. J Am Soc Mass Spectrom 15:424–430.

Lazar A, Reilly PTA, Whitten WB, Ramsey JM. 1999. Real-time surface analysis of individual airborne environmental particles. Environ Sci Technol 33:3993–4001.

Li Z, Hopke PK, Husain L, Qureshi S, Dutkiewicz VA, Schwab JJ, Drewnick F, Demerjian KL. 2004. Sources of fine particle composition in New York city. Atmos Environ 38:6521–6529.

Liggio J, Li S-M, McLaren R. 2005a. Heterogeneous reactions of glyoxal on particulate matter: Identification of acetals and sulfate esters. Environ Sci Technol 39:1532–1541.

Liggio J, Li S-M, McLaren R. 2005b. Reactive uptake of glyoxal by particulate matter. J Geophys Res Atmos 110:D10304.

Linstrom PJ, Mallard WG. 2001. The NIST Chemistry WebBook: A chemical data resource on the internet. J Chem Eng Data 46:1059–1063.

Liu BYH, Ziemman PJ, Kittelson DB, McMurry PH. 1995a. Generating particle beams of controlled dimensions and divergence: II. Experimental evaluation of particle motion in aerodynamic lenses and nozzle expansions. Aerosol Sci Technol 22:314–324.

Liu P, Ziemann PJ, Kittelson DB, McMurry PH. 1995b. Generating particle beams of controlled dimensions and divergence: I. Theory of particle motion in aerodynamic lenses and nozzle expansions. Aerosol Sci Tech 22:293–313.

Liu PSK, Deng R, Smith KA, Williams LR, Jayne JT, Canagaratna MR, Moore K, Onasch TB, Worsnop DR, Deshler T. 2006. Transmission efficiency of an aerodynamic focusing lens system: Comparison of model calculations and laboratory measurements for the aerodyne aerosol mass spectrometer. Aerosol Sci Tech (in press).

Marcolli C, Canagaratna MR, Worsnop DR, Bahreini R, de Gouw JA, Warneke C, Goldan PD, Kuster WC, Williams EJ, Lerner BM, Roberts JM, Meagher JF, Fehsenfeld FC, Marchewka ML, Bertman SB, Middlebrook AM. 2006. Cluster analysis of the organic peaks in bulk mass spectra obtained during the 2002 New England Air Quality Study with an aerodyne aerosol mass spectrometer. Atmospheric Chemistry & Physics Discussions 6:4601–4641.

Marr LC, Dzepina K, Jimenez JL, Riesen F, Bethel HL, Arey J, Gaffney JS, Marley NA, Molina LT, Molina MJ. 2005. Sources and transformations of particle-bound polycyclic aromatic hydrocarbons in Mexico City. Atmos Chem Phys Discuss 5:12741–12773.

McFiggans GH, Coe RB, Allan J, Cubison M, Alfarra MR, Saunders R, Saiz-Lopez A, Plane JMC, Wevill D, Carpenter L, Rickard AR, Monks PS. 2004. Direct evidence for coastal iodine particles from Laminaria macroalgae—Linkage to emissions of molecular iodine. Atmos Chem Phys Discuss 4:701–713.

McFiggans G, Alfarra MR, Allan J, Bower K, Coe H, Cubison M, Topping D, Williams P, Decesari S, Facchini C, Fuzzi S. 2005a. Simplification of the representation of the organic component of atmospheric particulates. Faraday Discuss 130:341–362.

McFiggans G, Artaxo P, Baltensperger U, Coe H, Facchini MC, Feingold G, Fuzzi S, Gysel M, Laaksonen A, Lohmann U, Mentel TF, Murphy DM, O'Dowd CD, Snider JR, Weingartner E. 2005b. The effect of physical and chemical aerosol properties on warm cloud droplet activation. Atmos Chem Phys Discuss 5:8507–8647.

McLafferty FW, Turecek F. 1993. Interpretation of mass spectra. Mill Valley, California: University Science Books.

McMurry PH. 2000. A review of atmospheric aerosol measurements. Atmos Environ 34:1959–1999.

McMurry PH, Wang X, Park K, Ehara K. 2002. The relationship between mass and mobility for atmospheric particles: A new technique for measuring particle density. Aerosol Sci Technol 36:227–238.

Morrical BD, Fergenson DP, Prather KA. 1998. Coupling two-step laser desorption/ionization with aerosol time-of-flight mass spectrometry for the analysis of individual organic particles. J Am Soc Mass Spectrom 9:1068–1073.

Morris JW, Davidovits P, Jayne JT, Jimenez JL, Shi Q, Kolb CE, Worsnop DR, Barney WS, Cass GR. 2002. Kinetics of submicron oleic acid aerosols with ozone; a novel aerosol mass spectrometric technique. Geophys Res Lett 29(9):71.1–71.4.

Murphy DM. The design of single particle laser mass spectrometers. Mass Spec Rev DOI 10.1002/mas.20113 (published online 16 October 2006).

Murphy DM, Middlebrook AM, Warshawsky M. 2003. Cluster analysis of data from the particle analysis by laser mass spectrometry (PALMS) instrument. Aerosol Sci Technol 37:382–391.

Murphy DM, Cziczo DJ, Hudson PK, Schein ME, Thomson DS. 2004. Particle density inferred from simultaneous optical and aerodynamic diameters sorted by composition. J Aerosol Sci 35:135–139.

Mysak ER, Wilson KR, Jimenez-Cruz M, Ahmed M, Baer T. 2005. Synchrotron radiation based aerosol time-of-flight mass spectrometry for organic constituents. Anal Chem 77:5953–5960.

NARSTO. 2004. In: McMurry P, Shepherd M, Vickery J, editors. Particulate Matter Science for Policy Makers—A NARSTO Assessment. Cambridge University Press.

Nash DG, Liu XF, Mysak ER, Baer T. 2005. Aerosol particle mass spectrometry with low photon energy laser ionization. Int J Mass Spectrom 241:89–97.

National Acid Precipitation Assessment Program. 1991. 1990 Integrated Assessment Report. In. Washington, DC 20503: The U.S. National Acid Precipitation Assessment Program, Office of the Director.

Noble CA, Prather KA. 2000. Real-time single particle mass spectrometry: A historical review of a quarter century of the chemical analysis of aerosols. Mass Spectrom Rev 19:248–274.

Northway MJ, Jayne JT, Toohey DW, Canagaratna MR, Trimborn A, Akiyama K-I, Shimono A, Jimenez JL, DeCarlo PF, Wilson KR, Worsnop DR. 2006. Demonstration of a VUV lamp photoionization source for improved organic speciation in an aerosol mass spectrometer. Aerosol Sci Tech (submitted).

NRC. 1996. Aerosol radiative forcing and climate change. Washington, DC: Council: National Academy Press.

O'Dowd CD, Jimenez JL, Bahreini R, Flagan RC, Seinfeld JH, Kulmala M, Pirjola L, Hoffmann T. 2002. Particle formation in the marine atmosphere controlled by biogenic iodine emissions. Nature 417: 632–636.

Öktem B, Tolocka MP, Johnston MV. 2004. On-line analysis of organic components in fine and ultrafine particles by photoionization aerosol mass spectrometry. Anal Chem 76:253–261.

Paatero P, Tapper U. 1994. Positive matrix factorization: A non-negative factor model with optimal utilization of error estimates of data values. Environmetrics 5:111–126.

Park K, Cao F, Kittelson DB, McMurry PH. 2003. Relationship between particle mass and mobility for diesel exhaust particles. Environ Sci Technol 37:577–583.

Pope CA, Burnett RT, Thun MJ, Calle EE, Krewski D, Ito K, Thurston GD. 2002. Lung cancer, cardiopulmonary mortality, and long-term exposure to fine particulate air pollution. JAMA 287:1132–1141.

Quinn PK, Bates TS. 2005. Regional aerosol properties: Comparisons of boundary layer measurements from ACE 1, ACE 2, Aerosols99, INDOEX, ACE Asia, TARFOX, and NEAQS. J Geophys Res 110: doi:10.1029/2004JD004755.

Ramanathan V, Crutzen PJ, Kiehl JT, Rosenfeld D. 2001. Aerosols, climate, and the hydrological cycle. Science 294:2119–2124.

Reilly PTA, Lazar AC, Gieray RA, Whitten WB, Ramsey JM. 2000. The elucidation of charge-transfer-induced matrix effects in environmental aerosols via real-time aerosol mass spectral analysis of individual airborne particles. Aerosol Sci Technol 33:135–152.

Rupakheti M, Leaitch WR, Lohmann U, Hayden K, Brickell P, Lu G, Li S-M, Toom-Sauntry D, Bottenheim JW, Brook JR, Vet R, Jayne JT, Worsnop DR. 2005. An intensive study of the size and composition of submicron atmospheric aerosols at a rural site in Ontario, Canada. Aerosol Sci Technol 39:722–736.

Salcedo D, Onasch TB, Dzepina K, Canagaratna MR, Zhang Q, Huffman JA, DeCarlo PF, Jayne JT, Mortimer P, Worsnop DR, Kolb CE, Johnson KS, Zuberi B, Marr LC, Volkamer R, Molina LT, Molina MJ, Cardenas B, Bernabé RM, Márquez C, Gaffney JS, Marley NA, Laskin A, Shutthanandan V, Xie Y, Brune W, Lesher R, Shirley T, Jimenez JL. 2006. Characterization of ambient aerosols in Mexico City during the MCMA-2003 campaign with Aerosol Mass Spectrometry: Results from the CENICA Supersite. Atmos Chem Phys 6:925–946.

Scheer V, Kirchner U, Casati R, Vogt R, Wehner B, Philippin S, Wiedensohler A, Hock N, Schneider J, Weimer S, Borrmann S. 2005. Composition of semi-volatile particles from diesel exhaust. SAE Paper 2005-01-0197.

Schneider J, Borrmann S, Wollny AG, Bläsner M, Mihalopoulos N, Oikonomou K, Sciare J, Teller A, Levin Z, Worsnop DR. 2004. Online mass spectrometric aerosol measurements during the MINOS campaign (Crete, August 2001). Atmos Chem Phys 4:65–80.

Schneider J, Hings SS, Hock BN, Weimer S, Borrmann S, Fiebig M, Petzold A, Busen R, Kärcher B. 2005a. Aircraft-based operation of an aerosol mass spectrometer: Measurements of tropospheric aerosol composition. J Aerosol Sci 37:839–857.

Schneider J, Hock N, Weimer S, Borrmann S, Kirchner U, Vogt R, Scheer V. 2005b. Nucleation particles in diesel exhaust: Composition inferred from in situ mass spectrometric analysis. Environ Sci Technol 39:6153–6161.

Schneider J, Weimer S, Drewnick F, Borrmann S, Helas G, Gwaze P, Schmid O, Andreae MO, Kirchner U. 2006. Mass spectrometric analysis and aerodynamic properties of various types of combustion derived aerosol particles. Int J Mass Spec: doi: 10.1016/j.ijms.2006.1007.1008.

Sinha MP, Giffin CE, Norris DD, Estes TJ, Vilker VL, Friedlander SK. 1982. Particle analysis by mass spectrometry. J Colloid Interface Sci 87:140–153.

Slowik JG, Stainken K, Davidovits P, Williams LR, Jayne JT, Kolb CE, Worsnop DR, Rudich Y, DeCarlo P, Jimenez JL. 2004. Particle morphology and density characterization by combined mobility and aerodynamic diameter measurements. Part 2: Application to combustion generated soot particles as a function of fuel equivalence ratio. Aerosol Sci Technol 38:1206–1222.

Stolzenburg M, Hering SV. 2003. Method for the automated measurement of fine particle nitrate in the atmosphere. Environ Sci Technol 34:907–914.

Suess DT, Prather KA. 1999. Mass spectrometry of aerosols. Chem Rev 99:3007.

Sullivan RC, Prather KA. 2005. Recent advances in our understanding of atmospheric chemistry and climate made possible by on-line aerosol analysis instrumentation. Anal Chem 77:3861–3886.

Sullivan AP, Weber RJ, Clements AL, Turner JR, Bae MS, Schauer JJ. 2004. A method for on-line measurement of water soluble organic carbon in ambient aerosol particles: Results from an urban site. Geophys Res Lett 31: doi:10.1029/2004GL019681.

Svane M, Hagstrom M, Pettersson JBC. 2004. Chemical analysis of individual alkali-containing aerosol particles: Design and performance of a surface ionization particle beam mass spectrometer. Aerosol Sci Technol 38:655–663.

Svane M, Janhall S, Hagstrom M, Hallquist M, Pettersson JBC. 2005. On-line alkali analysis of individual aerosol particles in urban air. Atmos Environ 39:6919–6930.

Sykes DC, Ephraim Woods I, Smith GD, Baer T, Miller RE. 2002. Thermal vaporization-vacuum ultraviolet laser ionization time-of-flight mass spectrometry of single aerosol particles. Anal Chem 74:2048–2052.

Takami A, Miyoshi T, Shimono A, Hatakeyama S. 2005. Chemical composition of fine aerosol measured by AMS at Fukue Island, Japan during APEX period. Atmos Environ 39:4913–4924.

Takegawa N, Miyazaki Y, Kondo Y, Komazaki Y, Miyakawa T, Jimenez JL, Jayne JT, Worsnop DR, Allan JD, Weber RJ. 2005. Characterization of an Aerodyne Aerosol Mass Spectrometer (AMS): Intercomparison with other aerosol instruments. Aerosol Sci Technol 39:760–770.

Tang YH, Carmichael GR, Horowitz LW, Uno I, Woo JH, Streets DG, Dabdub D, Kurata G, Sandu A, Allan J, Atlas E, Flocke F, Huey LG, Jakoubek RO, Millet DB, Quinn PK, Roberts JM, Worsnop DR, Goldstein A, Donnelly S, Schauffler S, Stroud V, Johnson K, Avery MA, Singh HB, Apel EC. 2004. Multiscale simulations of tropospheric chemistry in the eastern Pacific and on the US West Coast during spring 2002. J Geophys Res Atmos 109: D23S11, doi:10.1029/2004JD004513.

Tobias HJ, Kooiman PM, Docherty KS, Ziemann PJ. 2000a. Real-time chemical analysis of organic aerosols using a thermal desorption particle beam mass spectrometer. Aerosol Sci Technol 33:170–190.

Tobias HJ, Kooiman PM, Docherty KS, Ziemann PJ. 2000b. Real-time chemical analysis of organic compounds using a Thermal Desorption Particle Beam Mass Spectrometer. Aerosol Sci Technol 33:170–190.

Tobias HJ, Beving DE, Ziemann PJ, Sakurai H, Zuk M, McMurry PH, Zarling D, Waytulonis R, Kittelson DB. 2001. Chemical analysis of diesel engine nanoparticles using a nano-DMA/thermal desorption particle beam mass spectrometer. Environ Sci Technol 35:2233–2243.

Topping D, Coe H, McFiggans G, Burgess R, Allan J, Alfarra MR, Bower K, Choularton TW, Decesari S, Facchini MC. 2004. Aerosol chemical characteristics from sampling conducted on the Island of Jeju, Korea during ACE-Asia. Atmos Environ 38:2111–2123.

Trainer MG, Pavlov AA, Curtis DB, McKay CP, Worsnop DR, Delia AE, Toohey DW, Toon OB, Tolbert MA. 2004a. Haze aerosols in the atmosphere of early Earth: Manna from heaven. Astrobiology 4:409–419.

Trainer MG, Pavlov AA, Jimenez JL, McKay CP, Worsnop DR, Toon OB, Tolbert MA. 2004b. Chemical composition of Titan's Haze: Are PAHs present? Geophys Res Lett 31:L17S08.

Turpin BJ, Cary RA, Huntzicker JJ. 1990. An in-situ time-resolved analyzer for aerosol organic and elemental carbon. Aerosol Sci Technol 12:161–171.

Turpin BJ, Lim HJ. 2001. Species contributions to $PM_{2.5}$ mass concentrations: Revisiting common assumptions for estimating organic mass. Aerosol Sci Technol 35:602–610.

Voisin D, Smith JN, Sakurai H, McMurry PH, Eisele FL. 2003. Thermal desorption chemical ionization Mass Spectrometer for ultrafine particle chemical composition. Aerosol Sci Technol 37:471–475.

Volkamer R, Jimenez JL, San Martini F, Dzepina K, Zhang Q, Salcedo D, Molina LT, Worsnop DR, Molina MJ. 2006. Secondary organic aerosol

formation from anthropogenic air pollution: Rapid and higher than expected. Geophysical Research Letters 33:L17811.

Warscheid B, Kuckelmann U, Hoffmann T. 2003. Direct quantitative analysis of organic compounds in the gas and particle phase using a modified atmospheric pressure chemical ionization source in combination with ion trap Mass Spectrometry. Anal Chem 75:1410–1417.

Watson JG. 2002. Visibility: Science and regulation. J Air Waste Manage Assoc 52:628–713.

Weber RJ, Orsini D, Daun Y, Lee YN, Klotz PJ, Brechtel F. 2001. A particle-into-liquid collector for rapid measurement of aerosol bulk chemical composition. Aerosol Sci Technol 35:718–727.

Weimer S. 2003. University Mainz, 2003. Untersuchungen zum Nachweis von Russ- und Dieselabgaspartikeln am Aerodyne Aerosolmassen-spektrometer. Master Thesis. University Mainz.

Weimer S, Drewnick F, Hogrefe O, Schwab JJ, Rhoads K, Orsini D, Canagaratna M, Worsnop DR, Demerjian KL. 2006. Size-selective non-refractory ambient aerosol measurements during the PMTACS-NY 2004 winter intensive in New York City. J Geophys Res Atmos 111:D18305.

Williams Jonathan AD, Drewnick F, Hings SS, Curtius J, Eerdekens G, Klüpfel T, Wagner T. 2005. Firework emissions for satellite validation? Environ Chem 2:94–95.

Woods E III, Smith GD, Miller RE, Baer T. 2002. Depth profiling of heterogeneously mixed aerosol particles using single-particle mass spectrometry. Anal Chem 74:1642–1649.

Zahardis J, LaFranchi BW, Petrucci GA. 2005. Photoelectron resonance capture ionization-aerosol mass spectrometry of the ozonolysis products of oleic acid particles: Direct measure of higher molecular weight oxygenates. J Geophys Res 110: D08307 08301-08310.

Zelenyuk A, Yong C, Imre D. 2006b. From agglomerates of spheres to irregularly shaped particles: Determination of dynamic shape factors from measurements of mobility and vacuum aerodynamic diameters. Aerosol Sci Tech 40:197–217, 110.1080/02786820500529406.

Zelenyuk A, Cabalo J, Baer T, Miller RE. 1999. Mass spectrometry of liquid aniline aerosol particles by IR/UV laser irradiation. Anal Chem 71: 1802–1808.

Zelenyuk A, Cai Y, Chieffo L, Imre D. 2006a. High precision density measurements of single particles: The density of metastable phases. Aerosol Sci Technol 39:972–986.

Zhang X, Smith KA, Worsnop DR, Jimenez JL, Jayne JT, Kolb CE. 2002. A numerical characterization of particle beam collimation by an aerodynamic lens-nozzle system. Part I: An individual lens or nozzle. Aerosol Sci Technol 36:617–631.

Zhang Q, Stanier CO, Canagaratna MR, Jayne JT, Worsnop DR, Pandis SN, Jimenez JL. 2004a. Insights into the chemistry of new particle formation and growth events in Pittsburgh based on Aerosol Mass Spectrometry. Environ Sci Technol 38:4797–4809.

Zhang X, Smith KA, Worsnop DR, Jimenez JL, Jayne JT, Kolb CE, Morris J, Davidovits P. 2004b. Characterization of particle beam collimation. Part II: Integrated aerodynamic lens-nozzle system. Aerosol Sci Technol 38:619–638.

Zhang Q, Alfarra MR, Worsnop DR, Allan JD, Coe H, Canagaratna MR, Jimenez JL. 2005a. Deconvolution and quantification of hydrocarbon-like and oxygenated organic aerosols based on aerosol mass spectrometry. Environ Sci Technol 39:4938–4952, doi:4910.1021/es048568l.

Zhang Q, Canagaratna MC, Jayne JT, Worsnop DR, Jimenez JL. 2005b. Time and size-resolved chemical composition of submicron particles in Pittsburgh—Implications for aerosol sources and processes. J Geophys Res 110: doi:10.1029/2004JD004649.

Zhang Q, Worsnop DR, Canagaratna MR, Jimenez JL. 2005c. Hydrocarbon-like and oxygenated organic aerosols in Pittsburgh: Insights into sources and processes of organic aerosols. Atmos Chem Phys 5:3289–3311.

Douglas R. Worsnop was born in 1952 in Ann Arbor, MI. He received his B.A. from Hope College (1974) and Ph.D. from Harvard University (1982). He joined Aerodyne Research in 1985, where he is Vice President and Director of the Center for Aerosol and Cloud Chemistry. His research interests include gas phase chemical kinetics, atmospheric chemistry, heterogeneous chemistry, aerosol diagnostics, and mass spectrometry; focusing on the development and application of techniques for measuring size and composition of aerosol, both in the laboratory and in the field, in order to evaluate impacts on air quality and climate change.